THE NUMERICAL SIMULATION OF WHEEL LOADS ON AN ELECTRIC OVERHEAD TRAVELLING CRANE

Kim Anne M^{c}Kenzie

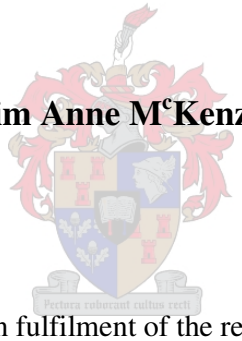

Thesis presented in fulfilment of the requirements for the
Degree of Master of Civil Engineering at the University of Stellenbosch

Supervisor: Prof. P.E. Dunaiski

December 2007

Declaration

I, the undersigned, hereby declare that the work contained in this thesis was my own original work and that I have not previously in its entirety or in part submitted it at any university for a degree.

Signature: ……

Date: ……

The financial assistance of the National Research Foundation (NRF) towards this research is hereby acknowledged. Opinions expressed and conclusions arrived at, are those of the author and are not necessarily to be attributed to the NRF.

Synopsis

The failure rate of electric overhead travelling crane supporting structures across the world is unacceptably high. Failures occur even when the supporting structures are designed within the relevant design codes. This demonstrates a lack of understanding of the dynamic behaviour of cranes in many design codes.

The current South African loading code is simplistic with respect to crane supporting structure design, relying on empirical factors to determine the correct loads. While these factors lead to predicted forces in the correct range of values, the Eurocode's methods are more scientifically based. In recognition of this the draft South African code predominantly incorporates the methods used by the Eurocode to calculate design forces for crane supporting structures.

The purpose of this thesis was to use an existing numerical model to determine the wheel loads induced by a crane into the crane supporting structure through hoisting, normal longitudinal travel, skewing and rail misalignment. The numerically obtained forces were then compared with the design forces estimated in the current South African code and the Eurocode, in order to determine whether the factors and methods used in the codes are accurate.

The current empirically based South African code was found to be highly conservative. In contrast the scientifically based design forces from the Eurocode were close to the numerically calculated forces, only failing to predict the behaviour of the crane in the case of skewing. Further work needs to be completed in the estimation of forces induced during this load case. Once this is achieved it is hoped that the better understanding of the crane forces adapted from the Eurocode into the draft South African code will lead to a reduction in failures of electric overhead travelling crane supporting structures.

Opsomming

Die falingskoers van elektriese oorhoofse hyskraan ondersteuningsstrukture is onaanvaarbaar hoog. Falings gebeur selfs indien die strukture met die relevante kodes ontwerp is. Dit demonsteer ‘n gebrek aan begrip aangaande die dinamiese gedrag van hyskrane soos vervat in die kodes.

Die Suid-Afrikaanse belastingskode vir hyskrane is simplisties met empiriese faktore vir die toegepaste belastings. Die Eurocode is meer wetenskaplik as die Suid-Afrikaanse kode en daarom inkorporeer die nuwe Suid-Afrikaanse kode baie van die Eurocode se ontwerpfaktore vir hyskraan ondersteuningsstrukture.

Die doel van hierdie tesis is om ‘n bestaande numeriese model te gebruik om die belastings op die struktuur gedurende oplig van las, gewone longitudinale beweging, wansporing en skuins beweging te ondersoek. Die numeriese model se kragte word vergelyk met die ontwerp kragte van die Suid-Afrikaanse kode en die Eurocode om te bepaal of die regte faktore en metodes in die kodes gebruik word.

Die empiriese Suid-Afrikaanse kode het konserwatiewe antwoorde gegee. Die Eurocode belastings was baie naby aan die numeriese model se antwoorde, met slegs ‘n groot verskil in die skuins beweging belastingsgeval. Verdere navorsing word benodig om die kragte vir hierdie belastingsgeval akkuraat te voorspel. Hierna kan ons hoop dat die nuwe Suid-Afrikaanse kode, wat ‘n meer wetenskaplike basis as die ou kode het, tot minder falings in die toekoms sal lei.

Acknowledgments

I would like to thank the following people whose enthusiasm, hard work and dedication throughout the last year have made this thesis possible.

Prof. P. E. Dunaiski

Thank you for your support and patience with my queries and problems throughout the year. It makes it easier when there is someone you can go to for help.

Bevan Timm

Thank you for your enthusiasm, support and encouragement whether helping with the endless checking and formatting required or simply being around. It means a lot to me.

Trevor Haas

Thank you for the many intense debates over cups of coffee. You've helped me solve innumerable problems and made the year an agreeable experience.

James Melvill

Thank you for keeping me on the right track even when it looked uncertain as to whether we would ever finish. You kept me sane through the year.

My Parents

Thank you for your tireless checking over the last few months and your constant encouragement. You've always supported me in all my endeavours and I thoroughly appreciate it.

TABLE OF CONTENTS

TABLE OF FIGURES

TABLE OF TABLES

1 INTRODUCTION

The design of electric overhead travelling cranes and their supporting structures is a contentious issue across the world. The concept of an electric overhead travelling crane holds the interest of mechanical, electrical and structural engineers whether trying to improve the mechanical functioning of the crane, the electrical control systems or predict the forces onto the supporting structure.

In the structural engineering industry the interaction of the crane and its supporting structure is of primary concern. As the crane moves, it induces horizontal and vertical forces that are transferred into the supporting structure through the rails.

Each country has its own relevant design code to discuss which forces must be taken into consideration. Despite this, the failure rate of electric overhead travelling crane supporting structures is unacceptably high, even when designed in strict accordance with the relevant codes. This demonstrates a lack of understanding in the codes of the forces in the crane and the crane's interaction with its supporting structure. This ignorance must be corrected in order to improve the lifespan of these structures.

1.1 Problem Description

In South Africa, and across the world, a large number of electric overhead travelling cranes have a reduced lifespan due to excessive rail and wheel flange wear. Occasionally misalignment of the wheels and rails or an incorrectly designed bracing system can lead to catastrophic failure.

Before a crane supporting structure can be designed, the multitude of forces that act on it must be understood. These forces can be caused by the position and weight of the payload the crane is carrying, the misalignment of the wheels and the rails and the interaction of the bridge and endcarriages with the supporting structure. All of these forces can complement or counteract each other.

The current South African loading code [1] considers many of these effects but does so in a simplistic manner. Empirical factors are applied to the weight of the crane and the payload to provide approximations of the forces that are likely to be induced in different scenarios. This shows little correlation to the actual behaviour of the crane which is inducing these effects. The factors are based on historical experience rather than scientific derivations.

In order to be updated to a more scientific approach, the South African code [1] is in the process of being revised. Many of the concepts in the draft South African code [3] concerning crane design are derived from the Eurocode [2]. For the most part, the Eurocode [2] methods show a more logical approach to determining forces induced by the crane. Nevertheless it does contain dynamic factors that are empirically based.

Before the draft South African code [3] is accepted, it is necessary to ascertain whether the forces, as predicted in the code, are a true reflection of the actual forces induced by the crane onto the crane supporting structure.

1.2 Brief History

There is a research group based at the University of Stellenbosch, South Africa, investigating overhead travelling cranes in a South African context. The research to date has included the establishment of a 5 ton, 8.28 m span, single girder crane on an independent supporting structure within the laboratory, the full calibration of the experimental crane, a series of experimental tests run on the crane to observe the crane's behaviour under all viable load cases and the establishment of a finite element model that reflects the behaviour of the crane accurately. A comparison between the reliability level of the current South African code [1] and the Eurocode [2] has also been completed. An investigation is underway as to best practice in the design of crane supporting structures in South Africa.

An essential part of this research was to calibrate and use the numerical model to model several of the load cases considered in the current South African code [1] and the

Eurocode [2]. This must be completed in order to determine if the dynamic factors and calculations used in the codes are appropriate. These analyses took into account the full dynamic movement of the crane with a swinging payload and considered the interaction of the crane and the crane supporting structure.

1.3 Aim

To use an existing numerical model to determine the wheel loads induced by the crane into the crane supporting structure through hoisting, normal longitudinal travel, skewing and rail misalignment.

To compare the numerically calculated forces with the design forces estimated in the current South African code [1] and the Eurocode [2] in order to determine whether the dynamic factors and calculation methods used in the codes are accurate.

1.4 Method

Four load cases were established in the numerical model. The four scenarios considered were: vertical payload movement, normal longitudinal travel, skewing and misalignment.

The **vertical payload movement** load case is the dominant case when considering the largest vertical force that can be induced into the crane supporting structure by the crane. It takes into account the dynamic vertical oscillations of the crane and the payload during the hoisting and lowering of the payload.

Normal longitudinal travel, according to both the current South African code [1] and the Eurocode, [2] is used to calculate the horizontal longitudinal forces imparted into the structure during acceleration and deceleration of the crane. It also provides insight into the normal behaviour of the crane.

Misalignment, according to the current South African code [1], is one of the dominant load cases for inducing lateral (transverse) horizontal forces into the crane supporting

structure. Rail misalignment was simulated by moving one point on the rail inwards and then outwards to determine the full range of lateral forces that could be obtained.

Skewing is considered by both the current South African code [1] and the Eurocode [2] to be a leading cause of lateral horizontal forces. For the purposes of this thesis, skewing was modelled as occurring as a result of the failure of one motor.

In each load case the numerical model was calibrated to the experimental results and then extended to acquire information difficult to obtain in the laboratory. The analyses were conducted for full range of payload positions and crane movements to ensure that the behaviour of the crane was fully represented.

The results from these analyses were compared to the design forces as described in the current South African code [1] and the Eurocode [2] to determine how accurately the codes represented the calculated crane behaviour. Recommendations were then made with regard to the draft South African code.

1.5 Conclusion

In order to ensure a long life for crane supporting structures it is essential to understand the behaviour of the electric overhead travelling crane it supports. With better understanding the forces induced into the crane supporting structure can be predicted and allowed for in the design codes.

The current South African code [1] is overly simplistic. To this end the draft South African loading code [3] has adopted most of the Eurocode's [2] crane design principles. The Eurocode [2] demonstrates a better representation of what occurs during the crane's movement than the current South African code [1]. Despite this many of the dynamic factors used in the code are empirical rather than scientifically based.

The purpose of this thesis is to extend the work done by the research group at the University of Stellenbosch by adapting the existing numerical crane model to study the

load cases of hoisting, normal longitudinal motion, misalignment and skewing. The results from these simulations are then used to confirm that the dynamic factors in the draft South African code [3] accurately represent the forces experienced at the crane wheels.

2 LITERATURE REVIEW

The failure of electric overhead travelling cranes and crane supporting structures designed in full accordance with the relevant design codes occurs on a frequent basis. This is deplorable and demonstrates a lack of understanding of general crane behaviour in the design codes.

During crane operation lateral, longitudinal and vertical loads are transferred from the crane into the crane supporting structure at the crane wheels. These dynamic forces are frequently higher than allowed for from static considerations. Under lateral forces the wheels move and interaction between the wheel flanges and the rail occurs. Excessive contact leads to accelerated wear of the rail and the wheel flanges, which in turn leads to uneven wear patterns and a reduced lifespan of both the crane and the supporting structure.

These dynamic forces in the crane can be caused in a variety of ways during normal and exceptional travel: hoisting of the payload; acceleration and deceleration of the crab and crane; misalignment of the rails or crane wheels; skewing of the crane; impact with the end buffers, steps and gaps in the rails and rough tracks.

2.1 History

Many studies have been conducted on modelling dynamic crane behaviour. Complex mathematical models have been put forward for calculating the different modes of oscillation of the crane [6] and using bond graph methods [7] to predict how the crane will behave and what loads will result. These models often assume that when the crane is in steady state motion the oscillations of the payload will have ceased, [8] and the forces at the wheels are constant. Other scenarios can then be superimposed over this to determine how the wheel forces change.

The mathematical models developed during the 1970s and 1980s to represent crane behaviour neglected the influence of the continuously swinging payload on the wheel

forces. The vertical oscillations induced by the moving payload during hoisting and lowering were studied but not the influence of the payload during longitudinal crane movement, whether normal motion or exceptional. The concept and mathematics of a swinging pendulum were well documented but not the interaction of the payload with the moving crane.

In 2000 research was completed by D.C.D. Oguamanam et al [9] on the pendulum motion of a payload during operation of the crane. Here the influences of the length of the pendulum cable, the mass of the pendulum and the acceleration and deceleration of the crane on the movement of the payload was studied in detail. The objective was to define a mathematical model representing the movement of the payload in order to develop an automatic controller to modify the swinging of the payload to allow for faster crane processing of goods. The influence of the payload motion on the forces at the crane wheels was not investigated.

Research into the computer modelling of cranes was done by Frank Taylor et al [10]. Here the behaviour of a real crane was compared to the behaviour of the virtual crane to determine the viability of using computers to model the real-life operation of heavy machinery. This study considered the overall behaviour of the crane rather than the forces induced in the crane supporting structure during crane motion. The swinging effect of the payload was taken into account in the model by representing the payload as a simple pendulum with one degree of freedom at the connection to the crane bridge. This ignores the payloads ability to swing laterally as well as longitudinally during crane movement.

In practice, electric overhead travelling cranes interact constantly with their supporting structures, at times inducing movement in the supporting structures and at others being forced to react to changes in the structures e.g.: rail misalignment. During the crane movement the payload is free to swing in any direction. Movement of the crane accentuates the movement of the payload, whether lateral or longitudinal, which in turn affects the forces induced at the crane wheels. It is important that the interaction of the crane and the crane supporting structure and the influence of the moving payload on the

crane wheel forces are taken into account in the relevant design codes when defining the loads for the design of the crane supporting structure.

2.2 South African Loading Code (SABS 0160-1989)

In the current South African loading code [1] cranes are categorised into four classes according to their safe lifting capacity and their frequency of operation. The class of crane is used to define the factors which are used for quantifying the dynamic effects of the moving crane into wheel loads.

2.2.1 Vertical Wheel Loads

The design vertical wheel load is taken as the maximum static vertical wheel load caused by an eccentric crab and supplied by the manufacturer, multiplied by the relevant dynamic factor. This dynamic factor depends on the class of crane and is included to account for the oscillation of the vertical wheel loads during hoisting and lowering of the payload. This method of calculating vertical wheel forces treats the dynamic movement of the payload and the crane together as the factor is applied to the combined weight of both.

2.2.2 Horizontal Lateral Forces

The design horizontal lateral forces induced by the crane, acting horizontally on top of the crane rail, are taken from the most adverse of the horizontal forces estimated to be induced by acceleration and braking of the crab, misalignment and skewing of the crane.

Acceleration and Braking of the Crab

The lateral force due to the acceleration and braking of the crab is assumed to be equal to the weight of the crab and the payload combined multiplied by a relevant factor as determined by the class of crane. This force is divided between the wheels of the crane with reference to the transverse stiffness of the rail supports at each wheel.

Misalignment

The lateral force due to misalignment is allowed for by a force P_1 applied either all inwards or outwards at all wheels simultaneously. This force is the horizontal equivalent of the total mass of the crane, including crab and payload, multiplied by a factor dependent on the class of crane and divided by the number of wheels.

Skewing

The lateral force due to skewing of a crane depends on the method of guidance employed at the crane wheels. Two of the most common types of wheel guidance are wheel flanges and rollers.

Where the crane is guided by wheel flanges, the horizontal forces (P_2) predicted at the wheels are equal to the force P_1 calculated from misalignment loads, multiplied by a factor of 1.5. This factor is irrespective of the class of crane but, as seen above, the value of P_1 is influenced by the class of crane. This force is applied at each wheel in directions that would induced either a positive or negative couple about the vertical axis on the crane body, depending on which causes the most severe effect.

Where the crane is guided by rollers located at one end of the bridge, a force P_3 is applied at each pair of rollers to induce either a negative or positive couple depending on which is the most severe case. This couple is calculated as 1.3 times the magnitude of the couple induced by the P_2 forces for a crane guided by wheel flanges.

2.2.3 Horizontal Longitudinal Forces

The horizontal longitudinal force induced into each crane rail is assumed to be a result of the acceleration and deceleration of the crane during normal longitudinal motion. The force in each rail is taken as 0.10 times the vertical load experienced by the crane rail.

2.2.4 South African Code Summary

All of these design forces work off a factor which is selected according to the class of the crane and multiplied by all or part of the dead weight of the crane and payload. These

factors have been empirically determined by past experience and lack scientific backing correlating the causes to the resultant forces. This code is easy to work to but simplistic, showing little understanding of the nature of the forces involved.

2.3 Eurocode (EN 1991-3)

In the Eurocode cranes are divided into four hoisting classes according to their use. A typical list of cranes and their classes is given in Annexure B of the Eurocode [2]. The majority of dynamic factors applied to the characteristic load values in order to obtain the design values for the forces do not depend on this classification, unlike in the South African code. An exception to the rule is the case of the vertical wheel loads.

2.3.1 Vertical Wheel Loads

The design vertical wheel load consists of two parts: the dead weight of the crane multiplied by its partial factor to account for dynamic effects of the crane vibration and the dead weight of the payload multiplied by its factor to account for the oscillation of the payload. This method of partial factors leads to a consistent reliability level as stated by Dymond et al. [11]

The dynamic factor applied to the dead weight of the crane remains constant for all crane classes but the factor applied to the payload is determined by the class of crane and the hoisting speed of the crane.

2.3.2 Horizontal Lateral Forces

Horizontal lateral forces are considered to be caused by either the normal longitudinal travel of the crane, the acceleration and deceleration of the crab, or the skewing of the crane. The most critical case is taken as the design horizontal lateral force.

Normal Longitudinal Travel

When the crane travels along its rails with an eccentric crab and non-synchronised motors, a moment is induced in the crane. This is counteracted by lateral wheel forces

which keep the crane running straight along the rails. These forces are calculated as the product of a dynamic factor, the ratio of maximum wheel load on a rail to the total wheel load and the moment induced by the drive force, divided by the spacing of the flanged wheels.

Acceleration and Deceleration of the Crab

The horizontal lateral forces caused by the acceleration and deceleration of the crab are considered to be at their worst when the crab impacts on its end stops. On condition the payload is allowed to swing, the horizontal force is taken as 0.1 times the sum of the weight of the payload and the weight of the crab. This correlates with the factor of 0.1 for a class 2 crane which the SABS code uses to determine lateral forces as a result of acceleration and deceleration of the crab.

Skewing

The skewing forces in the Eurocode are calculated for the concept of a crane rotating around an instantaneous centre of rotation. The force at each wheel is a function of the distance in the longitudinal and lateral directions from the wheel to this centre of rotation. Other factors which are taken into account in the equation include the maximum angle of skewing that can occur for each wheel-rail combination, considering wear of the wheel and flanges and the tolerances of the rail, and the number of pairs of wheels.

This is a more accurate representation of how skewing forces can occur when the crab is eccentrically placed than is found in the current South African Code [1]. The Eurocode does neglect the situations where skewing is induced by picking up the payload obliquely to the bridge or where the crane is run after one motor fails and is bypassed. These cases are considered bad practice; however, they occur frequently in actual situations.

2.3.3 Horizontal Longitudinal Forces

The horizontal longitudinal forces induced into the rails by the crane wheels are a result of the drive force experienced at the contact surface of the rails and the wheels. The design horizontal longitudinal force is calculated by multiplying the drive force by a

dynamic factor and dividing by the number of rails. The drive force is normally supplied by the manufacturer but can be calculated as the product of the coefficient of friction and the minimum dead load of the crane. It represents the force that can be applied onto the wheels with a minimum vertical load before the wheels start to slip.

This method of calculating the horizontal longitudinal forces takes into account the interaction of the driving wheels with the rails and should reflect the actual forces experienced in the rails.

2.3.4 Eurocode Summary

The Eurocode [2] calculates each of the relevant crane forces by determining the cause of the forces and how large these forces could become in an experimental situation. Dynamic factors are then applied to account for the unknown oscillation effects due to movement of the crane and payload. Although Prof. Gerhard Sedlacek does provide some insight to the Eurocode factors [12], for the most part these factors are empirical rather than based on scientific theory.

According to Warren et al [11] the level of reliability (β value) of a crane girder under the South African code [1] ranges from 5.4 for a class two crane to 5.7 for a class four crane. This is highly conservative. The Eurocode [2] achieves a more consistent reliability of 3.2 for all crane classes. The variation in level of reliability of the South African code is primarily due to the class dependent dynamic factors used in the South African code [1]. The only class dependent dynamic factor used in the Eurocode [2] is the factor modelling the dynamic effects of hoisting the payload on the crane structure. A more consistent reliability level was obtained in the Eurocode by separating the factors applied to the dead weight of the crane and payload into partial factors applied to each weight independently.

2.4 Draft South African Code

The draft South African code [3] moves away from the simplifications in the current South African code. For the most part it follows the processes laid out in the Eurocode [2], with partial load factors for the vertical loading and less reliance on the class of crane. The case of misalignment, which is not considered in the Eurocode [2], is included straight from the current South African code [1].

2.5 Conclusion

Historically there have been many mathematical models established to determine the loads induced by electric overhead travelling cranes on their supporting structure. These include dynamic effects such as vibrations in the crane bridge but seldom take the full influence of a swinging payload into account. When computer models have been designed to replicate the behaviour of these cranes and the motion of the payload has been included, the payload is only been free to swing in the longitudinal direction. This does not take into account the full three dimensional influence of the payload on the forces induced at the wheels.

In order to determine why there is a high frequency of failure in cranes, it is essential to study the forces at the wheels and the crane's interaction with its supporting structure. The design values in the codes need to take account of all the possible loads that can occur during normal and accidental crane travel. Although for the most this is the case, the dynamic factors used in each load case are empirical with little scientific support. In the case of the current South African code [1], the many different loads that can be induced at the wheels are considered but the models are simplistic, working simply on a factor multiplied by some or all of the dead weight of the payload and the crane. This means the loads are not calculated in relation to the factors that are causing them. In the Eurocode [2] this is handled in a more reliable manner with the wheel loads showing some correlation with the crane dynamics that created them. As a result, the draft South African code [3] adopts most of the calculations presented in the Eurocode [2] over those in the current South African code [1].

Further research is required to ensure that the dynamic factors used in the draft South African code are representative of the actual factors involved in the dynamic movement of the crane for all forces induced at the crane wheels. This must include the interaction of the crane with the crane supporting structure and the motion of the payload. The most convenient method of analysing this is using the computational power of a finite element analysis program to model the crane on its supporting structure. The various load cases considered in the code can then be run on the model to determine whether the code's dynamic factors provide an accurate representation of the forces involved.

3 DESCRIPTION OF EXPERIMENTAL AND NUMERICAL MODELS

An experimental setup of an electric overhead travelling crane was established in 2001 in the Structures Laboratory at the University of Stellenbosch by Hein Barnard. A number of experiments were completed on the system by Johan de Lange as part of his master's degree [5] from 2004 to 2006. During this time Trevor Haas developed a numerical model of the crane in Abaqus for his doctorate degree [4] which simulated the experimental behaviour of the crane and supporting structure on a computer. He then investigated the case of end buffer impact in the numerical model and compared it with impact results obtained in the laboratory by Johan de Lange.

Both the experimental results obtained by Johan de Lange and the finite element model created by Trevor Haas are used in my thesis and as such it is necessary to understand how the results were obtained and what the model entailed.

3.1 Experimental Setup

The crane is a 5 ton, single girder crane that runs along a supporting structure created within the laboratory. The supporting structure is designed to simulate a standard workshop layout.

3.1.1 Crane Supporting Structure

The structure is orientated such that the crane runs North-South. The southern end includes a bracing system that absorbs the loads generated by the acceleration and deceleration of the crane and impacts on the end stops (Figure 3-1).

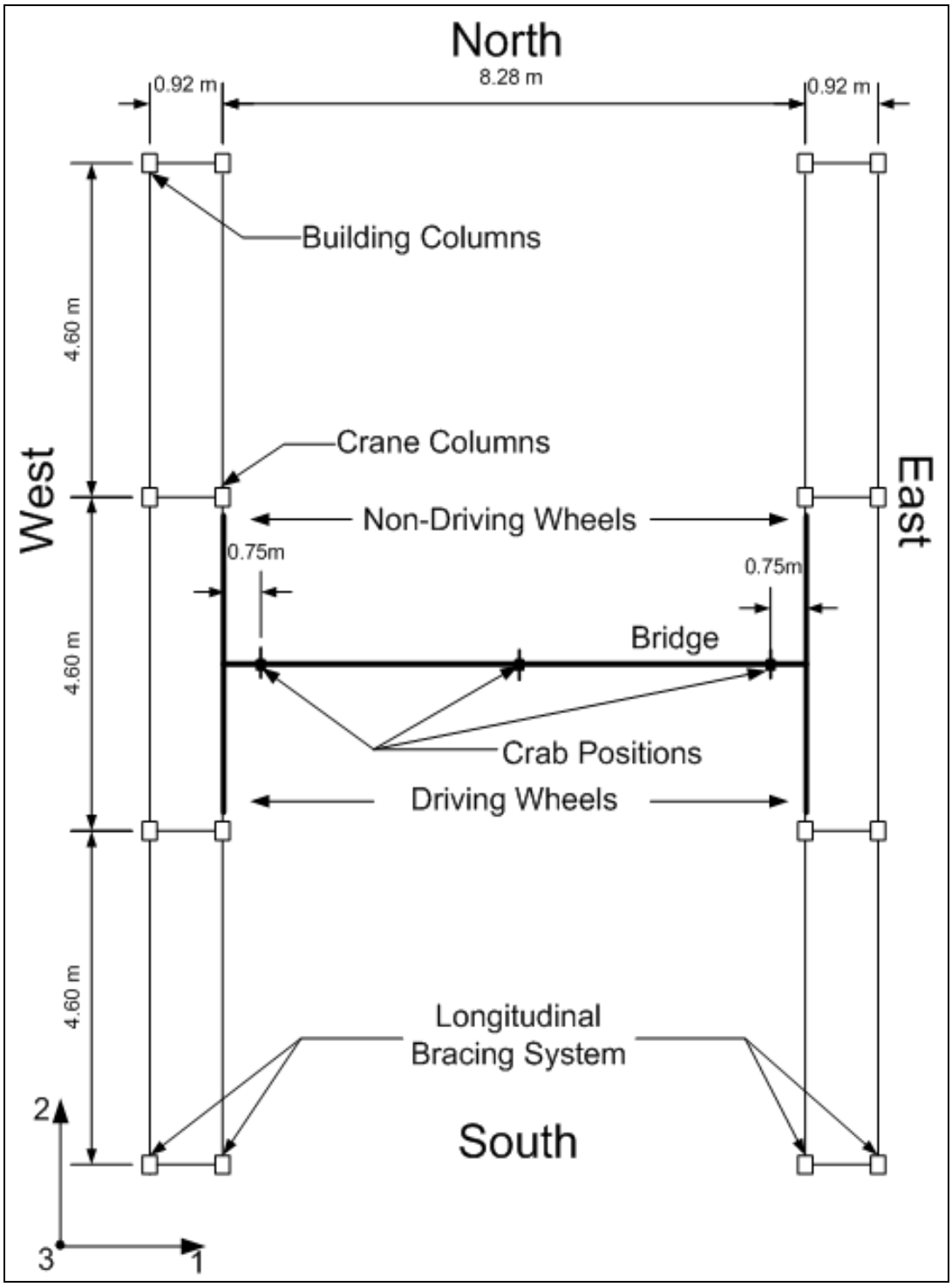

Figure 3-1: Layout of the crane supporting structure and crane in the Stellenbosch Laboratory

The crane supporting structure consists of eight crane columns (152x152x23 H sections) which directly support the crane girders. These are tied back to building columns (457x191x67 I sections) at the top and bottom of the crane column as would occur in a typical warehouse situation (Figure 3-2).

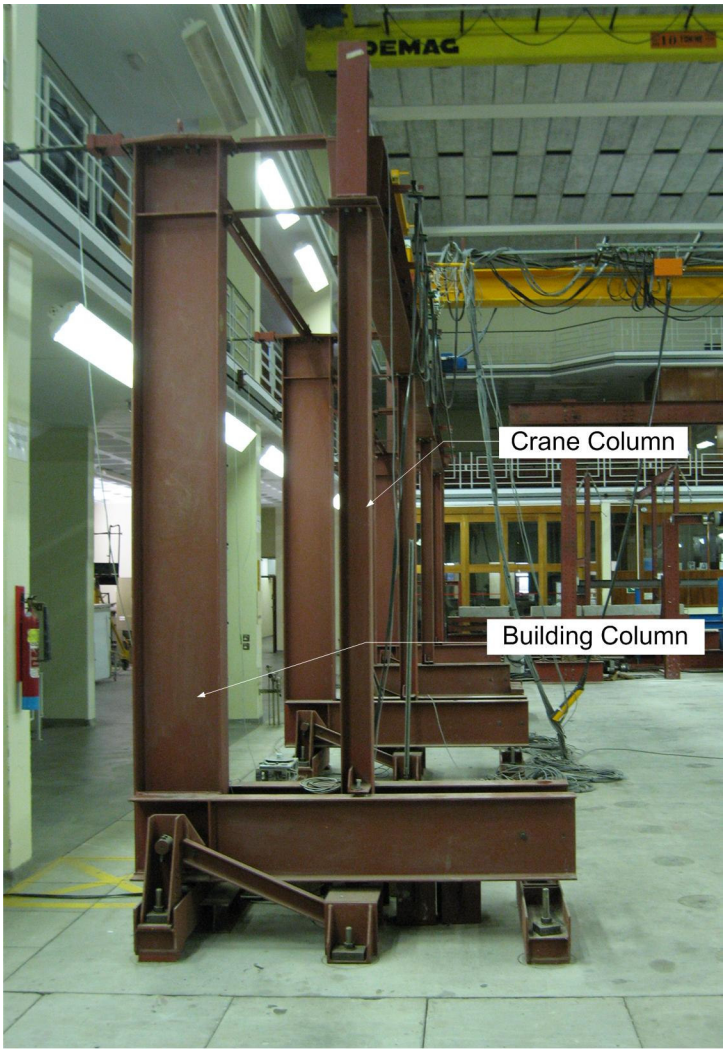

Figure 3-2: Crane column and building column connected top and bottom

The crane girders are simply supported monosymmetric plate girders that are single spanning between the crane columns. They support the crane rail which is fixed in place by rail clips at 0.4 m centre to centre and separated from the girder by a 7 mm continuous elastomeric Gantrax pad. The top flange of the crane girder is laterally braced at each of the column positions. The crane rail is a 30 $kg.m^{-1}$ rail with a 57.2 mm rail width, which

is larger than would normally be specified for a 5 ton crane. This is due to limited resources at the time of establishment. The distance between the crane wheel flanges and the rail when the wheel is perfectly aligned is only 2.4 mm on each side.

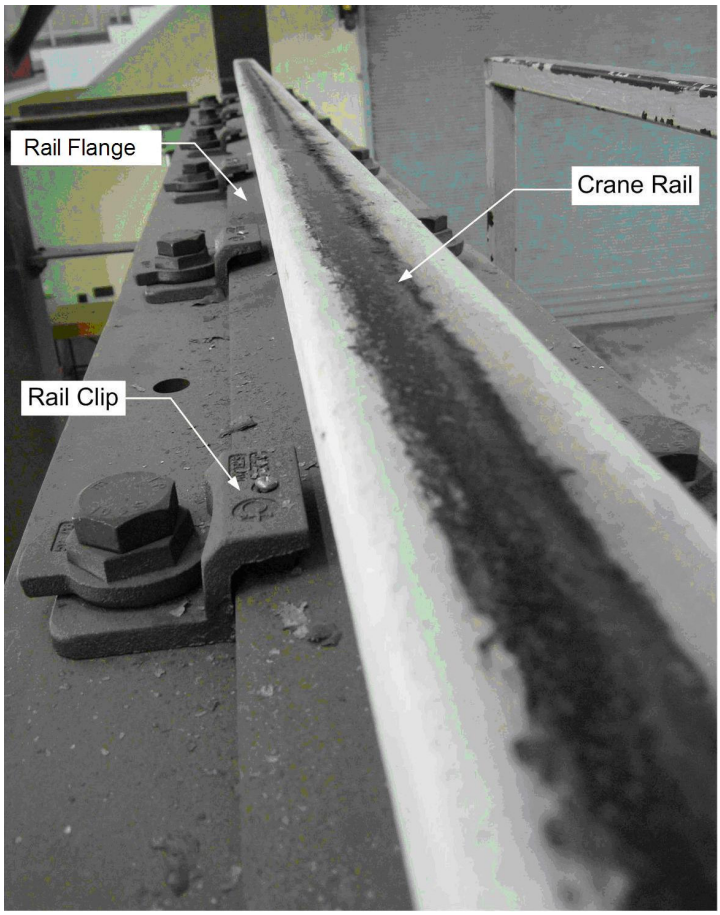

Figure 3-3: Crane Rail on Gantrax pad fixed to crane girder

3.1.2 Crane

The crane is a 5 ton, 8.28 m span, single girder crane. The bridge is a 305x305x118 H-section bolted on top of 203x203x60 H-section endcarriages. The distance between the wheels under the endcarriages can be adjusted but for these tests was kept at 4.26 m. The driven wheels are at the southern end of the crane.

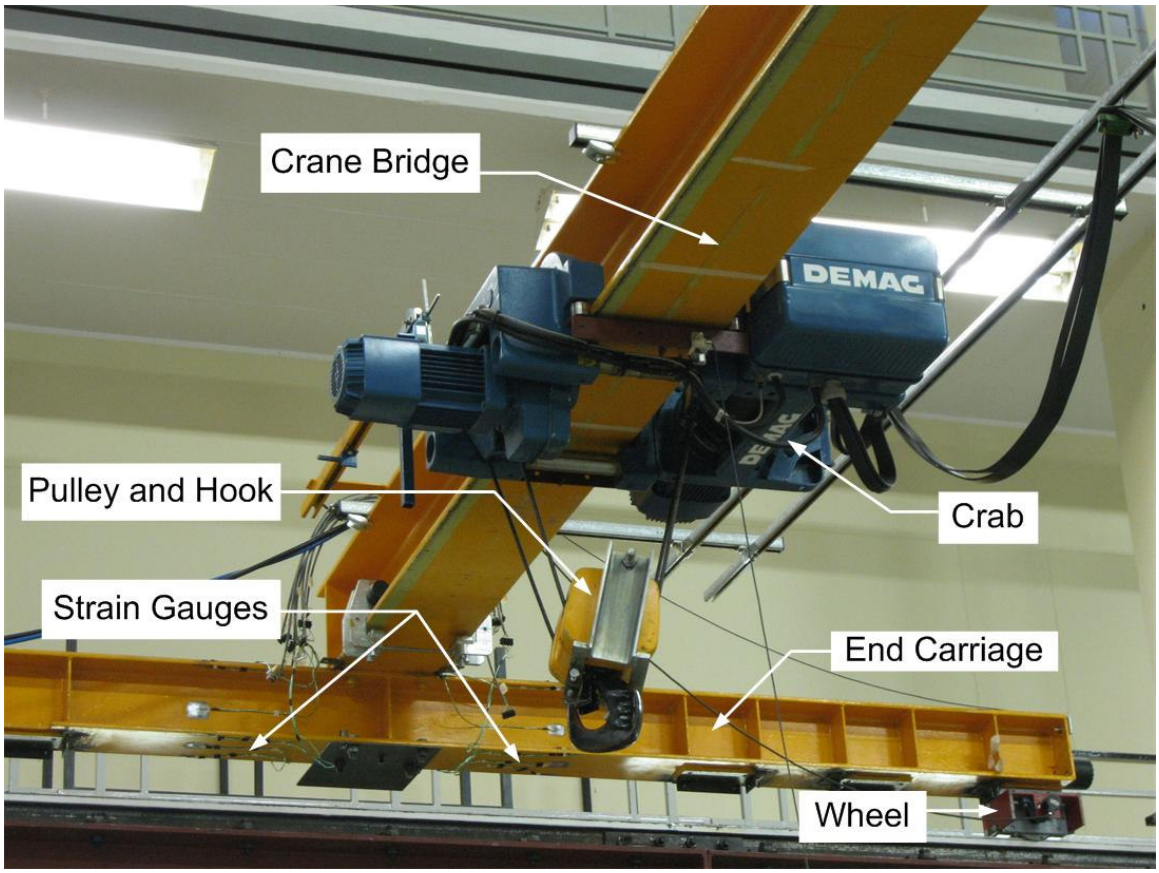

Figure 3-4: Crane Body with crab and measuring instruments

The control box containing the control systems for the crane is positioned at the centre of the crane bridge to minimize load eccentricities. The hoisting system consists of two 9.25 mm diameter twisted strand cables. These loop from a fixed point on the crab, through the pulley at the hook and then back to a winder drum. The fixed point is 0.5 m away from the winder drum, ensuring a constant distance is maintained between the ends of the cables irrespective of the height of the payload.

Figure 3-5: 5 ton lead and concrete payload

The payload was constructed to give a lifting weight of 5 tons in a compact form. It is approximately 1 m^3 and consists of concrete and lead weights. The payload can be hoisted with the crab in any position along the crane bridge up to 0.75 m away from each end carriage. This limit is established by the crane manufacturer and is due to the size of the crab.

3.1.3 Measurement Systems

Strain gauges, encoders and load cells were placed in key positions on the crane in order to record results from the experimental experiments.

48 strain gauges were placed on the crane to calculate 24 stress results. From these gauges it was possible to calculate the vertical and horizontal forces experienced at each wheel and deflections at key points.

An encoder was fixed to each of the crane's non-driving wheels to measure velocity. Although the driving wheels would have been a more appropriate place to gather information there were space limitations due to the positioning of the motors. For the most part the northern, non-driving wheels have an identical velocity to the southern, driving wheels on condition no slip occurs and thus the information gathered by the encoders is still relevant.

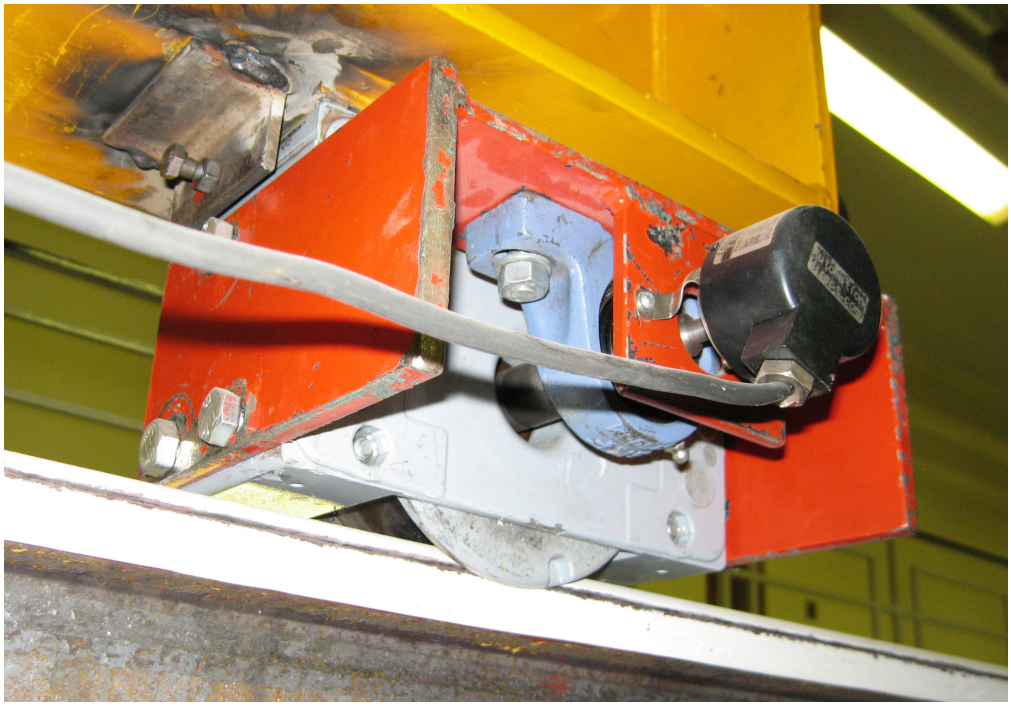

Figure 3-6: Encoder on Northern wheels

For the purposes of the vertical payload movement load case it was essential to quantify the force being exerted on the system by the payload. To this end a load cell was

positioned under the hook on the payload. This gives the exact force that is being transferred by the payload through the hook and cables into the crane.

Each crane column was constructed so that a load cell could be incorporated without affecting the integrity of the structure. This is to determine the vertical loads experienced by the columns.

3.2 Numerical Model

The finite element crane model was created in Abaqus by Trevor Haas for his doctorate degree[4]. Unless otherwise stated, all beams and columns were modelled using beam elements, typically the B31 Abaqus element, a 2-node, 6 degree of freedom per node, Timoshenko beam element. The results obtained from a 3-node Timoshenko beam element had a difference of less than 0.5 % from that of the 2-node elements. To minimise computational time it was considered sufficient to use the 2-node elements.

3.2.1 Crane Supporting Structure

The longitudinal bracing system at the southern end of the structure was modelled using boundary conditions rather than modelling the elements themselves. The work was more concerned with the forces travelling into the bracing system than the actual behaviour of the bracing members under those loads.

The crane rail and girder were combined into one section to minimise computational time. This section was given the combined physical properties of both elements but the Gantrax pad was excluded due to its minimal effect on the section properties. The shape of the rail was modelled as a flat surface with perpendicular flanges that matched the dimensions of the physical rail. The thickness of the surface was reduced to 0 mm so that the rail had no physical influence on the model other than a surface for the crane wheel to interact with. The position of the rail was then linked to the neutral axis of the crane rail and girder combination using connectors (Figure 3-7).

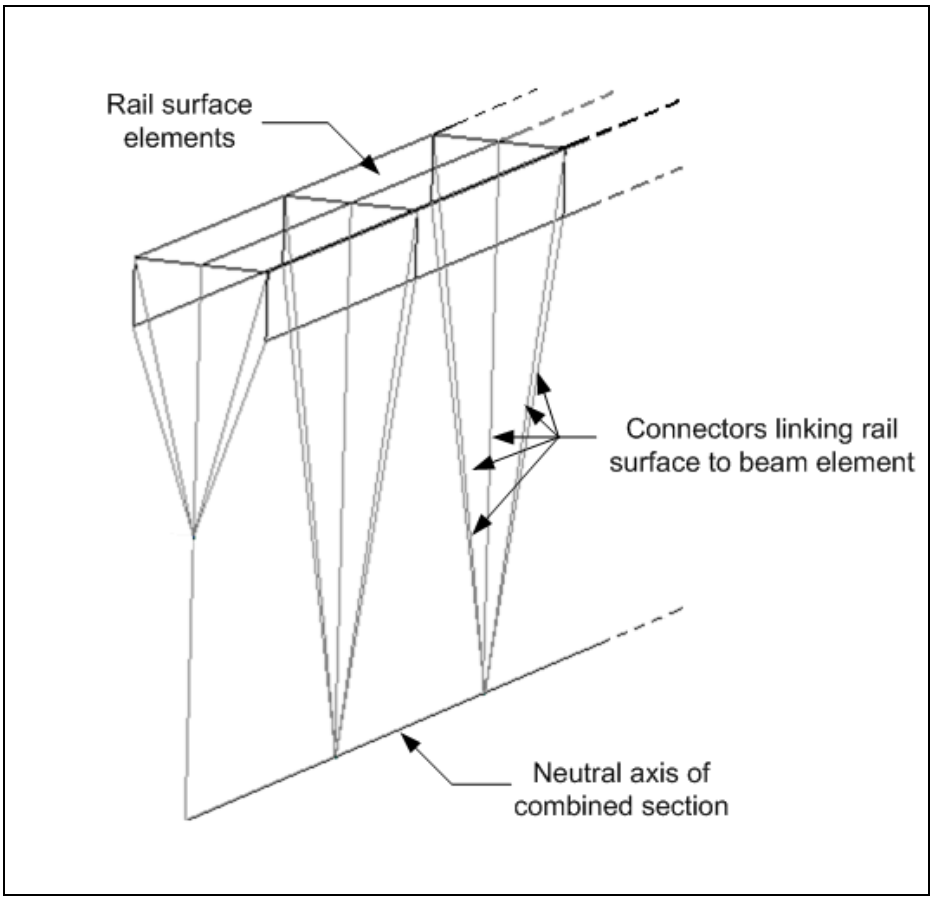

Figure 3-7: Finite element representation of a crane rail

3.2.2 Crane

The crane bridge and endcarriages were both modelled with beam elements; the bridge with the same B31 elements mentioned previously and the endcarriages with B310S elements (2 node, 7 degree of freedom per node, Timoshenko beam elements). The B310S elements are suitable for open, thin-walled sections subjected to torsion. As these contain an extra degree of freedom representing warping, it was possible to restrain warping at certain points and model the end carriages more accurately. The end carriages are relatively flexible members which are continuously subjected to torsion under the flexing of the crane bridge. These elements take this into account. A version of the crane bridge was modelled with B310S elements to determine whether torsional flexing had an effect on the bridge. No material differences were noted in the results so the crane bridge was reverted to B31 elements.

The cables were modelled with T3D2 elements (2 node, 3 degrees of freedom per node, truss elements) and joined using connectors to the crane bridge. These connectors spaced the tops of the cables away from the bridge to model the experimental situation (Figure 3-8).

The pulley at the base of the cables was a solid element that could rotate or slide along the cables as required. It was linked by a chain of two connectors representing the crane hook and the connection to the centre of gravity of the payload. These connectors allowed for the rotation that could occur at these points. The payload, crab and control box were modelled as point loads with set moments of inertia located at their centres of gravity. The payload could therefore swing and rotate as it would in the physical experiments and would still be computationally efficient, being modelled by a point rather than a solid.

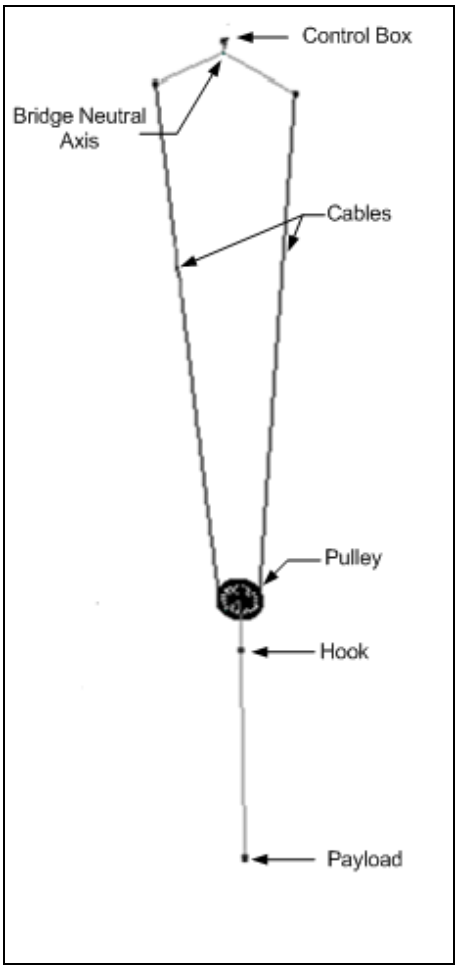

Figure 3-8: Numerical model representation of the cable, pulley and payload system

The crane wheels in the numerical model were modelled substantially differently compared to the experimental setup. Round wheels caused problems with contact interaction and the element size of the crane beams would have needed to be drastically reduced before accurate results could have been obtained. To avoid this problem, the wheels were modelled as flat surfaces 200 mm long. This length was chosen to ensure a smooth interaction between the rails and the wheels while permitting the rail mesh size to remain large enough to be computationally efficient. The positions of the wheel flanges in the numerical model were modelled to correlate with the experimental wheel flanges but the finite element flanges run the full length of the wheel and hence are substantially longer than the existing experimental flanges. Using this method with the coefficients of friction in both horizontal directions adjusted appropriately, the surface represented the

physical behaviour of the wheel without the numerical errors that occurred with the round wheel. Further explanation of the wheel system can be found in Trevor Haas' work [4].

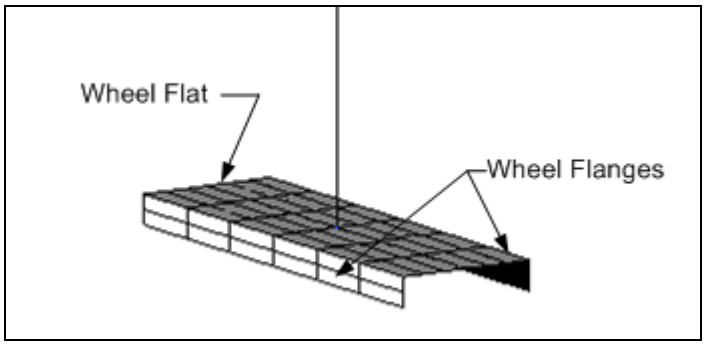

Figure 3-9: Finite element representation of a wheel

3.2.3 Measurement Systems

The numerical model allows information to be gathered at any point on the crane or crane supporting structure. To keep the information at a manageable level, this output was restricted to the following key points:

- deflection in all directions at the wheels, payload, midspan of the endcarriages and midspan of the bridge;
- forces in all directions at the wheels, payload, columns and bracing systems;
- velocity at the wheels.

This data was selected to correlate the numerical model with the physical data obtained by Johan de Lange as well as to calculate forces and deflections in areas difficult to measure in the experiments, such as longitudinal force transmitted into the rails.

3.3 Conclusion

This thesis builds on the work already completed by others at the University of Stellenbosch, primarily Trevor Haas and Johan de Lange. During their doctorate and master's research respectively, they established an accurate numerical model in Abaqus

to represent the crane and completed all the experiments with which to calibrate this model.

The above describes the work done primarily by these two students so that a better understanding of how the crane system works, both in the laboratory and in the numerical model, can be acquired. Further information can be obtained by referring to their theses – Reference 4 and Reference 5 in the Bibliography.

4 VERTICAL PAYLOAD MOVEMENT

The Vertical Payload Movement load case refers to the hoisting and lowering of the payload. This occurs at the beginning and end of every cycle of crane loading and is essential for determining the maximum vertical wheel load that can be exerted by the crane on the crane supporting structure.

During hoisting and lowering the oscillations of the payload introduce dynamic vibrations into the crane. These vibrations amplify the static loads on the structure. The design vertical wheel load for the crane supporting structure in the relevant code is determined using dynamic factors to represent this amplification.

4.1 Codification

In the current South African Loading Code [1] the dynamic effect of the vertical movement of the payload is taken into account in paragraph 5.7.3, "Make allowance for impact and other dynamic effects in the vertical direction by multiplying the static wheel load by the appropriate of the following factors:". The appropriate factor for a class 2 crane, such as the 5-ton crane in the Stellenbosch University laboratory, is $\varphi = 1.2$.

The Eurocode[2] gives a more detailed breakdown of the factors to be applied to the vertical static wheel loads to account for the dynamic amplification effect of hoisting and lowering of the payload. The dynamic effects are broken up into the effect caused by the excitation of the crane structure under the moving payload (φ_1) and the effect caused by the movement of the payload itself in lifting off the ground or stopping suddenly (φ_2).

Under this method the dynamic factor φ_1 is applied to the self weight of the crane (Q_c) while φ_2 is applied to the payload (Q_h). The maximum vertical load experienced by the crane supporting structure is then $F_V = Q_c\varphi_1 + Q_h\varphi_2$ which is then distributed through the wheels according to the position of the crab.

For the 5 ton crane used in the Stellenbosch laboratory the relevant factors according to the Eurocode [2] are:

$0.9 < \boldsymbol{\varphi_1} < 1.1$ (Table 2.4 [2])

where the two values reflect the upper and lower limits of the oscillations

$\boldsymbol{\varphi_2} = \varphi_{2,\,min} + \beta_2 v_h$ (Table 2.4 [2])

where: v_h =0.075 $m.s^{-1}$ is the steady hoisting speed of the Stellenbosch crane

$\varphi_{2,\,min}$ = 1.10 (Table 2.5, HC2 [2])

β_2 = 0.34 (Table 2.5, HC2 [2])

The draft South African Loading Code [3] closely resembles the current Eurocode [2] where provisions and allowances are made for the same two dynamic factors during hoisting. Both factors are calculated using the same values and equations given in the Eurocode [2] for an equivalent class 2 crane.

4.2 Experimental Setup

The vertical movement of the payload was considered as a load case during the experiments completed by Johan de Lange [5]. Four cases were investigated:

- The lifting of the payload off the ground to a height of 1.2 m;
- The hoisting of the already hanging payload from 1.2 m to the cut-off point at 2.2 m;
- The lowering of the payload from 2.2 m to 1.2 m
- The lowering of the payload from 1.2 m to the ground.

These experiments were completed for a centralised crab and then repeated for an eccentric crab. (Figure 4-1)

Vertical Payload Movement

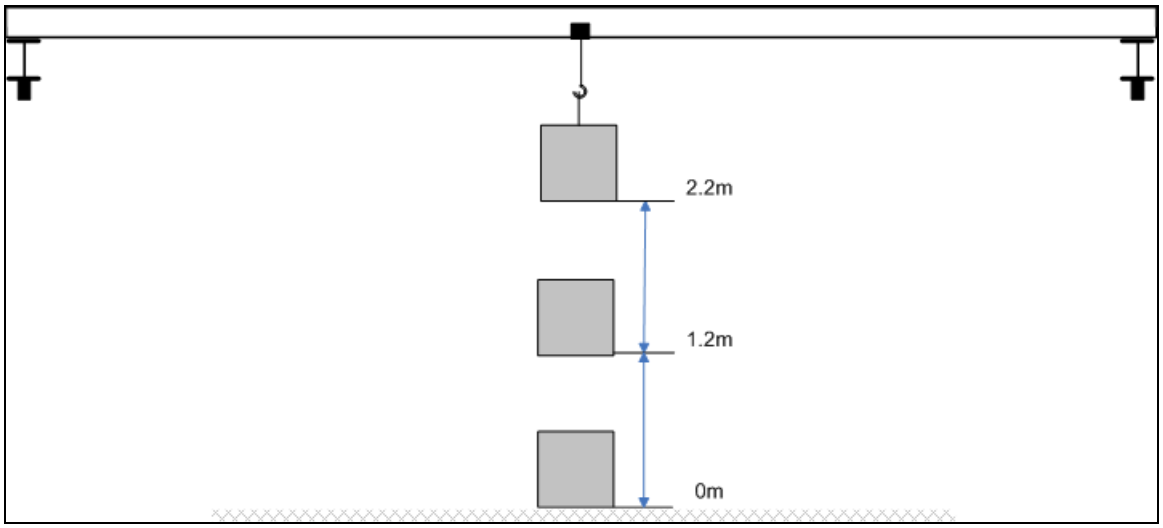

Figure 4-1: Positions of the payload during hoisting and lowering with a centralized crab

When lifting the payload off the ground the crane operates at a creep speed of 0.02 $m.s^{-1}$. Once the full weight of the payload is taken by the cable this speed increases to 0.075 $m.s^{-1}$. When the payload is hoisted to 2.2 m above the ground the height limit is reached and an emergency cut-out occurs. This is a sudden, full stop as opposed to the gradual slowing down that occurs during a normal stop.

As detailed in Section 3.1.3, a load cell was placed on the payload under the hook to allow for measurement of the vertical force at the payload. The values obtained from this load cell reflect the dynamic behaviour of the payload itself during hoisting and correlate to the φ_2 factor, multiplied by the self weight of the payload, mentioned in Eurocodes [2].

4.3 Finite Element Model

The vertical payload movement load cases were simulated in the numerical model using the base model of the crane developed by Trevor Haas during his PhD research [4].

Due to the difficulty in modelling the shortening of the cables under the hoisting process another approach was found to simulate the movement. The experiments yield a graph of the force exerted by the payload on the crane while it is being hoisted and lowered. Figure 4-2 shows an example of the variable force as it is measured by the load cell on

the payload. Here time = 13.8 seconds is the moment when the payload reaches 2.2m above ground and the hoisting motor is cut off.

By inputting this variable force as a function of time into the numerical model the difficulties regarding the dynamic contribution of the shortening cables and the payload are avoided. This makes it difficult for the numerical model, as it is currently set up, to confirm the payload dynamic factor (φ_2) but the results will show the total amplification of the vertical wheel loads. From this it is possible to calculate the dynamic factor due to the vibration of the crane alone (φ_1). This is then compared to the measured results and the codes.

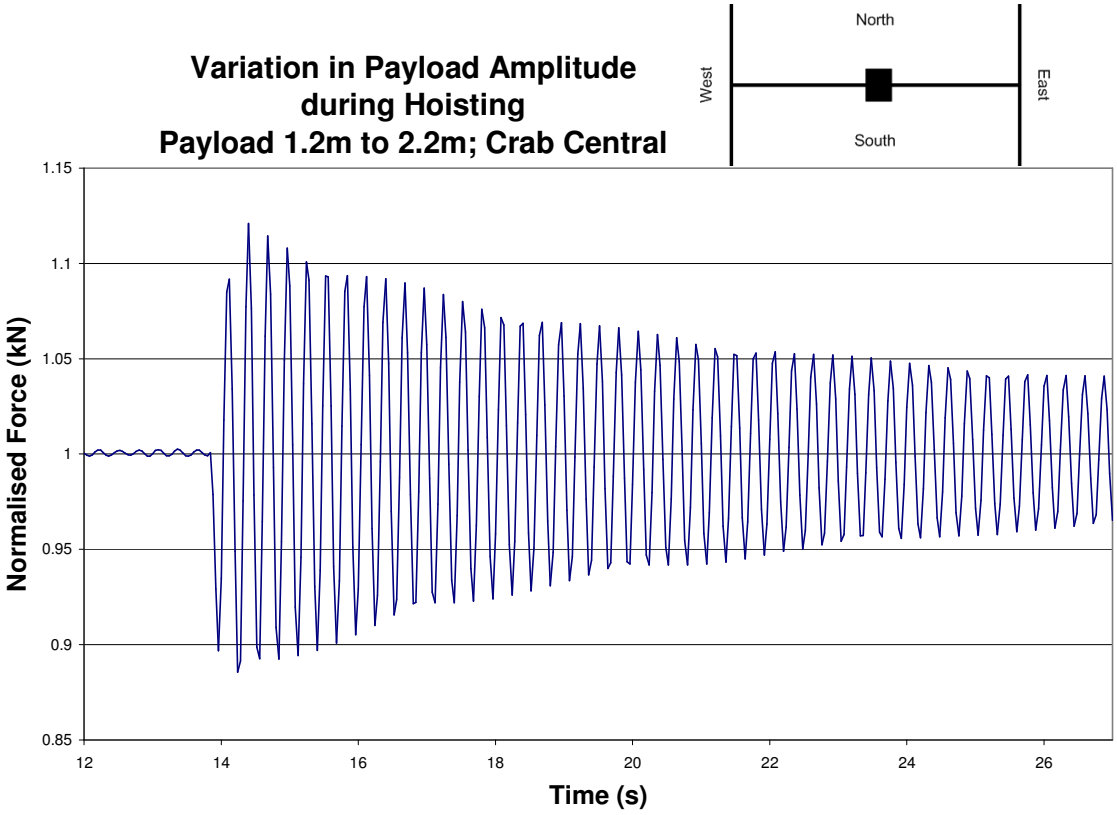

Figure 4-2: Normalized payload amplitude experienced during hoisting from 1.2m to 2.2m

The four hoisting and lowering scenarios were completed for a centralised and eccentric crab and the results checked against the experimental findings.

Vertical Payload Movement

4.4 Verification

The numerical model was initially verified against the static experimental results obtained from the laboratory experiments. Horizontal and vertical forces at the wheels and deflection at midspan of the crane bridge (Figure 4-3) as a result of the central payload were compared between the numerical model and the experimental results (Table 4-1).

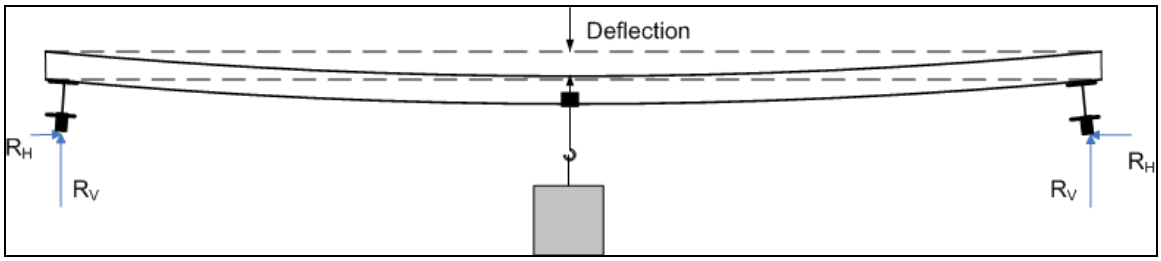

Figure 4-3: Midspan deflection and horizontal and vertical forces for a statically loaded crane

	Vertical Force (kN)	**Horizontal Force (kN)**	**Deflections (mm)**
Experimental	12.52	0.67	12.64
Numerical	12.45	0.63	13.69

Table 4-1: Correlation of experimental and numerical results for a statically loaded crane

These values exclude the contribution of the dead weight of the crane due to the difficulties of measuring absolute values in the experimental experiments.

Good correlation is found in both the vertical and horizontal wheel forces; however a slight error exists in the deflection measurement. While this error is most probably from the lack of torsional rigidity in the end carriages of the crane in the numerical model and can be corrected by stiffening the end carriages, it was found that the crane behaviour was more consistent with experimental measurements as a whole if this additional stiffening was neglected.

The four vertical payload movement cases discussed in 4.2 above, were run in the numerical model for both the central and eccentric crab positions.

Vertical Payload Movement

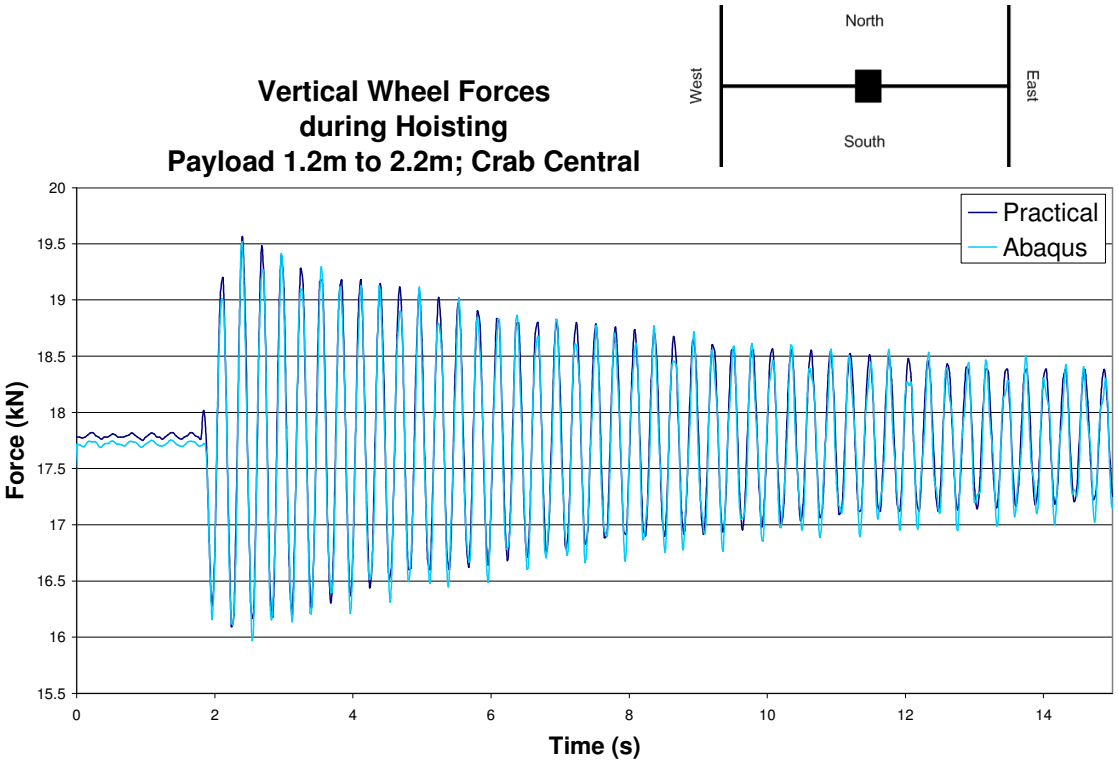

Figure 4-4: Correlation between experimental and numerical results for a payload hoisted from 1.2m to 2.2m

Figure 4-4 shows the correlation between the physical experiments and the numerical results for the hoisting of the payload from 1.2 m to 2.2 m with the crab centrally positioned. Time = 13.8 seconds is the moment when the payload reaches 2.2 m above ground and the hoisting motor is cut off.

When the peak vertical wheel load in each case is divided by the average wheel load, for both the experimental and the numerical results, the following results are obtained:

	Hoisting		Lowering	
	0m → 1.2m	**1.2m → 2.2m**	**2.2m → 1.2m**	**1.2m → 0m**
Central Crab				
Experimental	1.06	1.10	1.09	1.08
Numerical	1.05	1.10	1.10	1.09
Eccentric Crab				
Experimental	1.06	1.10	1.07	1.09
Numerical	1.05	1.10	1.09	1.09

Table 4-2: Correlation between experimental and numerical results for a global dynamic factor

A high correlation was obtained between the experimental results and the numerical model's results with the numerical model's results a maximum of 0.02 higher than the experimental. It was therefore considered that the finite element model accurately reflected the experimental behaviour of the crane during hoisting. The following graphs are all results obtained from the numerical model.

4.5 Results

4.5.1 Vertical Wheel Loads

Central Crab

Initially the payload is lifted off the ground up to a height of 1.2 m with the crab in a central position (Figure 4-5). The crane operates at a creep speed while starting to lift the payload and then switches to a higher speed once the payload is suspended (time = 1.2 s). At 1.2 m above the ground the hoisting is stopped and this results in a jerk in the cables sending dynamic oscillations through the crane into the wheels (time = 5.7 s). This oscillation is affected by a secondary vibration that exists at this frequency (1.9 Hz). A modal analysis would probably have determined the source of the secondary vibration, but was deemed an unnecessary step as this lifting scenario is dominant in neither the experimental nor numerical results.

Graph (Figure 4-6) represents the vertical load experienced at each wheel as a result of the payload being lifted from 1.2 m to 2.2 m above the ground. The critical region of the

Vertical Payload Movement

graph is shown and the first 12 seconds of constant hoisting are disregarded. At the highest point the motor cuts out suddenly to prevent the cable from being wound too far (time = 14 s). This sudden cut-out causes a jerk in the system and the resulting oscillations induce the peak vertical wheel load. The amplitude of the oscillations as a result of the cut-out far exceeds those occurring during normal payload hoisting.

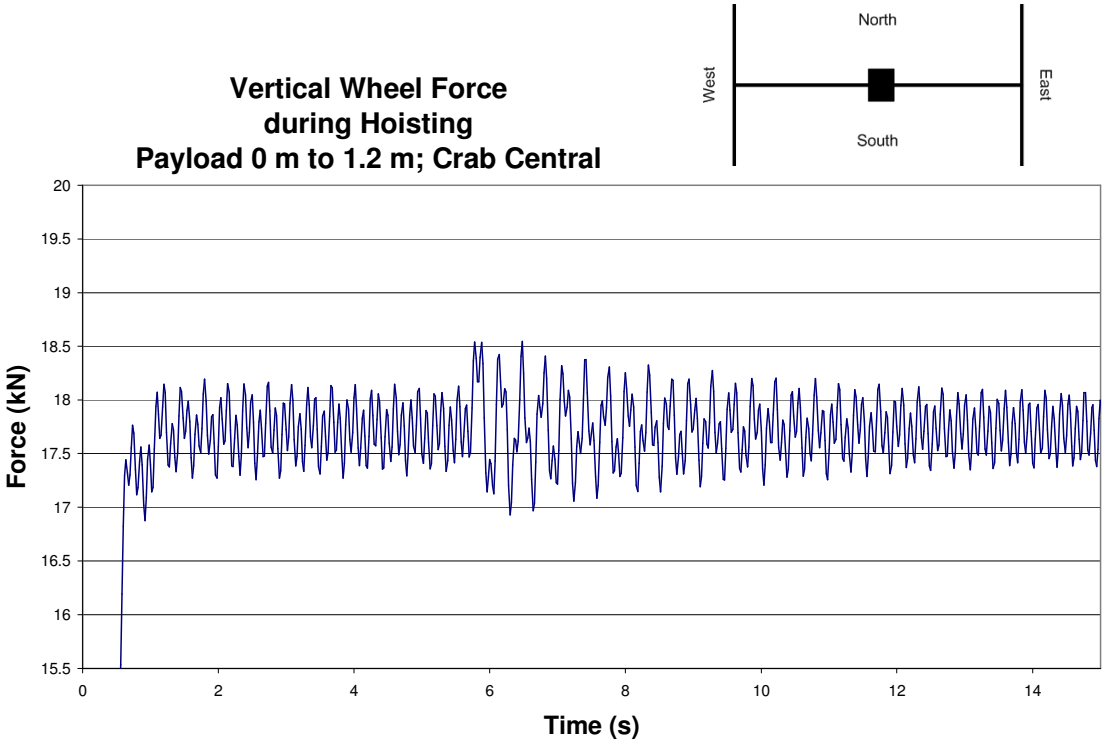

Figure 4-5: Vertical wheel forces as a result of hoisting the payload from 0 m to 1.2 m with a central crab

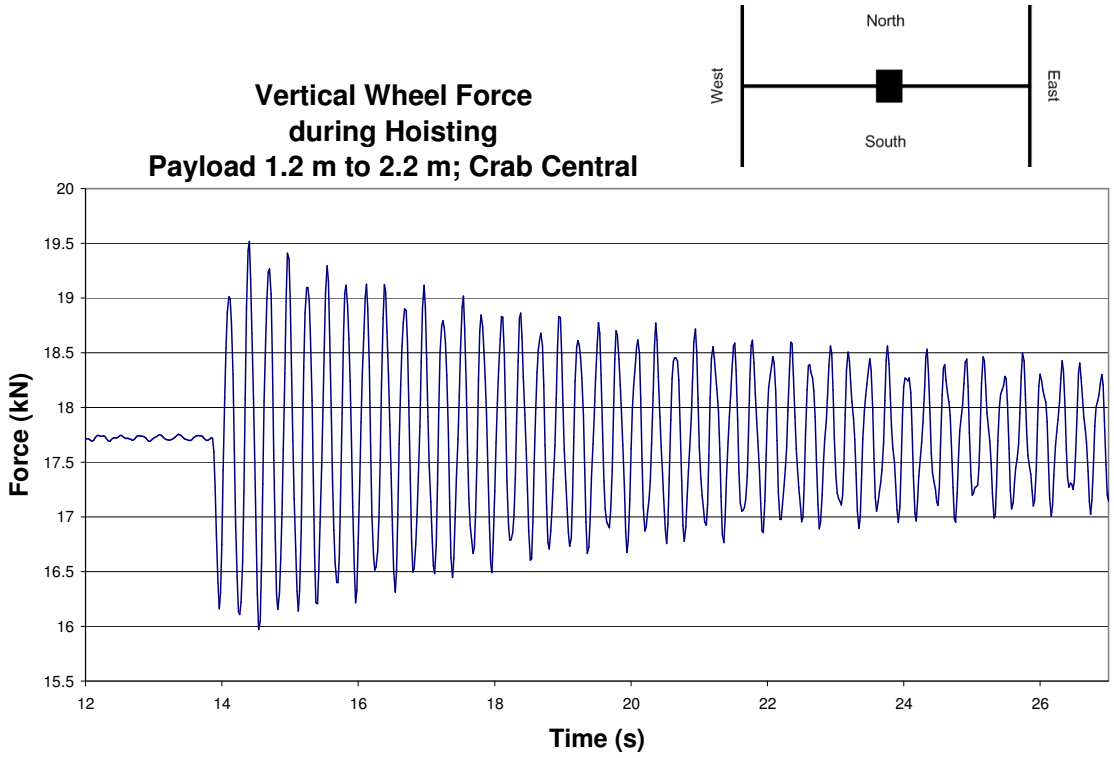

Figure 4-6: Vertical wheel forces as a result of hoisting the payload from 1.2 m to 2.2 m with a central crab

Both lowering load cases display very similar patterns. The movement that causes the dominant oscillation is the initial starting of the motor (time = 1.9 s for both graphs) rather than the moving or the stopping action (time = 13.2 s in the graph representing lowering from 2.2 m to 1.2 m). This is true whether lowering from a 2.2 m height or from a 1.2 m height. Small differences do occur due to the frequencies of oscillation set up as a result of the different length of the cables. In both cases you can see the destructive interference that was apparent in the lifting to 1.2 m load case. This interference is most pronounced when the payload is between 1.2 m and the ground.

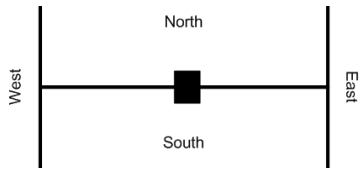

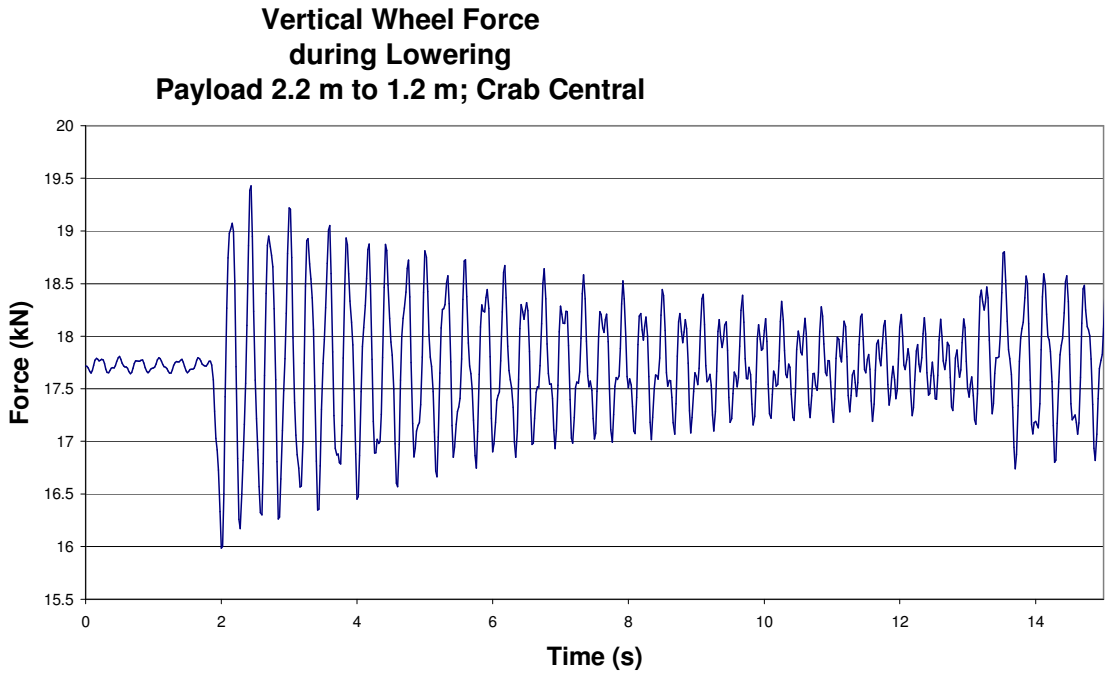

Figure 4-7: Vertical wheel forces as a result of lowering the payload from 2.2 m to 1.2 m with a central crab

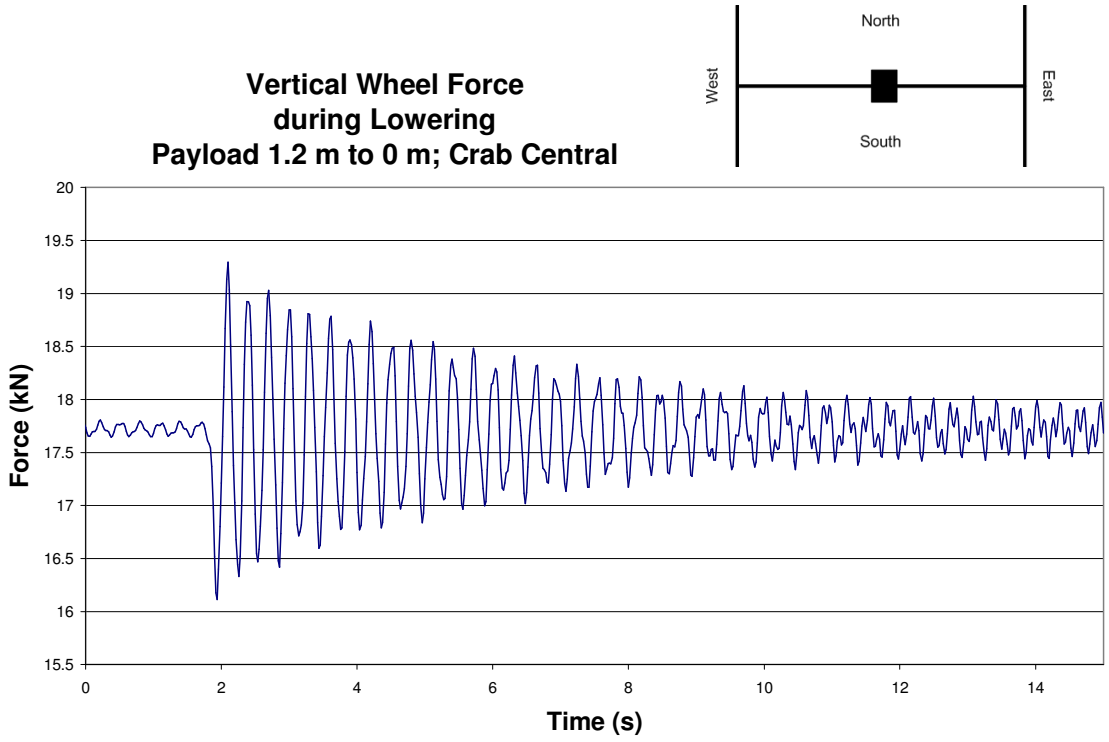

Figure 4-8: Vertical wheel forces as a result of lowering the payload from 1.2 m to 0 m with a central crab

Eccentric Crab

The behaviour of the crane with the crab in an eccentric position closely resembles that of the crane with the crab in a central position. The oscillations induced in the crane by the payload being hoisted with an eccentric crab are consistently smaller than those induced by the payload movement with a central crab, in the same way that midspan deflections with an eccentric crab will always be smaller than with a central crab. Although the dominant vertical wheel force will come from the eccentric crab position, the vibration behaviour of the crane is more apparent in the case of the central crab, so this crab position has been dealt with in detail. The most dominant loading scenario with an eccentric crab is hoisting from 1.2 m to 2.2 m. This is shown in Figure 4-9 below. The full set of graphs for the eccentric crab is given in Appendix A.

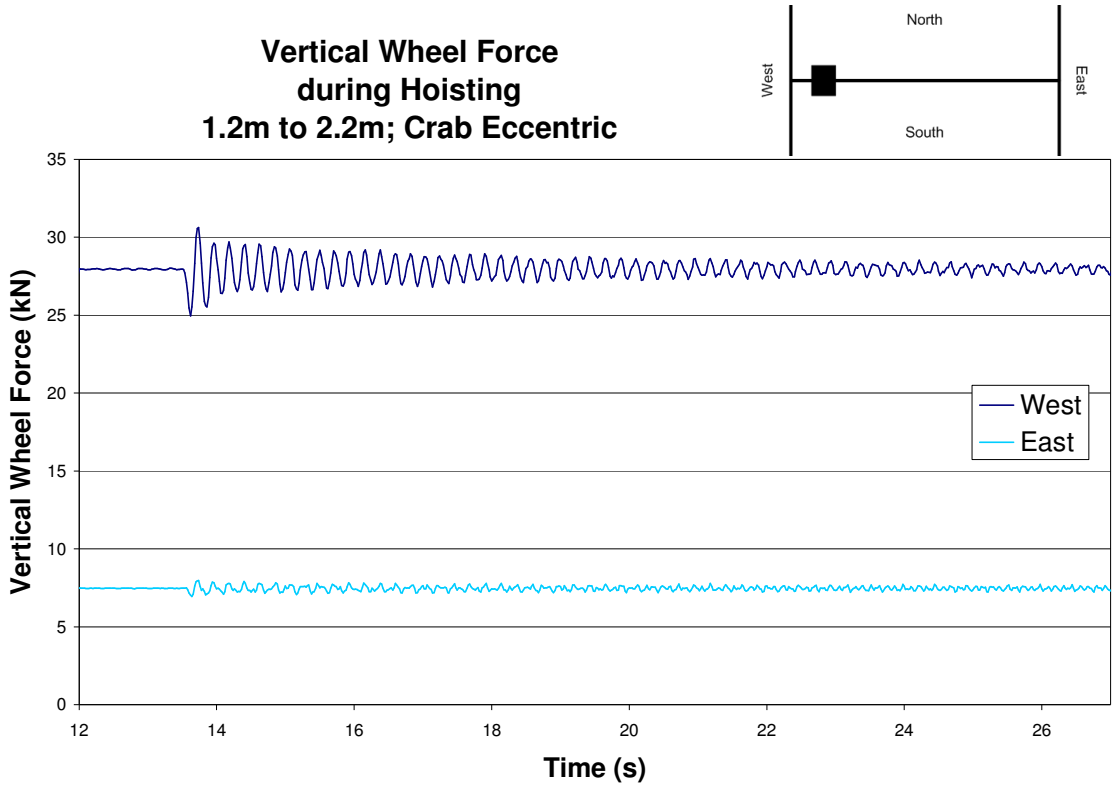

Figure 4-9: Vertical wheel forces as a result of hoisting the payload from 1.2m to 2.2m with an eccentric crab

Once again the critical part of the graph is shown and the initial 12 seconds of lifting disregarded. Here the wheels closest to the payload (west) carry the majority of the vertical load as expected with the load distribution being spread to the wheels according to normal static mechanics. The oscillations induced by the hoisting motor being cut-off (time = 13.8 s) are substantially more pronounced in the closer wheels (west) with the further wheels (east) receiving only a slight vibration.

4.5.2 Horizontal Wheel Forces

Vertical payload motion does not only induce vertical forces at the wheels but horizontal lateral forces as well due to the portal frame action of the bridge, endcarriages and wheels.

The horizontal wheel forces closely follow the behaviour pattern of the vertical wheel forces. The largest dynamic effects on the horizontal loading are found during the hoisting of the payload from 1.2 to 2.2m with the emergency cut-off occurring at the top.

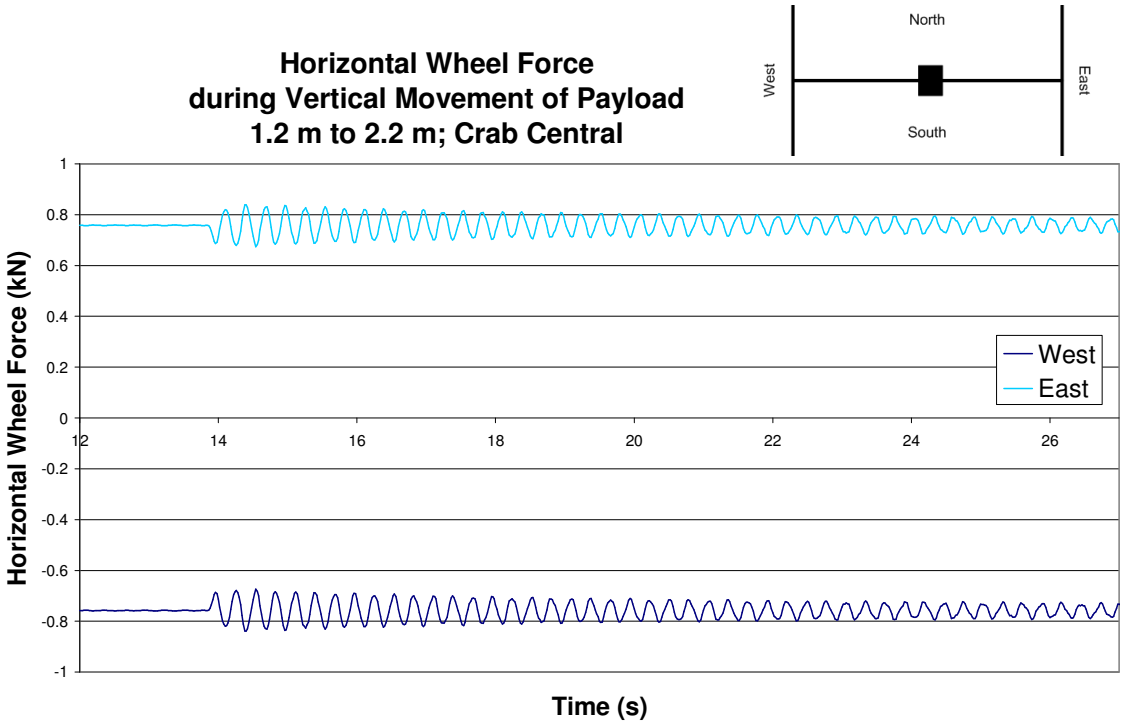

Figure 4-10: Horizontal wheel forces as a result of lifting the payload from 1.2m to 2.2m with a central crab

Vertical Payload Movement

The average horizontal force experienced with a central crab is 0.76 kN outwards at each wheel. This is substantially more than the average horizontal force of 0.33 kN outwards when the crab is eccentrically placed. This is an expected result due to the portal frame action of the crane bridge on its end carriages. The more centralized the load the larger the horizontal forces.

It is also important to note that while the crane remains stationary the wheels do not slip horizontally. The static frictional force is sufficient to counteract the horizontal force induced by the lifting and lowering of the payload.

4.6 Discussion

Using the equations from the Eurocode mentioned in 4.2, it is possible to calculate the φ_1 and φ_2 values which occur in each hoisting and lowering scenario.

φ_2 can be calculated from the maximum amplitude of the force measured in the payload's loadcell. This is purely based on experiments and was used as input into the numerical model (Table 4-3).

	Hoisting		**Lowering**	
	0m → 1.2m	**1.2m → 2.2m**	**2.2m → 1.2m**	**1.2m → 0m**
Crab Central φ_2	1.07	1.12	1.10	1.10
Crab Eccentric φ_2	1.06	1.11	1.09	1.10

Table 4-3: φ_2 values as calculated from the experimental results

According to Eurocode [2] the value of φ_2 to be used for calculating the vertical wheel loads is:

$$\varphi_2 = \varphi_{2,\,min} + \beta_2 v_h$$
$$= 1.1 + 0.34*0.075$$
$$= 1.13$$

The maximum design vertical wheel load will exist in the case of an eccentric payload so the greatest measured factor (φ_2 = 1.11) is slightly lower than the given factor in the codes. The code calculated factor is therefore representative of the results measured.

Using these measured φ_2 values and knowing both the dead weight of the crane and the dead weight of the payload, it is possible to calculate the dynamic factor caused by the vibration of the crane for each load case (φ_1) according to the formula:

$$F_V = Q_h\varphi_1 + Q_c\varphi_2$$

This yields the following factors:

	Hoisting		**Lowering**	
	0m → 1.2m	**1.2m → 2.2m**	**2.2m → 1.2m**	**1.2m → 0m**
Crab Central φ_1	0.98	1.05	1.08	1.06
Crab Eccentric φ_1	1.00	1.04	1.07	1.02

Table 4-4: φ_1 values as calculated from the numerical results

The low values for the payload being lifted from 0 m to 1.2 m are considered an anomaly. In the numerical model there are clear secondary modes of vibration which have a destructive influence on the primary mode for this case (as has been noted in Figure 4-5). This dampens the oscillations rapidly and reduces the dynamic factor of the oscillation of the crane.

From this table it is clear that with both a central crab and an eccentric crab, the maximum amplification of the vertical force due to the vibration of the crane occurs when the payload is lowered from 2.2 m to 1.2 m. Interestingly this does not correlate with the maximum payload amplification which occurs when the payload is lifted from 1.2 m to 2.2 m.

According to the European Code, φ_1 is given as 1.1. This value comfortably exceeds any of the values obtained by the numerical model, remaining conservative but not overly so.

Vertical Payload Movement

When the overall behaviour of the crane is considered the following global dynamic factor is observed (Table 4-5). The global factor is the amount the maximum static vertical wheel load is multiplied by to form the maximum dynamic vertical wheel load.

	Hoisting		**Lowering**	
	0m → 1.2m	**1.2m → 2.2m**	**2.2m → 1.2m**	**1.2m → 0m**
Central Crab	1.05	1.10	1.10	1.09
Eccentric Crab	1.05	1.10	1.09	1.09

Table 4-5: Global φ factors as calculated from the numerical results

It is observed that although the dominant scenario for crane vibration is the lowering of the payload from 2.2m to 1.2m, the overall dominant scenario is the hoisting from 1.2m to 2.2m with the emergency cut-off at the top of the hoist. This is due to the large payload vibrations which are set off during this stop. These large oscillations override the marginal differences in the crane structure vibration that exist between scenarios.

This global dynamic factor observed at the wheels is a result of the combined effect of the dynamic oscillation of the payload and the vibration in the crane itself. Calculated according to the Eurocode [2] with the weight of the payload and the crane as recorded in the laboratory, this global dynamic factor should be $\Phi_e = 1.12$ for both the central and eccentric crabs. This value is comparable to the general factor given in the current South African code [1] of $\Phi_s = 1.2$.

As the maximum observed factor is $\Phi_o = 1.10$ one can conclude that the current SABS code [1] is extremely conservative with regards to the global dynamic factor. The Eurocode [2] is far more representative of the crane behaviour with an individual dynamic factor for both the payload and the crane movement. Both factors are slightly conservative and as a result the combined effect is conservative but appropriately so.

4.7 Conclusions

The hoisting and lowering of a payload is a crane's most frequent operation. It is the dictating case for the maximum vertical load experienced per wheel in the crane design

codes and in practice. Horizontal loads are also passed into the crane supporting structure during this action.

The experimental results showed that the greatest dynamic factor (φ_2) induced by the payload itself on the vertical wheel forces was 1.11 in the eccentric crab position (the critical position for determining maximum vertical wheel loads). The numerical model showed that the greatest dynamic factor (φ_1) caused by the vibration of the crane on the horizontal wheel forces was 1.07 in the eccentric crab position.

Both φ_1 and φ_2 values as estimated by the Eurocodes [2] are slightly higher than the numerically calculated φ_1 and φ_2 values. The resultant global factor of these combined dynamic factors is 1.12, slightly higher than the global factor measured numerically of $\varphi_o = 1.10$ and considerably lower than the value predicted by the current South African code of $\varphi_o = 1.2$.

The Eurocode [2], and by proxy the new South African loading code [3] as it is based on the Eurocode [2], provides an accurate representation of what is occurring during the hoisting of the payload and a far closer estimate of the dynamic factors involved than the current South African code [1]. The factor in use by the South African code is conservative and shows little understanding of the mechanics behind the hoisting and lowering of the load.

5 NORMAL LONGITUDINAL MOTION

Normal longitudinal motion covers the crane behaviour when the crane is behaving exactly as the manufacturer intended. There is no skewing or impact taking place, the rails are not misaligned and contain no large gaps; the crane is simply running back and forward along the rails carrying its payload.

As a result this is seldom a dominant load case. The only codified factor this case gives rise to is the horizontal longitudinal forces due to acceleration and deceleration of the crane under normal use.

It is still important to study this case as it gives insight into how the crane is behaving under normal loading conditions. This can then be extrapolated when studying the more complicated cases of skewing and misalignment.

This chapter analyses the Eurocode [2] and the current South African code's [1] approach to normal longitudinal travel. It follows with the methods that were used to imitate normal longitudinal travel in the laboratory and the numerical model, analyses the results obtained from the numerical model and compares them to the codes.

5.1 Codification

In the current South African code [1] the horizontal force considered to be imposed by the acceleration and deceleration of the crane on each line of rails (acting longitudinally along the rail) is equal to the maximum static wheel load multiplied by a factor of 0.1. (SABS 0160 Ch 5.7.5)

In the current Eurocode [2] the acceleration and deceleration of the crane is taken into account by the following equation:

$$H_{L,i} = \varphi_5 K/n_r$$

where: n_r is the number of rails

K is a drive force factor given by the crane supplier

φ_5 =1.5 is a dynamic factor (Table 2.6 [2])

i is the integer to identify the rail considered

The crane section in the draft new South African code [3] is heavily based on the Eurocode [2]. As such the calculations for the longitudinal horizontal forces imposed on the rails by the acceleration and deceleration of the crane in the draft South African code [3] follows the same method as stated above.

5.2 Experimental Setup

During the experiments completed by Johan de Lange the crane was always started from the most southerly bay of the crane supporting structure. It was then accelerated (0.18 $m.s^{-2}$) in a northerly direction for 3 seconds, allowed to run at a constant velocity (0.54 $m.s^{-1}$) for 12.30 seconds and decelerated (0.20 $m.s^{-2}$) to a stop over 2.7 seconds. This pattern was immediately repeated for the crane running in a southerly direction to gain a full spectrum of results of the crane's behaviour. At the end of the cycle the crane was started on its northward journey again to ensure that the effects of the payload swinging through were fully taken into account. The velocity of the crane was measured by a pair of encoders on the northern wheels.

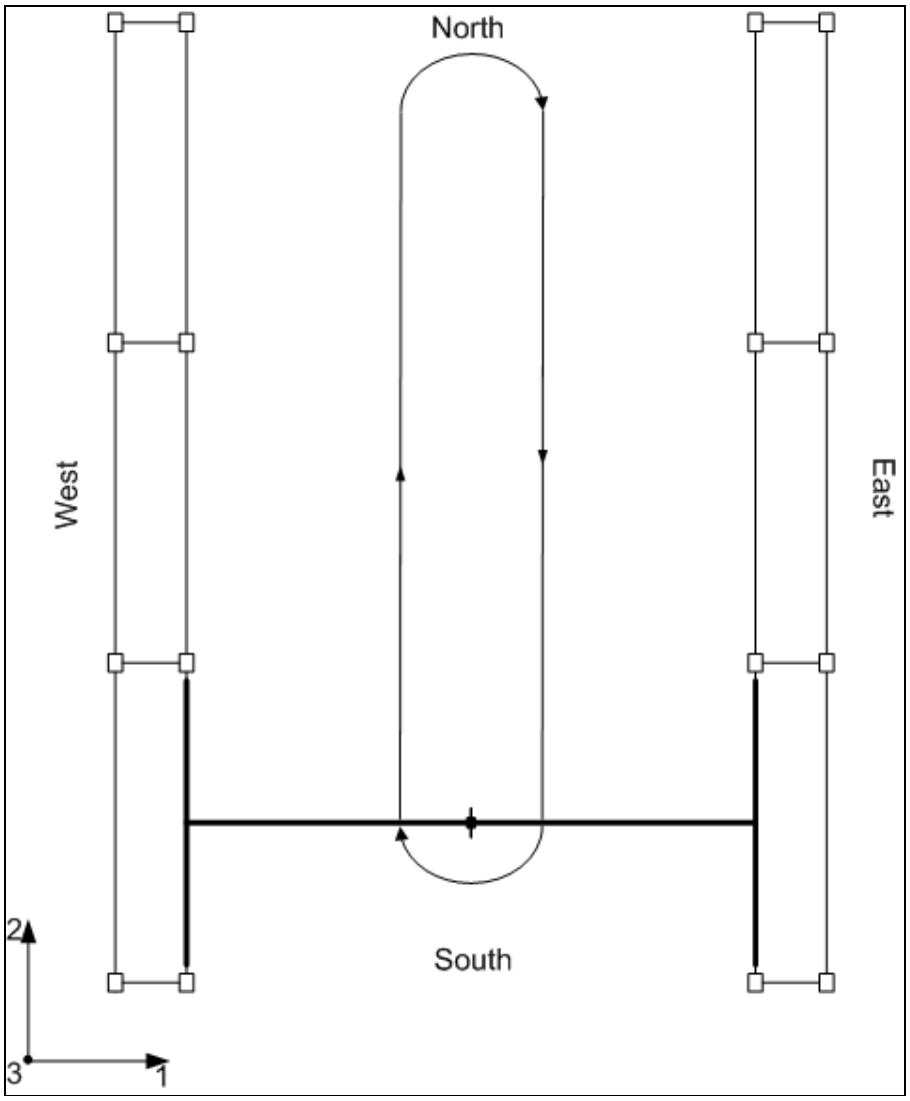

Figure 5-1: Route followed by crane during longitudinal motion

The southern wheels are the driving wheels of the crane. During northward travel the crane is being pushed and during southward travel the crane is being pulled by the driving wheels. This is important to note as it can affect the behaviour of the crane especially with an eccentric payload.

For the purposes of clarity, the global referencing system is as in Figure 5-1. The Lateral (transverse) direction refers to the West-East axis (East positive), the Longitudinal direction to the South-North axis (North positive) and the Vertical direction to the vertical axis (positive upwards).

Normal Longitudinal Motion

5.3 Numerical Model Setup

In the numerical model the crane was positioned in the southernmost bay to duplicate the experimental results. The acceleration, constant velocity and deceleration boundary conditions in the model were matched with the measured velocity at the northern wheels from the experiments (Figure 5-2).

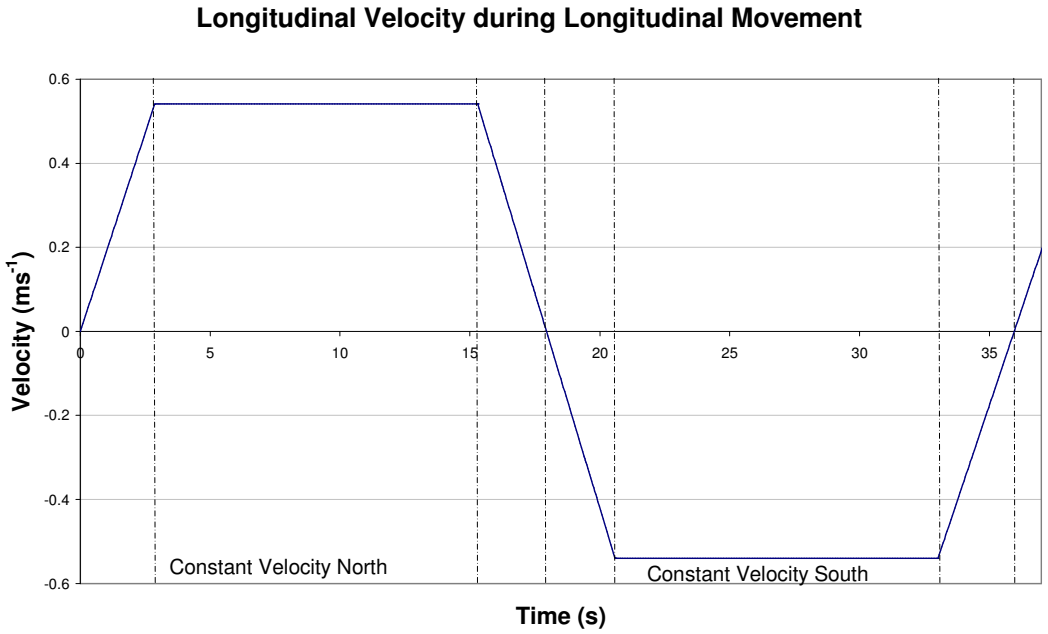

Figure 5-2: Velocity of crane wheels during longitudinal travel used as input for finite element model

The crane was run for both a central and eccentric payload with the load at the bottom (0.15m above the ground) and the load at the top (2.2 m above the ground).

5.4 Calibration

The numerical model was calibrated to the experimental model using the simplest form of normal longitudinal travel. The crane was accelerated at 0.17 $m.s^{-1}$ for 1.78 seconds, decelerated at 0.18 $m.s^{-1}$ for 1.46 seconds and then allowed a period of free motion. During this period of free motion the payload is allowed to swing. This movement results in a sudden increase in velocity when the payload pulls the crane forward. The numerical model's results should match this if it is modelled correctly.

Normal Longitudinal Motion

Initially the velocity graphs for the northern wheels were calibrated to the experimental results. The acceleration and deceleration restrictions are treated as boundary conditions within the finite element model and are set during the acceleration and deceleration phases but during the free motion phase the wheels are required to follow the motion of the experimental crane of their own accord. Once the wheel velocities were calibrated the horizontal lateral loads experienced at the wheels were compared to ensure the full calibration of the model.

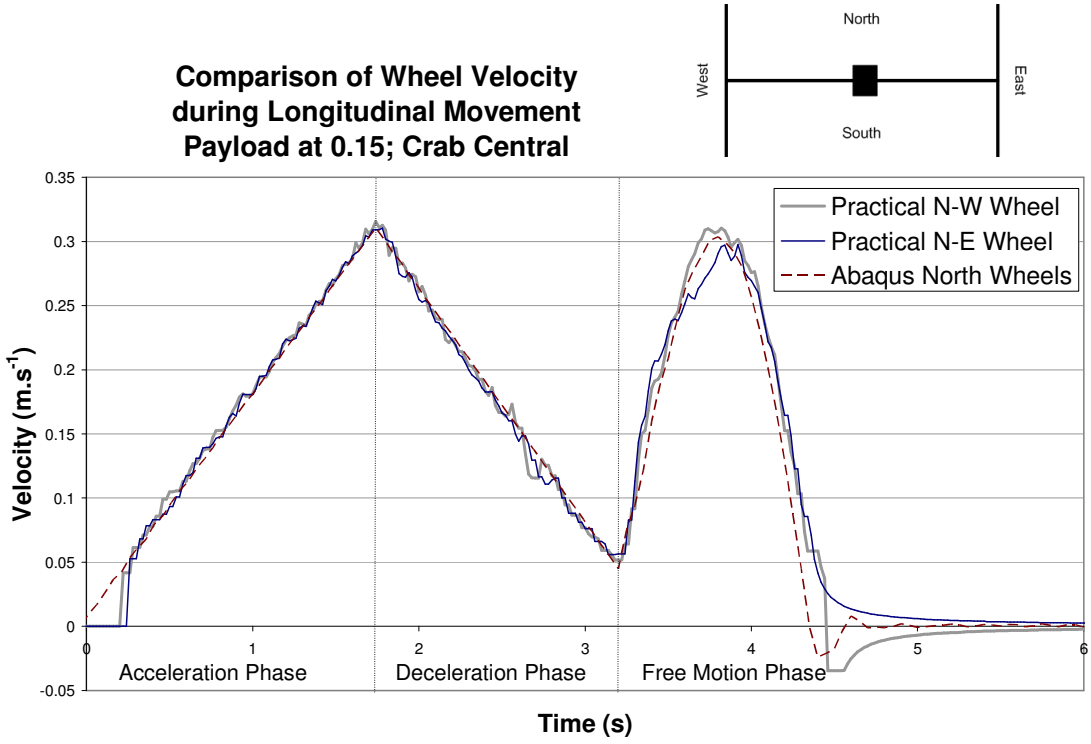

Figure 5-3: Comparison of the experimental measurements and the numerical results of the wheel velocities at the northern wheels for a central crab at 0.15m above the ground.

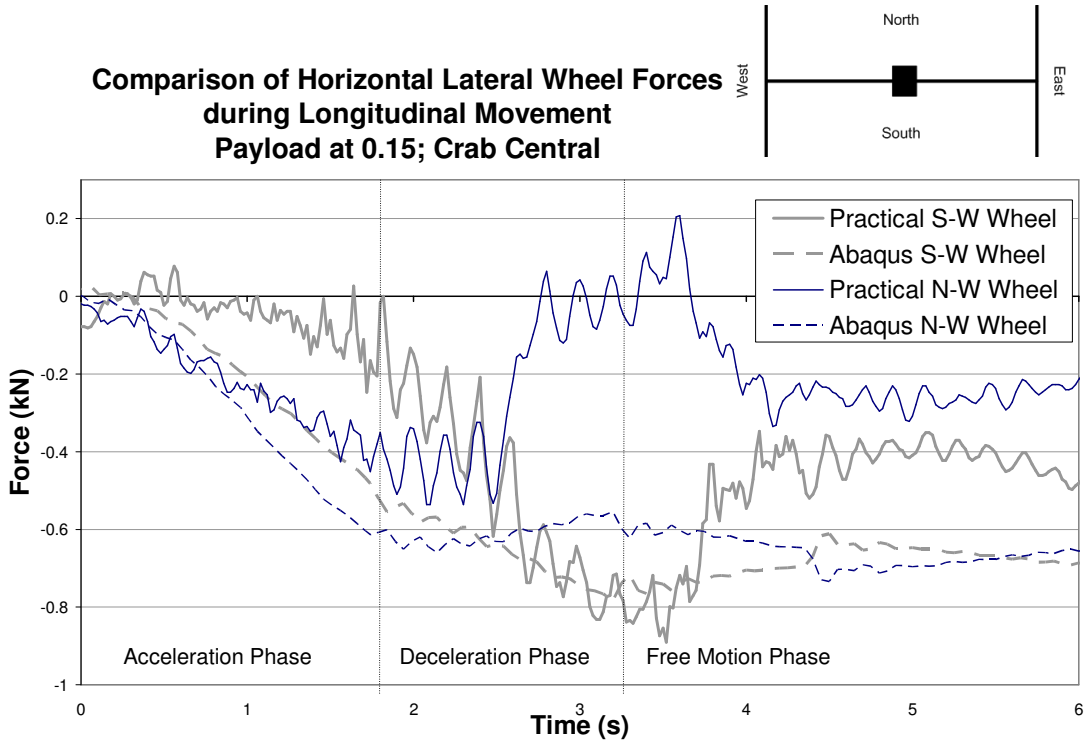

Figure 5-4: Comparison of the experimental measurements and the numerical results of the horizontal lateral forces at the northern wheels for a central crab at 0.15 m above the ground.

The numerical wheel velocities show a close correlation to the experimental even during the free motion phase. In the numerical model both northern wheels experience identical velocities and as such only one has been represented in the graph.

The horizontal lateral forces show a larger disparity than was seen in the velocity graph. In the experimental results the difference between the north and south wheels is marked while in the numerical results this difference is far slighter. It is possible that this difference is a result of the weight distribution on the wheels of the experimental crane. It is observed that the behavioural pattern the forces follow and the maximum peak reached by the forces in the finite element model do still accurately represent the experimental solution. The numerical model results in a larger average lateral force experienced on each endcarriage than occurs in practice but this will lead to slightly conservative modelling.

5.5 Results

The following graphs are all results obtained from the numerical model once it had been calibrated and checked against the experimental results. They relate to a full circuit of northward and southward travel of the crane.

5.5.1 Vertical Wheel Forces

The average vertical wheel forces calculated by the numerical model during normal longitudinal travel matched static vertical force calculations and are included here (Figure 5-5) for reasons of completeness. In eccentric travel the crab is positioned closest to the western wheels.

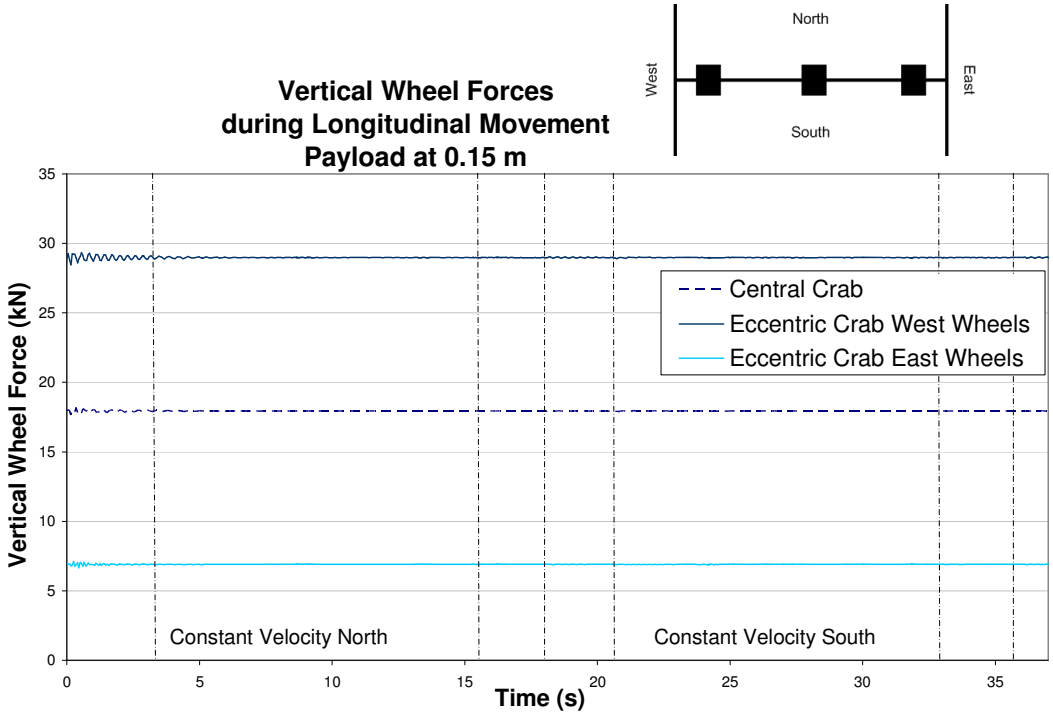

Figure 5-5: Vertical Wheel Forces for a central crab with payload at 0.15 m above the ground

The oscillation of the payload is predominantly in the longitudinal direction with the motion of the crane travel and as a result the vertical oscillations are far more muted than in the case of vertical payload movement.

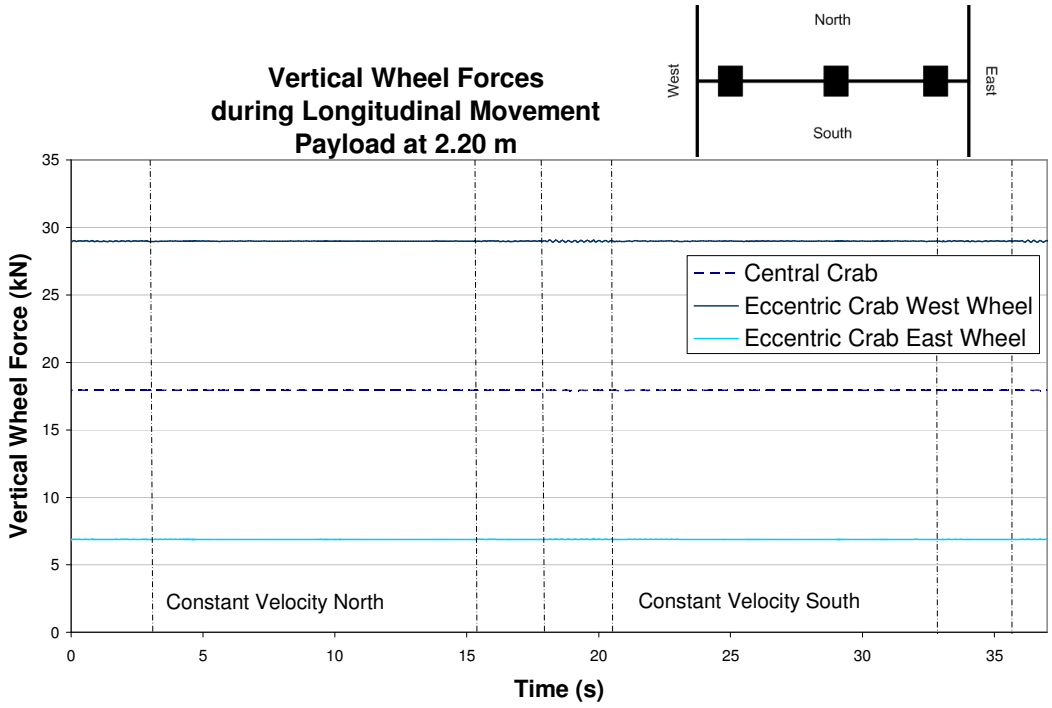

Figure 5-6: Vertical Wheel Forces for a central crab with payload at 2.2 m

When the payload is fully hoisted (2.2 m above the ground), the oscillations are reduced even further but the average vertical wheel forces still match the static calculations. The position of the cables at the crane bridge is fixed. This means that as the payload is hoisted the angle the cables form at the pulley increases. When the payload is fully hoisted the pulley tends to run along the cables as opposed to forcing the cables to sway. This decreases the volatility of the payload during crane movement.

5.5.2 Horizontal Lateral Wheel Forces

Central Crab

The horizontal lateral wheel forces are the forces experienced at the wheel in the lateral direction (perpendicular to the direction of motion). These forces start at the average force of 0.76 kN which occurs during the lifting of the payload. As the crane begins to move the wheels slide out laterally as the static frictional coefficient that was restraining them is no longer valid.

The crane wheels are expected to move laterally outwards until they find a new point of equilibrium with the moving system or until the wheel flanges make contact with the rails. In the case of the laboratory crane the starting distance between the wheel flange and the rail is

only 2.4 mm which is very slight. As a result the wheel flanges come into contact with the rails early in the crane's movement (t = 3.7 s) and the lateral deflection of the wheels remain at 2.4 mm outwards for the duration of the crane's movement (Fig 5.7).

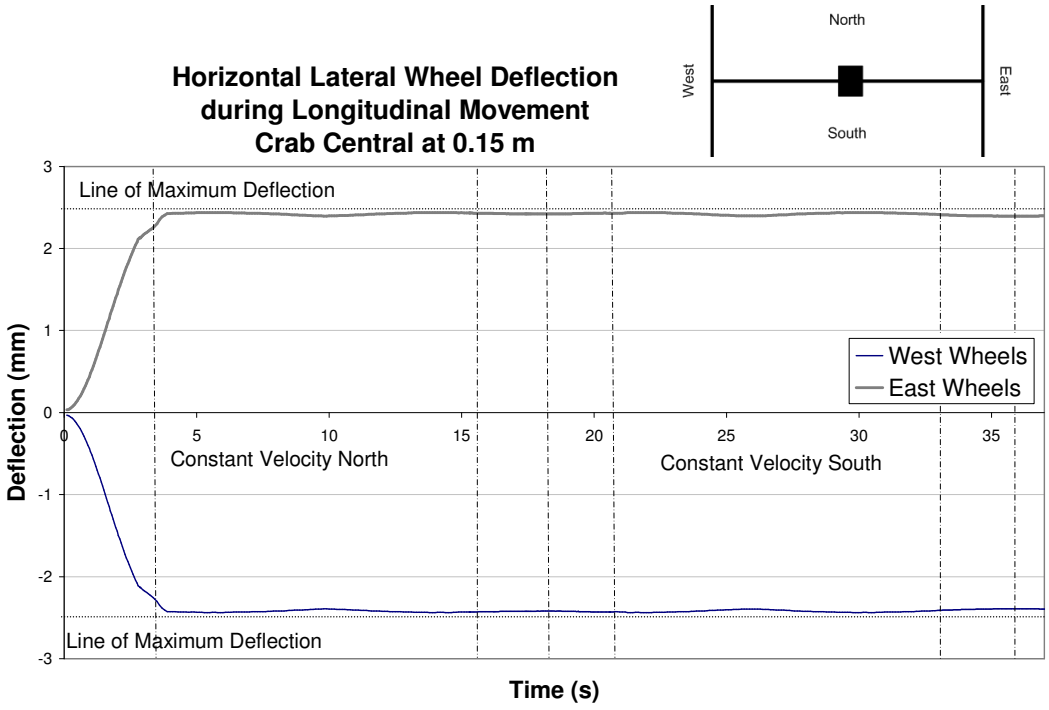

Figure 5-7: Horizontal Lateral Wheel Deflection for a central crab with payload at 0.15m

The sliding of the wheels leads to a rapid decrease in the horizontal loads experienced during the acceleration phase of the crane motion (Fig 5.8). By the constant motion phase the forces have settled into a gently oscillating pattern that matches the oscillation of the payload.

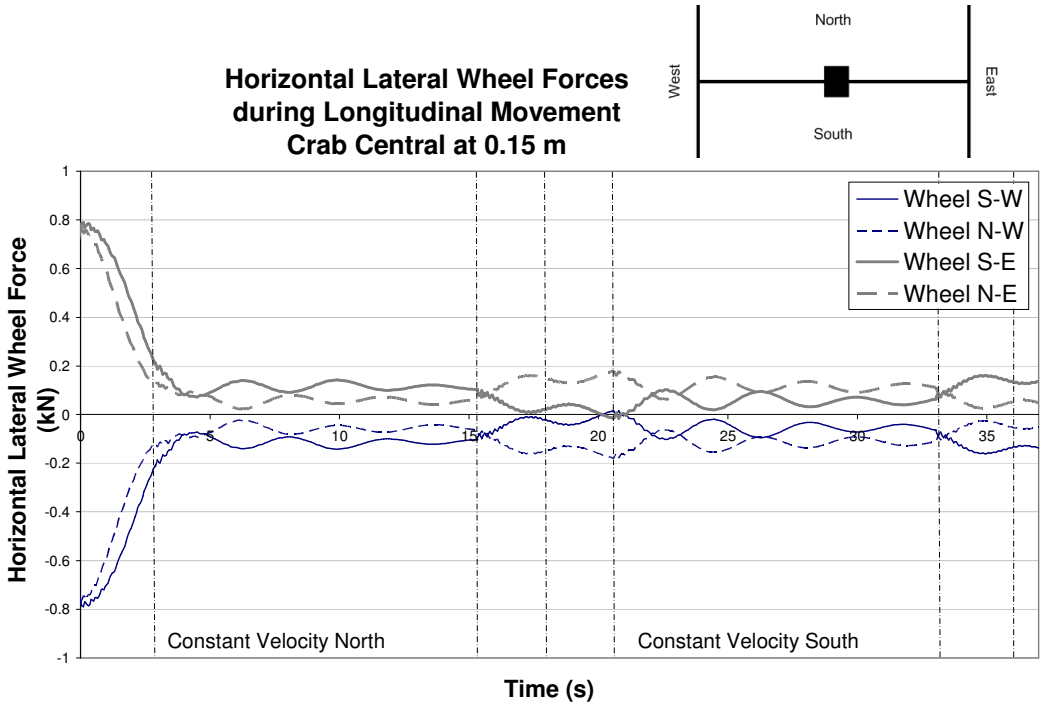

Figure 5-8: Horizontal Lateral Wheel Forces for a central crab with payload at 0.15 m

At no point do the lateral forces reobtain their static loading peak (0.76 kN). This reinforces the fact that normal longitudinal travel of the crane is not a dominant load case for transverse horizontal forces. It is interesting to note that both with the payload at 0.15m and the payload at 2.2 m it is the back wheels that experience the greater forces irrespective of whether the back wheels are the driving wheels or not. The forces increase marginally at the point where the crane stops moving north and starts south (18 s). This is due to the payload swinging through as the crane starts to accelerate in the opposite direction.

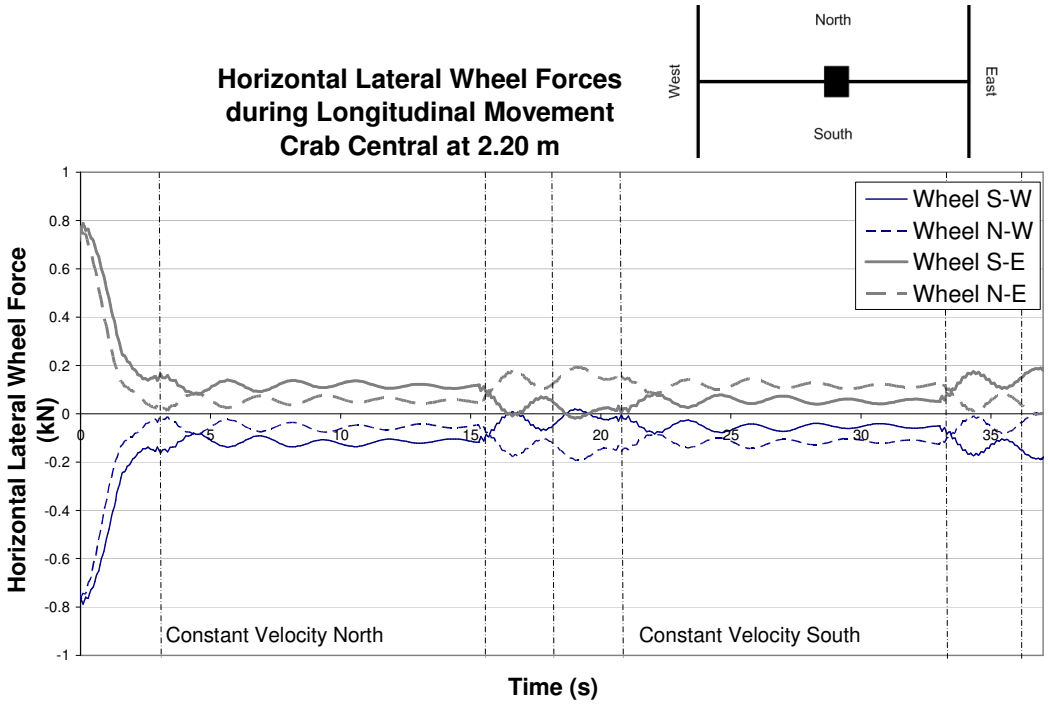

Figure 5-9: Horizontal Lateral Wheel Forces for a central crab with payload at 2.20 m

The main difference between the lateral forces obtained when the payload is at the bottom (Figure 5-8) and the payload is at the top (Figure 5-9) is the frequency of oscillation, which increases with the shorter cable length from 0.27 Hz to 0.4 Hz.

Eccentric Crab

With the eccentric crab it is interesting to note that both sets of wheels do not immediately move outwards until their flanges are touching the rail (Figure 5-10). It is only the lightly loaded wheels furthest from the crab (east wheels) that slide outwards during acceleration.

As the crane starts to move the eccentric payload causes slight skewing to occur. Although the motors are synchronised to prevent this, the eccentricity of the load is still felt throughout the motion of the crane. During the constant velocity period the motor on the west side carrying the majority of the load is not as strained as during acceleration and the crane reaches an equilibrium position with the non-driving west wheel almost touching the rail. Little change occurs as the crane decelerates and starts to move south but after constant velocity is reached a period of rapid lateral movement is observed as the crane tries to find a new position of equilibrium in which to travel. When the crane decelerates during its northward travel and starts to accelerate south again, the payload continues to swing north. It is only after the

constant velocity south phase is reached that the payload has the opportunity to swing in front of the crane bridge and this causes the rapid lateral adjustment seen in the graph below. It is also important to note that the driving wheels (south) are considerably more stable than the driven wheels (north).

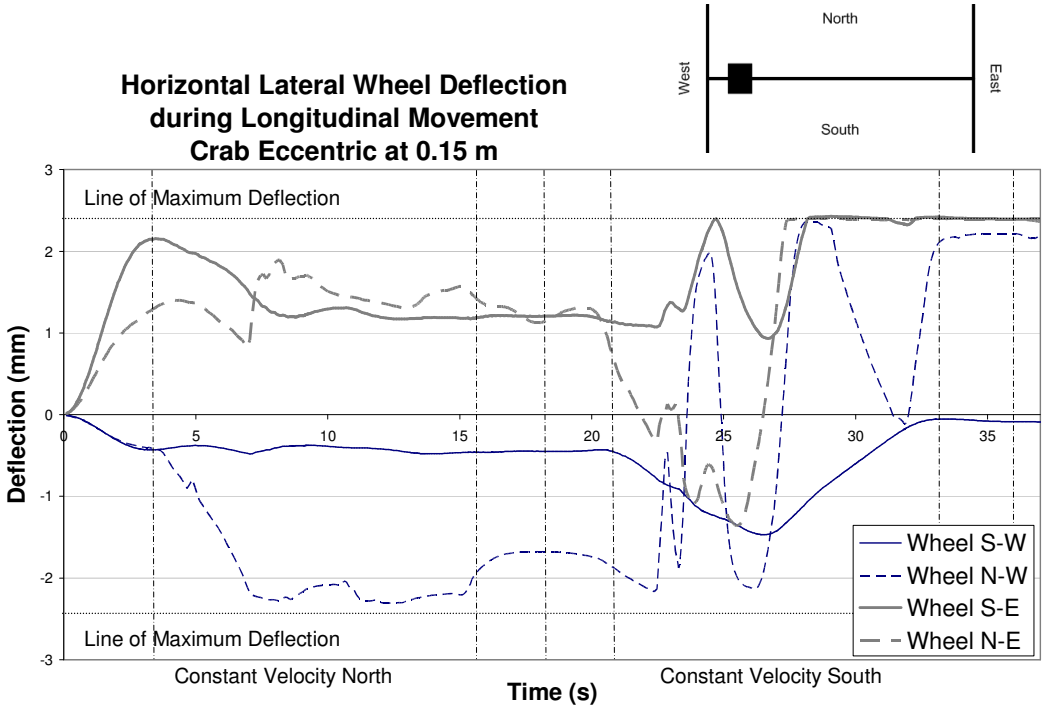

Figure 5-10: Horizontal Lateral Wheel deflection for an eccentric crab with the payload at 0.15m

The forces associated with this movement are more erratic than those for the central payload. As with the central crab, the forces decrease rapidly from the static frictional force obtained during the hoisting of the payload (Figure 5-11). For the majority of the movement of the crane, the two driving wheels experience minimal lateral wheel loads and the non-driving wheels experience the skewing forces caused by the eccentric payload.

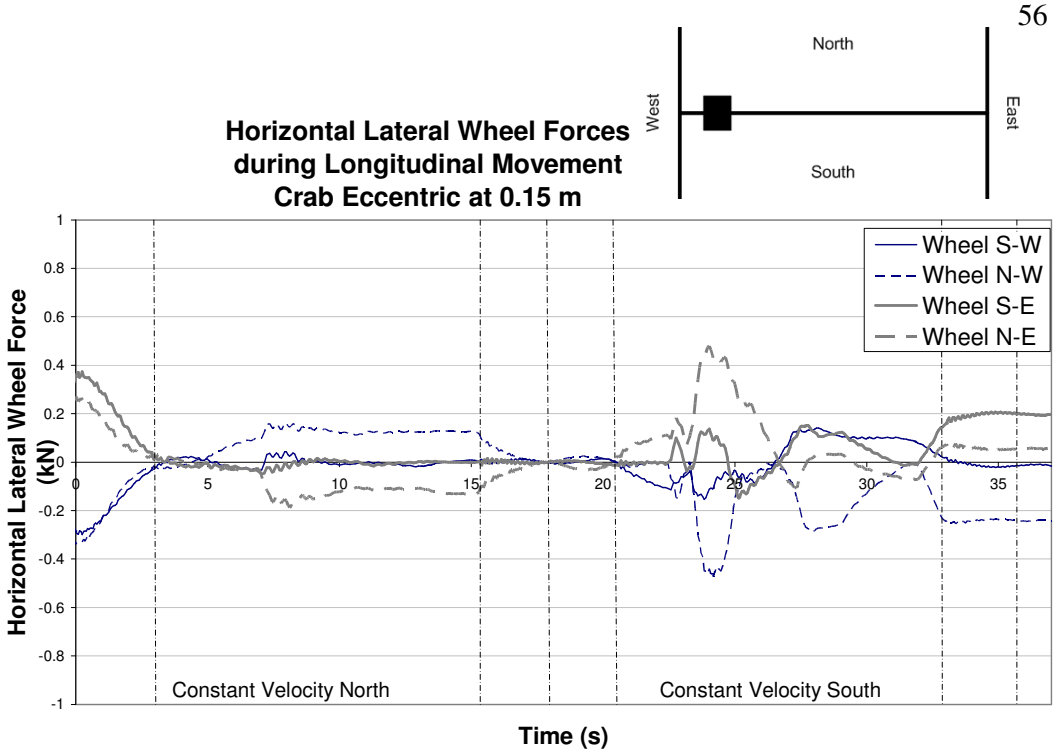

Figure 5-11: Horizontal Lateral Wheel Forces for an eccentric crab with payload at 0.15 m

During the constant velocity northbound phase the crane is experiencing mild skewing. As the crane bridge and end carriages are light H-sections (305x305x118 and 203x203x60 respectively) the crane itself is fairly flexible. This will be dealt with in greater detail in Chapters 6 and 7. While the west endcarriage of the crane is lagging slightly due to the extra weight of the payload, the east endcarriage maintains its specified speed. As the crane is flexed, forces are induced into the crane structure that attempt to return the crane to its original shape. As a result of this interaction the forces in the exaggerated diagram below are experienced at the wheels.

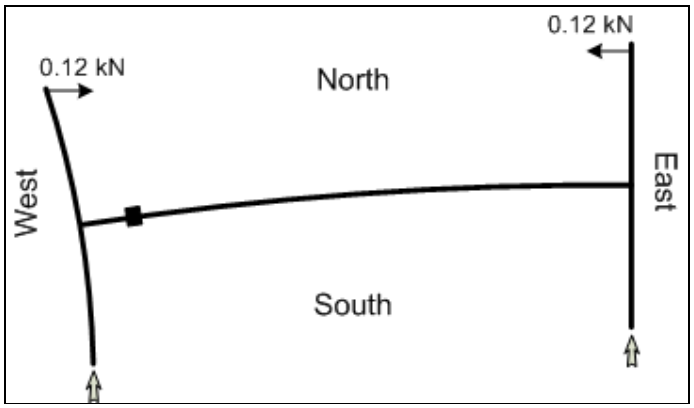

Figure 5-12: Lateral Forces acting on wheels during northerly motion with an eccentric crab after time t = 10 seconds.

When the crane is decelerated and then accelerated in a southerly direction, the lateral forces are again diminished. When the crane is moving at a constant velocity in the southerly direction the forces shown are responding to the lateral movement of the crane discussed earlier. Eventually equilibrium is reached with the east end carriage straight with its wheel flanges touching the rails and the west end carriage skewed with the non-driving wheel flange touching the rail. The lateral forces are then carried by the north-west (non-driving) wheel and the south-east (driving) wheel on opposite endcarriages as per Figure 5-13.

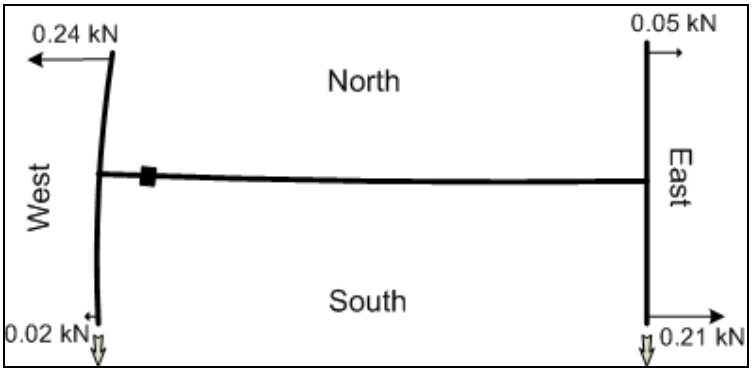

Figure 5-13: Lateral Forces acting on wheels during southerly motion with an eccentric crab after time t=35 seconds.

Although these skewing forces can reach 0.5 kN, the initial forces of 0.76 kN experienced by the crane with the crab in a central position are still the largest lateral forces produced during longitudinal movement.

When the payload is at the top (2.20 m) a similar pattern of results emerges to the payload at the bottom (0.15 m) but the forces are far smaller. In all cases considered the payload at the bottom has a larger affect on the results than the payload at the top.

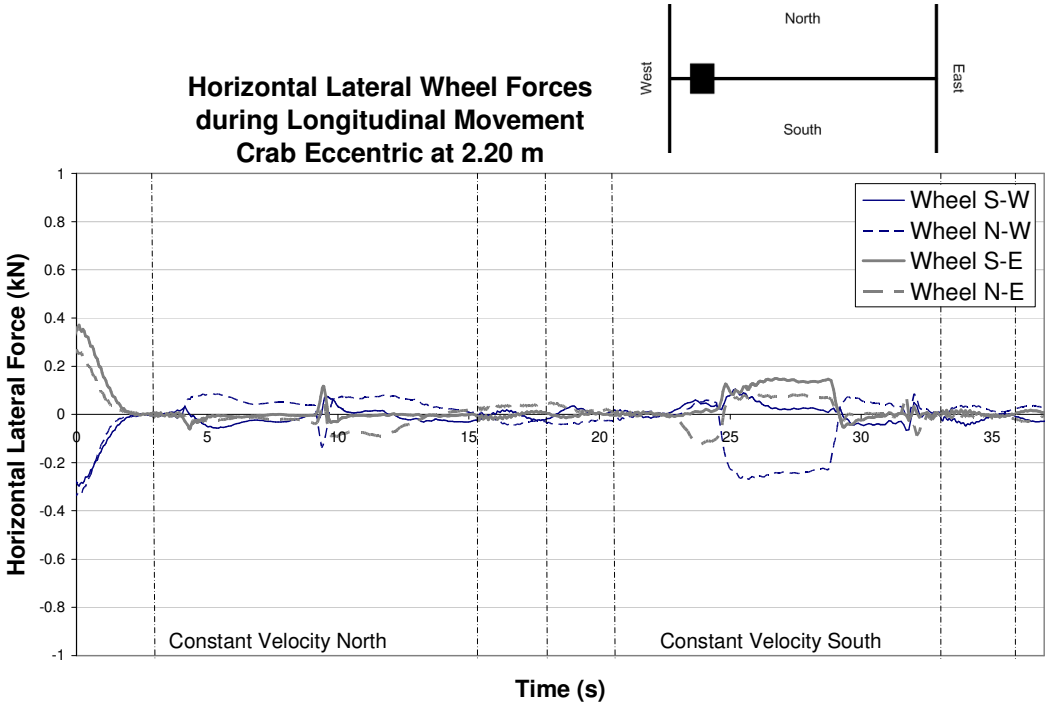

Figure 5-14: Horizontal Lateral Wheel Forces for an eccentric crab with payload at 2.2m

5.5.3 Horizontal Longitudinal Wheel Forces

This is the force experienced in the longitudinal direction (parallel to the direction of movement) along the crane rails as the crane accelerates and decelerates.

In the experiments the motors appeared to modulate the torque given to the wheels in order to maintain a set acceleration, constant velocity or deceleration. It is only during free motion of the crane after the motors have been switched off that the swinging of the payload has a direct influence on the longitudinal motion of the crane.

This is modelled by giving an input in the numerical analysis that the crane driving wheels must run at a set acceleration, constant velocity and then set deceleration again. The model calculates the force at the driving wheel required to maintain these boundary conditions. As a result when the payload is pulling the crane forward the force required to drive the wheel is considerably less than when it is pulling the crane back.

Normal Longitudinal Motion

Central Crab

With a centralised crab the highest negative force is experienced while accelerating in the northward direction and the highest positive when accelerating south. The highest peaks reached are 1.31 kN with the payload 0.15 m off the ground (Figure 5-15), and 1.30 kN with the payload 2.20 m above the ground (Figure 5-16). It is apparent from the graphs below that the oscillations induced by the swinging of the payload are of a higher frequency when the payload is at the top and the cable is shorter.

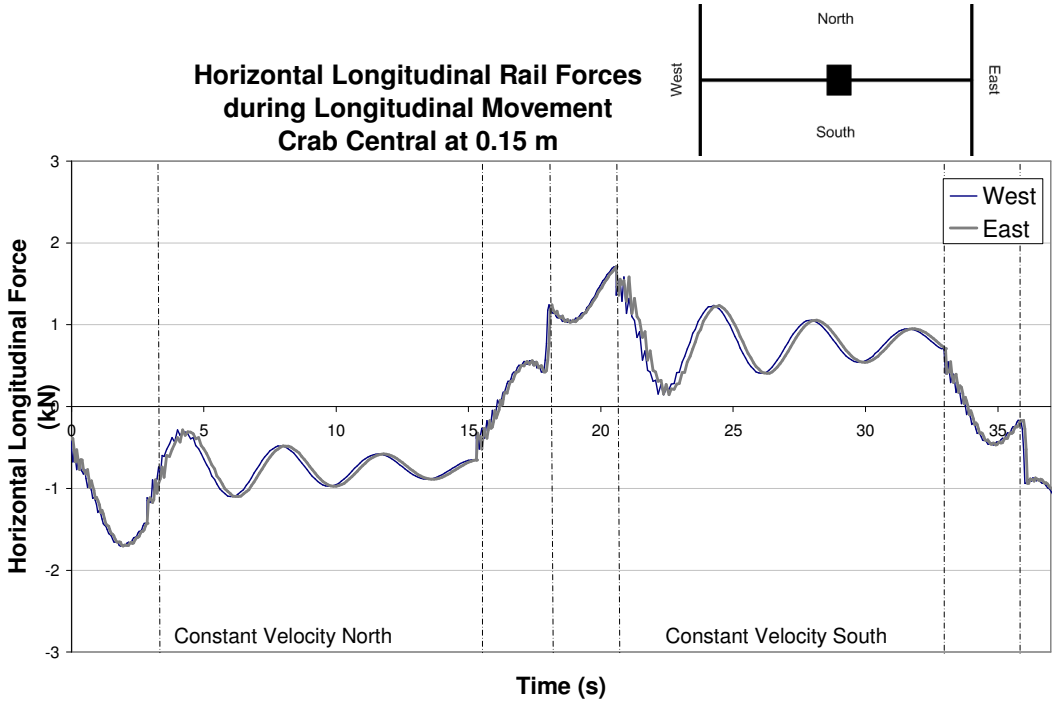

Figure 5-15: Horizontal Longitudinal Rail Forces for central crab with payload at 0.15 m

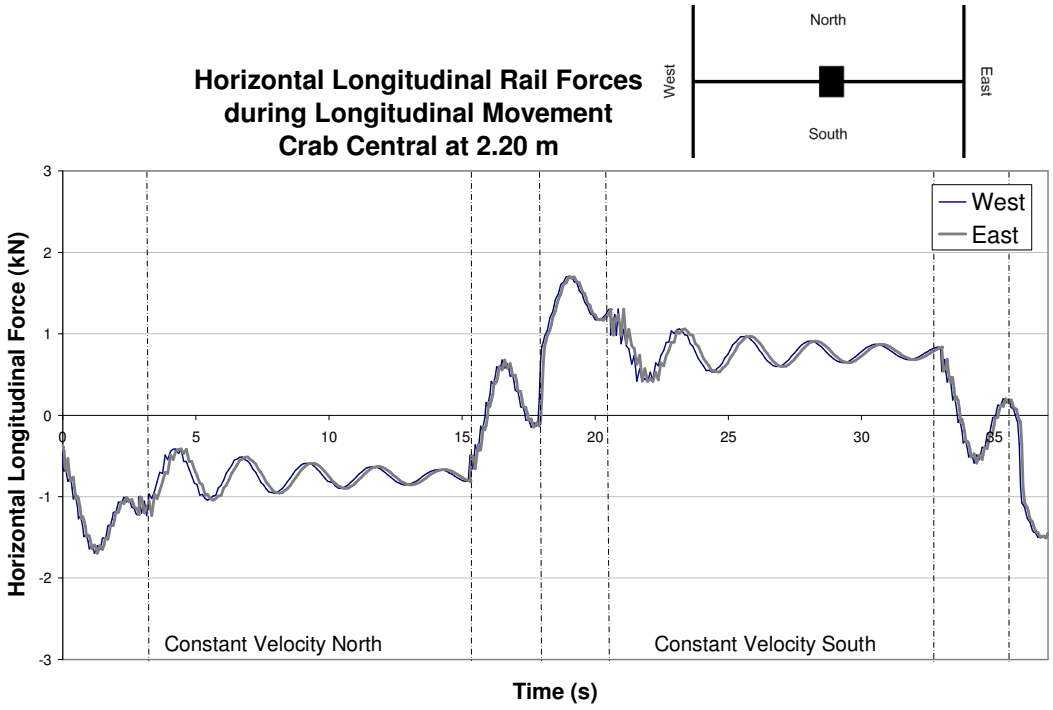

Figure 5-16: Horizontal Longitudinal Rail Forces for central crab with payload at 2.2 m

Eccentric Crab

When the crab is placed eccentrically a far greater difference in the longitudinal forces at the driving wheels is observed.

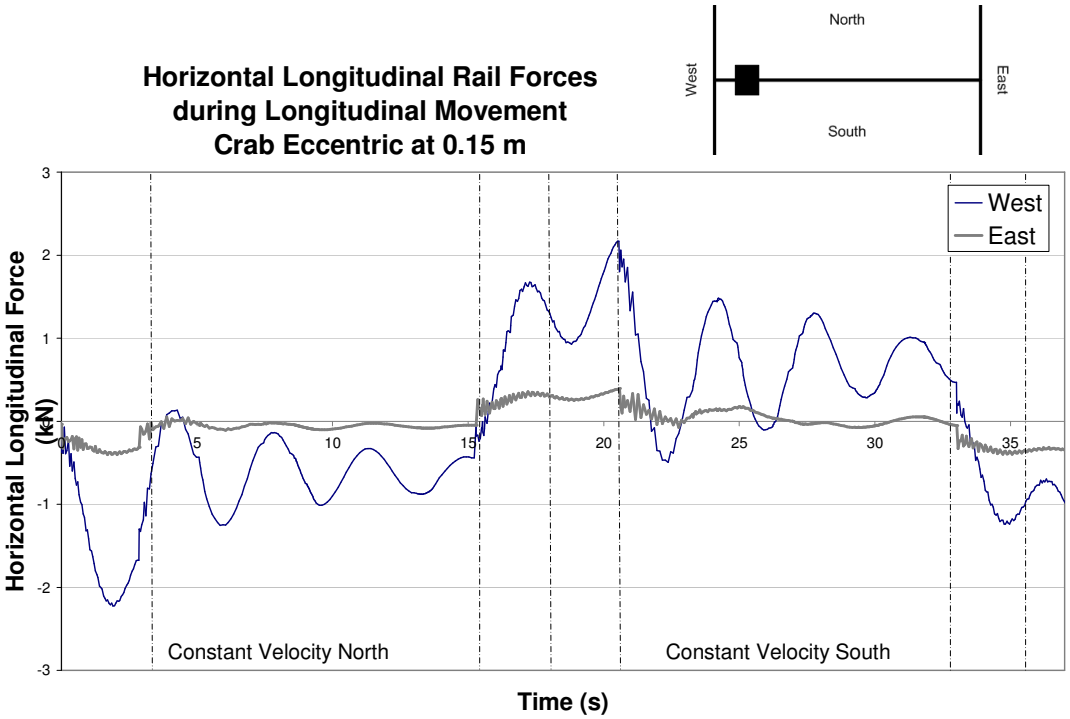

Figure 5-17: Horizontal Longitudinal Rail Forces for an eccentric crab with payload at 0.15 m

Normal Longitudinal Motion

The south-west wheel, as the driving wheel carrying most of the weight of the payload, requires considerably more force to maintain the set movement boundary conditions than the south-east wheel. It is also notable that the payload movement affects the west wheel far more than the east as is expected from the positioning of the payload. The maximum force experienced by the rail is 2.17 kN. This is slightly higher than the force of 2.13 kN experienced when the payload is at the top (Figure 5-18) and considerably higher than the maximum force of 1.31 kN experienced when the payload is central (Figure 5-15)

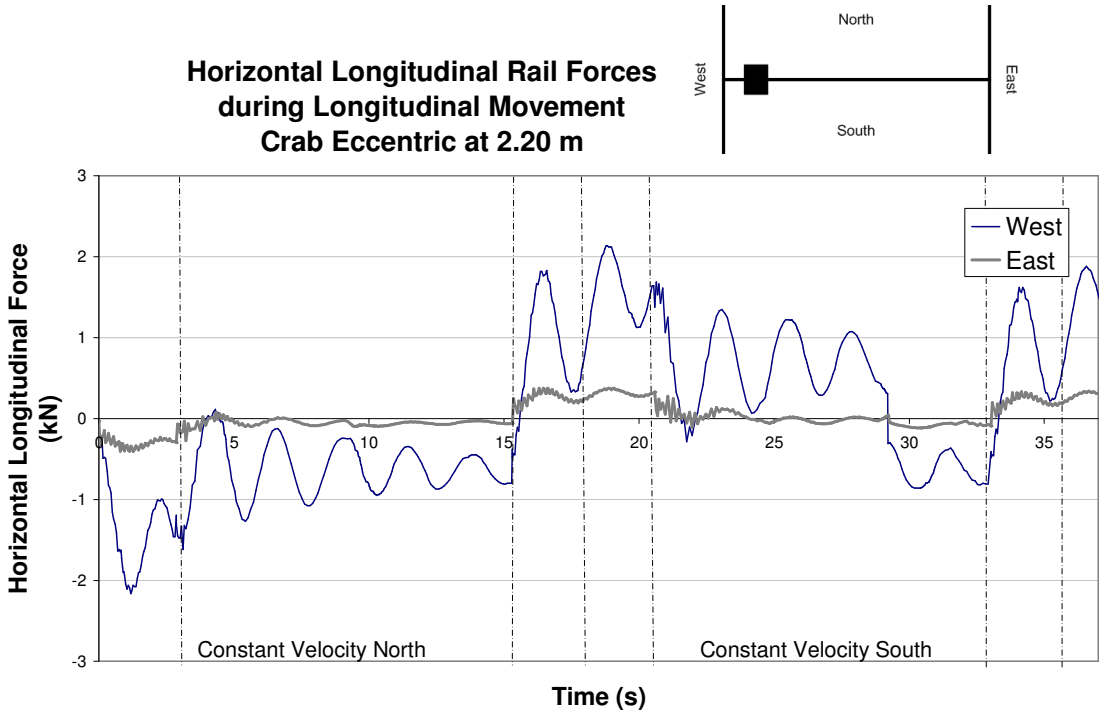

Figure 5-18: Horizontal Longitudinal Rail Forces for an eccentric crab with payload at 2.2 m

As with the other forces it is clearly apparent that the oscillations are of a much higher frequency when the payload is positioned at the top than at the bottom due to the shorter cable length.

5.6 Discussion

The maximum static wheel load for this crane is Q_v = 28.9 kN. According to the current South African code [1], an appropriate force to account for the acceleration and deceleration of the crane can be obtain by multiplying the maximum static wheel load by a factor of 0.1 and applying it longitudinally at each rail. This leads to a design force of 2.89 kN.

According to the Eurocode:

$H_{L,i} = \varphi_5 K/n_r$
$= 1.5* 3.82 *1/2$
$= 2.86$

The actual force experienced by each rail is a maximum of 2.17 kN according to the numerical model. This is considerably lower than the force estimation in both the South African code [1] and the Eurocode [2].

When regarding the code on crane loading factors as a whole, it is clear that in most cases the longitudinal force that needs to be taken through the crane beams into the bracing system is dominated by the impact on end stops loading case as covered by Trevor Haas in his doctoral thesis. This force far exceeds the force experienced as a result of the acceleration and deceleration of the crane as covered here. It is still important to note that the Eurocode on which the SABS draft loading code is based is overestimating the longitudinal forces involved during acceleration and deceleration of the crab.

5.7 Conclusion

The normal longitudinal travel of a crane does not lead to any dominant loading factors, but is essential to obtain an understanding of how the crane behaves.

When the payload is central the forces are mirrored for east and west whether one is considering the vertical, horizontal lateral or horizontal longitudinal forces. The wheels slide laterally once the crane begins to move and, as the gap between the wheel flange and the rail is only 2.4 mm on the crane, they slide the full gap and make contact with the rail. The wheels then remain against the rails for all northward and southward crane movement.

When the payload is eccentric, skewing occurs despite the synchronised motors. This is clear from the difference in lateral forces between the east and west wheels and the lateral movement of the crane. When the payload is at the bottom (0.15 m above the ground) the forces are larger and more movement occurs than when the payload is fully hoisted. With the

payload swinging at 0.15 m above the ground the flexing of the crane bridge and end carriages as the crane travels becomes more apparent.

When the payload is fully hoisted, the frequency of the vibrations of all forces (vertical, horizontal lateral and horizontal longitudinal) is higher than when the payload is just above the ground. This is an expected result due to the shortening of the payload cable and therefore higher frequency of oscillation of the payload itself. When fully hoisted the angle the cables form is greater with the higher payload and the pulley tends to run along cables rather than forcing the cables themselves to sway. As a result when the payload is at the top the graphs are generally smoother and more predictable with a higher frequency oscillation.

Whether the driving wheels are pushing or pulling the crane (northwards or southwards travel) makes minimal difference in the case of a central payload but considerable difference in the case of an eccentric payload where the crane is skewing.

The forces induced in the rails longitudinally due to the acceleration and deceleration of the crane reach a peak when the crab is eccentric. Here the maximum force reached is overestimated by the current South African code [1] and the current Eurocode [2] and hence will be overestimated by the draft South African code [3].

Longitudinal travel highlights some issues which become vital in the following load cases, such as lateral movement of the wheels, the extra skewing caused by the eccentricity of the payload and the flexibility of the crane itself. Although not resulting in a dominant load case it provides a useful insight into the behaviour of the crane.

6 MISALIGNMENT

Misalignment occurs when the crane wheels are not parallel to the rails. This could be due to a cant in the wheels or the rail. This situation often leads to the wheel flanges touching the rails and considerable wear on both. Large lateral forces, which must be designed for are also induced into the crane supporting structure.

The scenario where the crane rails are misaligned is the only situation considered here. The allowable tolerance on the rails is given by SANS 2001: CS1 in South Africa and prEN 1993-6 in the Eurocode. This tolerance allows for the rails to be misaligned either inwardly or outwardly and accordingly both cases are considered here in order to determine which leads to the most adverse forces.

This chapter analyses the Eurocode [2] and the current South African code's [1] approach to misalignment. It follows with the methods that were used to imitate misalignment in the laboratory and the numerical model, analyses the results obtained from the numerical model and compares them to the codes.

6.1 Codification

The current South African loading code [1] regards misalignment as one of the three leading causes of large horizontal loads on the crane structure. It is allowed for in Section 5.7.4b in the following manner:

A force P_1 is considered to be acting on each of the wheels as shown in Figure 6-1

$P_1 = (X*M) / N$

where: M = combined weight of the crane bridge, crab and payload
N = total number of crane travel wheels
X = 0.12 for a Class 2 crane

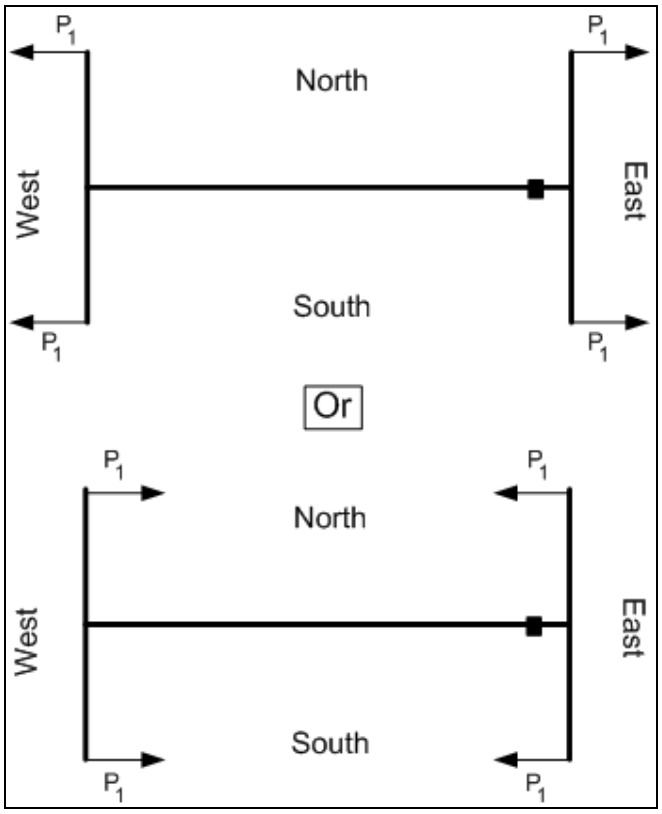

Figure 6-1: SABS diagram demonstrating the application of misalignment forces.

The Eurocode [2] does not allow for rail or wheel misalignment, assuming that the dominant lateral horizontal forces occur as a result of acceleration and deceleration of the crab or through skewing.

The draft new South African loading code [3], although using different terminology, follows the same method as used in the current South African code for calculating forces due to misalignment. Forces are applied at the wheels as in Figure 6-1 above.

6.2 Experimental Setup

As part of the experiments completed by Johan de Lange in the laboratory a threaded lateral support rod was positioned at the east rail above a column in order to induce outward and inward misalignment. This permitted a maximum misalignment of 15 mm to be induced into the rail. The position of this misalignment is shown in Figure 6-2 below.

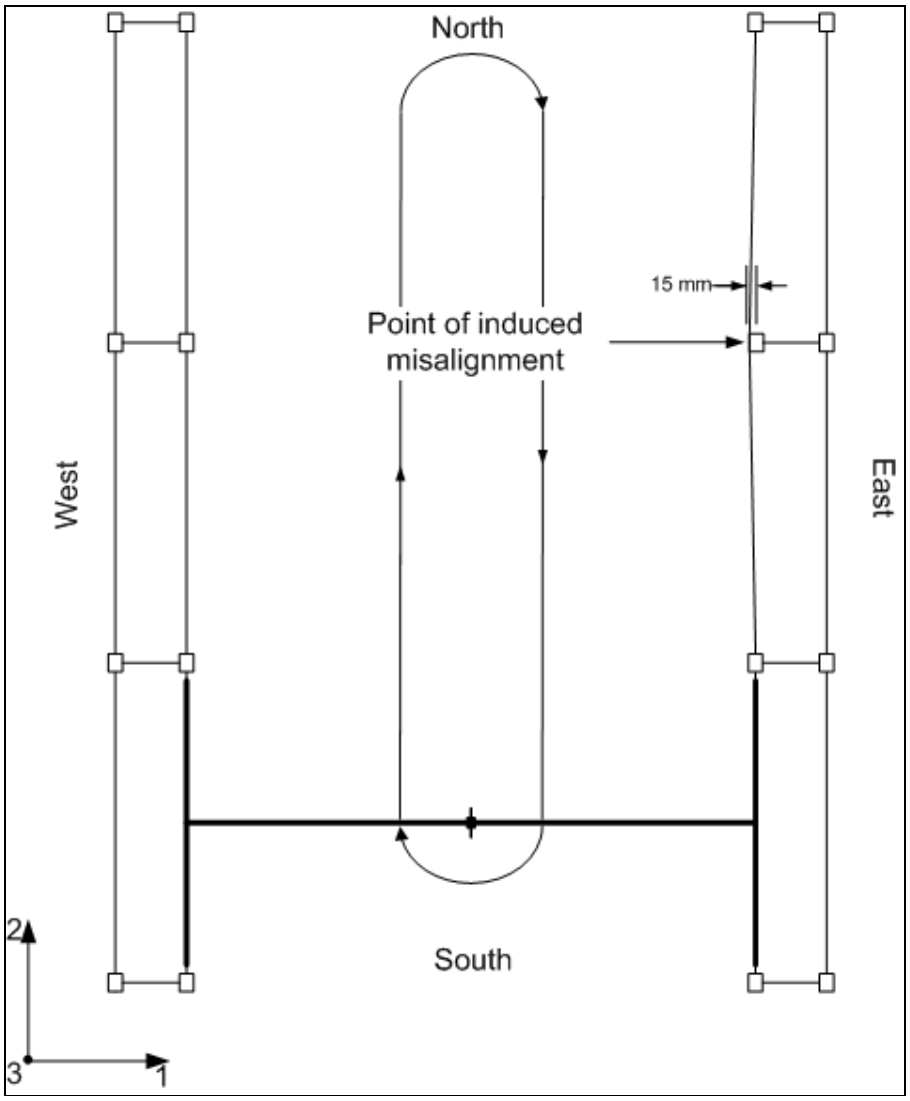

Figure 6-2: Plan of route taken by crane during misalignment showing the position of the induced misalignment.

The crane was positioned at the southernmost point of the rails and run north the full extent of the rails and returned south again. The wheels moved sufficiently far north so that both the north wheels and the south driving wheels passed the point of maximum misalignment. This method was followed to investigate whether a difference occurred between the driving and non-driving wheels when passing the point of misalignment. The effect of the direction of travel on the longitudinal forces induced at the wheels was also investigated.

These tests were conducted with the payload placed centrally, eccentrically west and eccentrically east, using the same acceleration, constant velocity and deceleration conditions as used in normal longitudinal travel.

6.3 Numerical Model

In the numerical model, the surface representing the crane rail was initially kinked inward by 15 mm. This was to correlate with the inward misalignment induced in the experimental setup. The beam elements providing the physical characteristics of the rail and crane girder were not altered. This allowed the rail surface to be moved without changing the line of the crane girder.

A problem associated with the use of finite elements in this context is the sharp angle that is induced in the model at the misalignment. In the experimental setup an enforced deviation pulls the steel rail into deflecting but it is achieved in a gentle manner with a gradual curve rather than a kink. In the numerical model the sudden change of angle of 0.0065 radians is induced as can be seen in Figure 6-3 below. It is possible to model this rail with a curved surface that accurately represents the experimental scenario but this requires a fine element mesh in the vicinity of the misalignment and substantially more connectors from the surface to the beam element modelling the physical properties of the rail and girder combination. This is a computationally intensive method and should only yield a slightly higher level of accuracy.

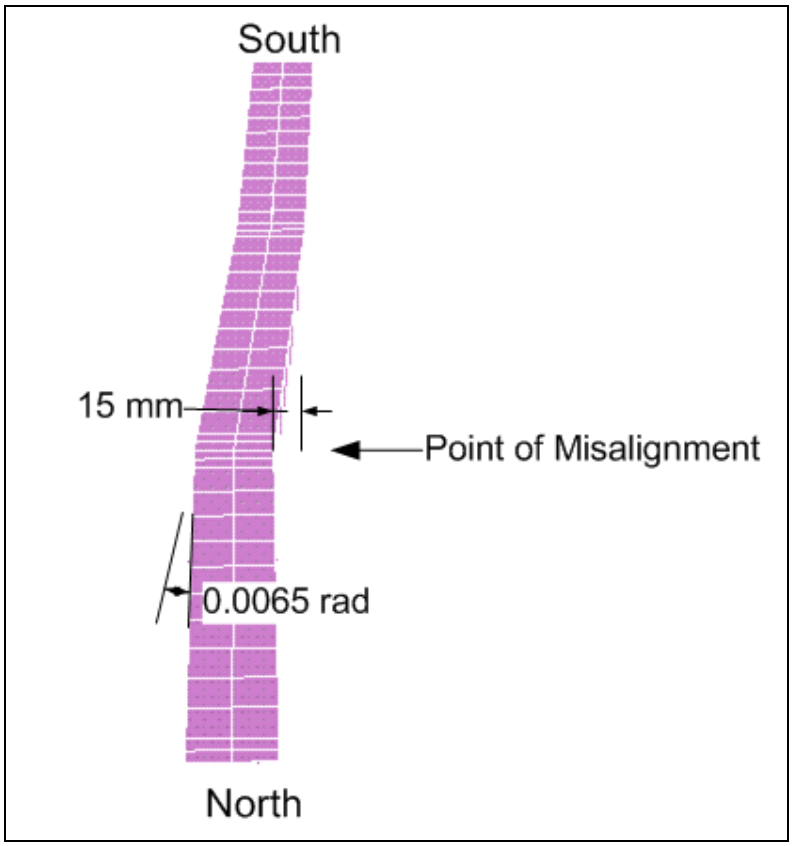

Figure 6-3: Looking South down the east rail in the finite element model. Point of outward misalignment indicated.

The wheel shape in the finite element model (Figure 3-9) has wheel flanges that are longer than the experimental flanges. This partially alleviates the problems induced by the kinked rail in the finite element model as it has a softening effect on the bend. The front edges of the wheel flanges in the numerical model touch the rail earlier than would occur in the experimental setup and hence the wheel starts to turn earlier. This causes the numerical results to have a close correlation with the experimental results despite the modelling errors.

Once the correlation with the experimental results was verified, several runs were analysed on the numerical model to examine the effect of the positioning of the crab and the height of the payload. All of these runs were repeated with the model adjusted to an outward misalignment to determine where the maximum horizontal lateral forces would occur.

Misalignment

6.4 Results

Results were obtained from the numerical model for inward and outward misalignment. Six sets of analyses were run for each case varying the height of the payload (0.15 m and 0.22m) and the position of the crab (Central, East Eccentric, West Eccentric). This provides a full spectrum of results for the misalignment case.

Only slight differences in results were found between the tests run with the payload at the top (2.2 m) and the payload at the bottom (0.15 m). Where the payload had a noticeable influence, it was always the payload at the bottom that was the dominant case. To simplify the presentation of results, the cases where the payload is fully hoisted are not discussed in detail here but a full set of graphs can be found in Appendix B.

Vertical wheel loads are covered in detail in Chapter 4 and, as the misalignment load case has little influence on the vertical forces, will not be discussed again here.

6.4.1 Horizontal Lateral Forces

Inwards Misalignment

For the purposes of inwards misalignment the east rail is moved west by 15 mm at one point.

Central Crab

As the crane starts to move the wheels slide laterally outwards towards the rails (Figure 6-4). This is part of the normal longitudinal travel of the crane. The north east wheel is the first wheel to experience the effects of misalignment. At time = 2.4 seconds the rail forces the north east wheel to move in a westerly direction. It continues to deflect an increasing amount until the point of maximum misalignment is reached (12.6 mm) at time = 10.3 seconds. Shortly before this point is the south east wheel, 4.26 m behind the north east wheel, reaches the start of the misaligned rail and begins to deflect west.

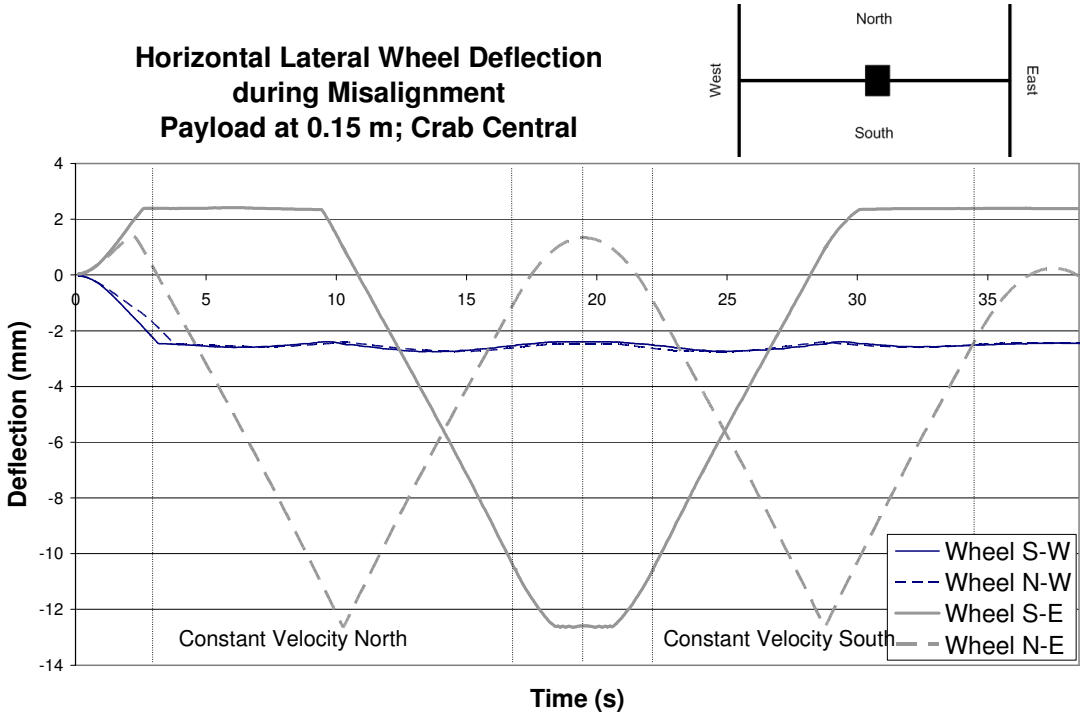

Figure 6-4: Horizontal lateral wheel deflection experienced at the wheels during inward misalignment with the payload at 0.15 m and the crab central on the bridge.

As the south east wheel reaches the point of maximum misalignment (time = 19.7 seconds) the north east wheel reaches the northernmost point of the rail and the crane starts to move south again. This process repeats itself for southward movement with the north east wheel moving past the point of maximum misalignment at time = 28.8 seconds.

Throughout this process the western wheels are forced outwards against their rail. As the misalignment moves the crane west, the west wheels are pressed against their rails so the force between the west wheel flanges and the rail flanges increases (Figure 6-5). When both eastern wheels are being affected by the misalignment, the forces at the western wheels remain relatively constant at 1.2 kN. The peak force in the eastern wheels is 2.12 kN, at the north east, non-driving wheel when the crane is moving south (time = 28.8 seconds).

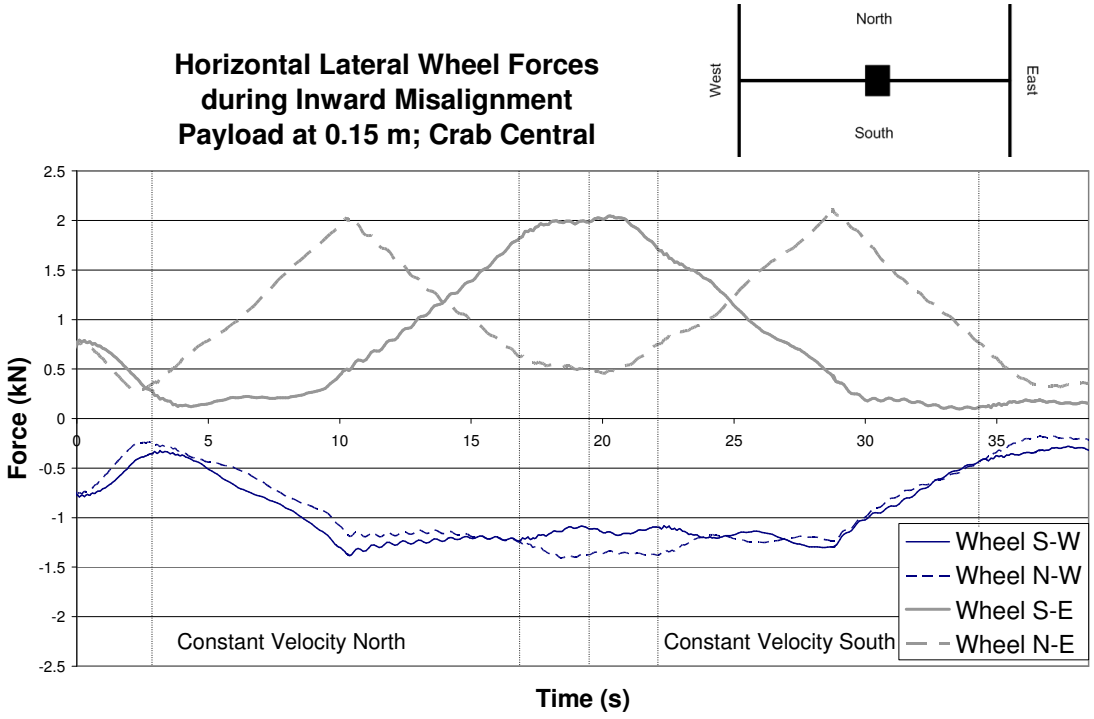

Figure 6-5: Horizontal lateral forces experienced at the wheels during Inward Misalignment the payload at 0.15m and the crab central on the bridge.

Crab West Eccentric

As the crane starts to move the eastern wheels, only lightly loaded as the crab is eccentric on the western side of the bridge, move outwards rapidly as per normal longitudinal travel (Figure 6-6). At time = 2.55 seconds the north east wheel reaches the start of the misalignment and starts to move west. The remaining wheel deflections closely follow the pattern of the central crab with two minor exceptions. At time = 7 seconds and time = 24.4 seconds there are two anomalies. These are caused by the lateral swinging of the payload and will be discussed in greater detail under outward misalignment.

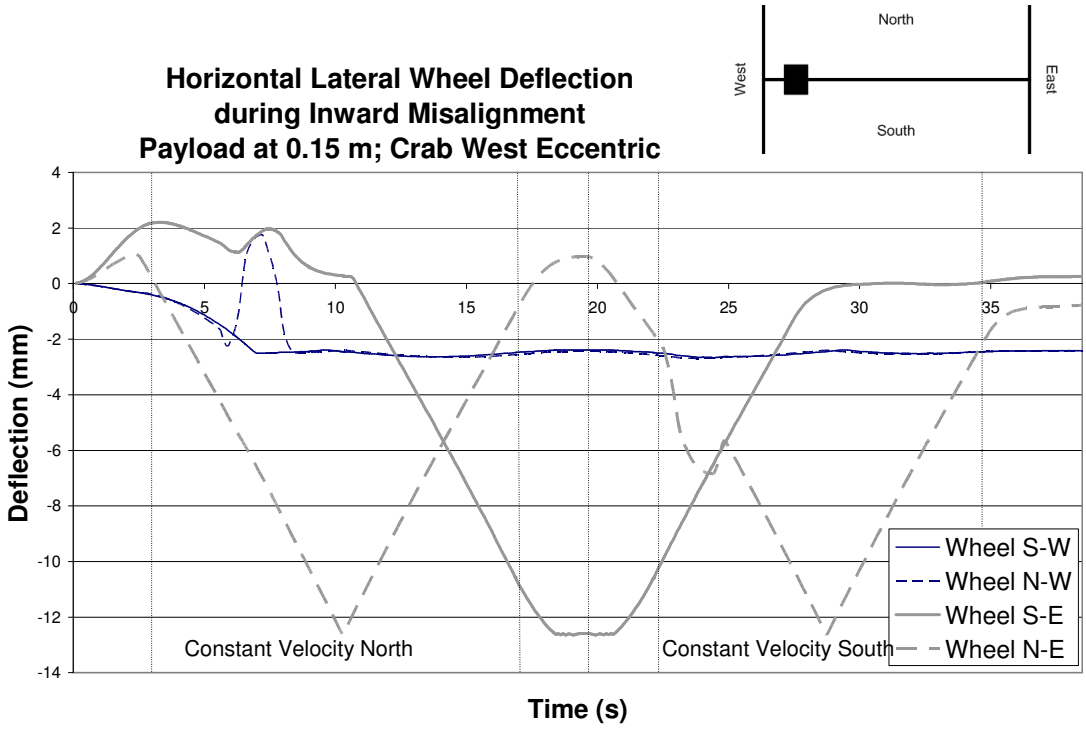

Figure 6-6: Horizontal lateral deflection experienced at the wheels during inward misalignment with the payload at 0.15 m and the crab placed eccentrically West on the bridge.

The forces are observed to follow a similar pattern to the case with a central crab (Figure 6-7). Where the anomaly is visible in the deflections it is apparent that a jump in forces also occurs. From this one can see that although only the north west wheel moves substantially, all wheels, with the exception of the south west wheel, experience a rapid change in force, although this is slight in comparison to the magnitude of the forces considered throughout the misalignment case.

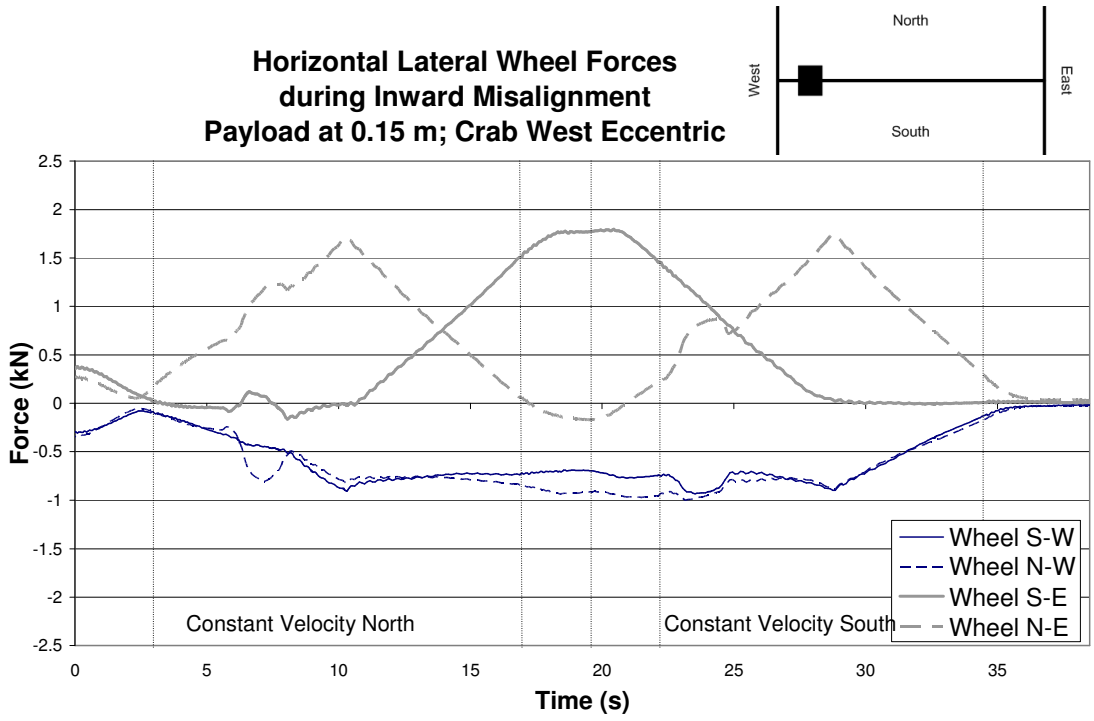

Figure 6-7: Horizontal lateral forces experienced at the wheels during inward misalignment with the payload at 0.15m and the crab placed eccentrically West on the bridge.

The maximum force (1.78 kN) occurs at the south east wheel as the crane turns and starts to run in a southerly direction. This is only slightly larger than the force (1.75 kN) that occurs at the northern wheel on the south section of the crane's run.

Crab East Eccentric

When the crane starts to move, the wheels initially behave in the same way as with the crab eccentric on the west side of the crane. The lightly loaded, west wheels move out to the rails (Figure 6-8). The misalignment induces movement in the north east wheel at time = 2.4 seconds. The remainder of the deflection graph then follows the pattern of the central crab. Before the south east wheel starts to be affected by misalignment it moves east. This is induced by the skewing of the east endcarriage as the north wheel is forced west by the misalignment. This graph shows none of the payload related anomaly seen with the west eccentric crab as the payload is now closely situated to the rail that is misaligned.

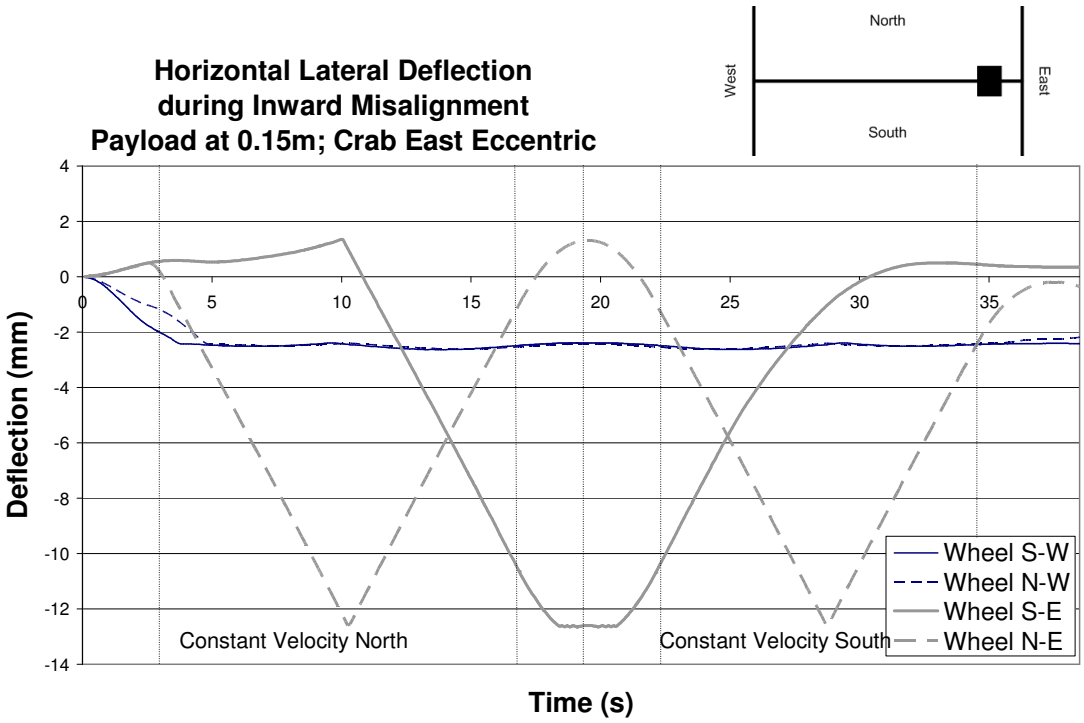

Figure 6-8: Horizontal lateral deflection experienced at the wheels during inward misalignment with the payload at 0.15 m and the crab placed eccentrically east on the bridge.

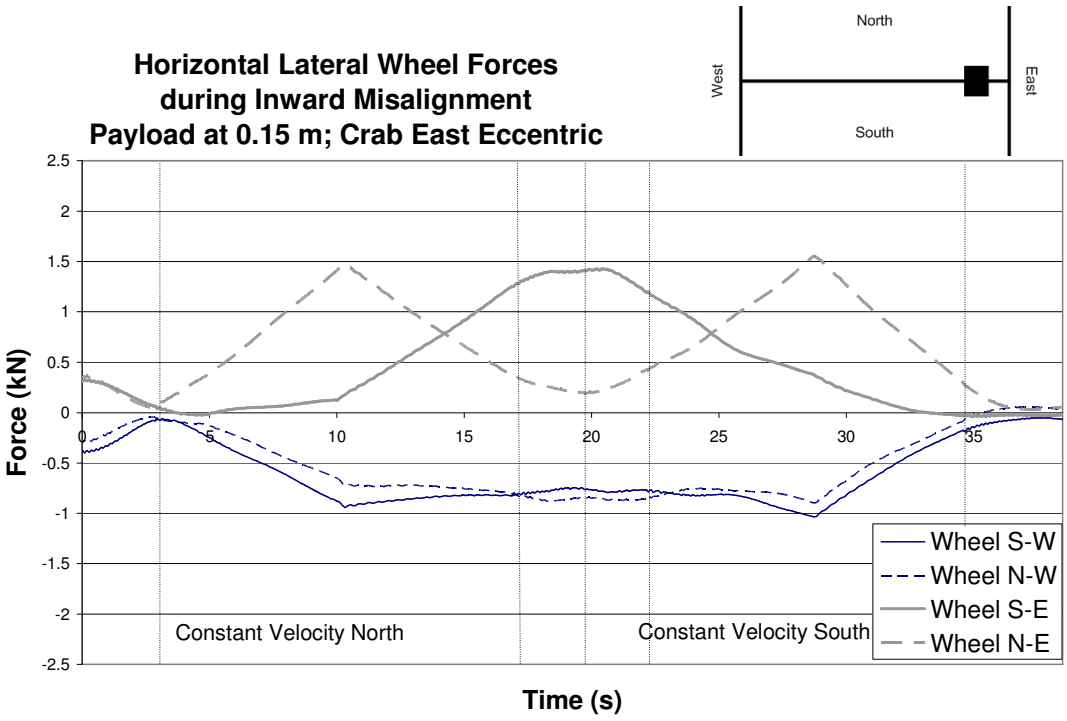

Figure 6-9: Horizontal lateral forces experienced at the wheels during inward misalignmet with the payload at 0.15 m and the crab placed eccentrically east on the bridge.

It is observed that the maximum force (1.56 kN) occurs at the north east wheel when the crane is moving south (time t = 28.8 seconds, Figure 6-9). This is slightly higher than the force (1.45 kN) at the north east wheel during the northern section of the crane's run and the force (1.42 kN) at the south east wheel as the crane starts to move south. The forces at the west wheels remain steady during misalignment with an average force of 0.81 kN.

All of the above results for forces due to inward misalignment include the static outwards lateral forces that exist due to the dead weight of the payload and the crane (0.76 kN per wheel for a central crab and 0.33 kN per wheel for an eccentric crab). If these initial forces are removed so the forces due to inward misalignment alone are considered, the maximum forces are as follows:

Central Crab:	1.36 kN
Eccentric West Crab:	1.45 kN
Eccentric East Crab:	1.23 kN

It can be observed that the further away the crab is from the rail with misalignment, the greater the lateral force that is induced into the rail by the wheels.

Outward Misalignment

In outward misalignment the east rail is moved east by 15 mm at one point.

Central Crab

As the crane starts to move, all wheels slide laterally outwards to their rail as per normal longitudinal motion (Figure 6-10). The start of the misalignment is felt at time t = 2.36 seconds. At this point the north east wheel continues to move east with the misaligning rail. This wheel reaches its peak deflection at time t = 10.36 at the point of maximum misalignment before returning to normal travel. Shortly before the north east wheel reaches its first peak the effects of the misalignment are felt by the south east wheel. This wheel has maximum misalignment at time t = 19.08 seconds. After the south east wheel has passed the point of maximum misalignment the crane stops moving north and starts to move south (time t = 19.4 seconds). The process is then repeated for southbound travel.

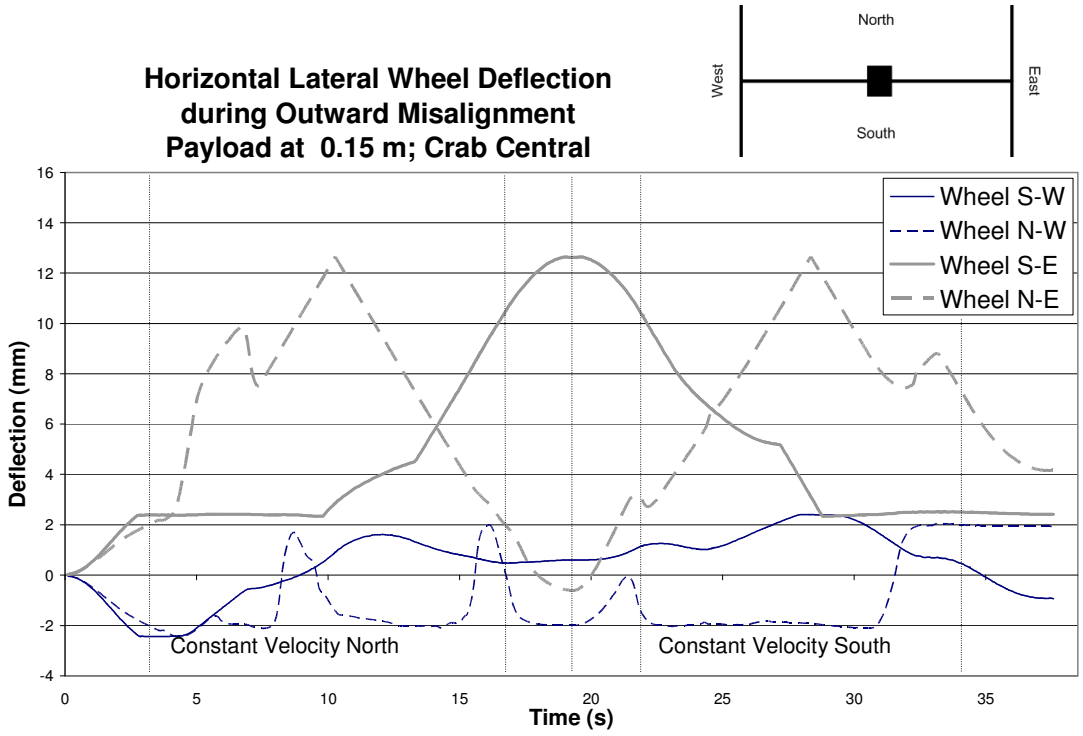

Figure 6-10: Horizontal lateral deflection experienced at the wheels during outward misalignment for the payload at 0.15 m and the crab central on the bridge.

The west wheels behave in a less predictable manner than in inward misalignment. One would expect both west wheels to move east, following the east wheels as they are forced outwards by the rail misalignment. When the crab is centrally placed the initial lateral horizontal forces outwards at the wheels from the weight of the payload and the crane are considerably larger than when the crab is placed eccentrically. These forces counteract the forces induced by the misalignment and as such the west wheels do not move east. The driving south west wheel, which was observed as being more stable in the case of longitudinal motion, does not touch either flange while the non-driving, north wheel remains pressed outwards against the eastern flange of the rail as per normal longitudinal motion.

The anomalies that can be seen at time $t = 6.76$ seconds and time $t = 33.22$ seconds are induced by the swinging of the payload in the lateral direction. As the east rail misaligns, the payload follows the motion of the crane with a slight delay and starts to swing east. When the payload is at the maximum lateral displacement from the midpoint of the crane bridge, it pulls the crane in the easterly direction and causes the rapid movement visible in the displacement graph. This can be clearly seen in Figure 6-11 which demonstrates the lateral deflection of the payload and the midpoint of the crane bridge over time.

Misalignment

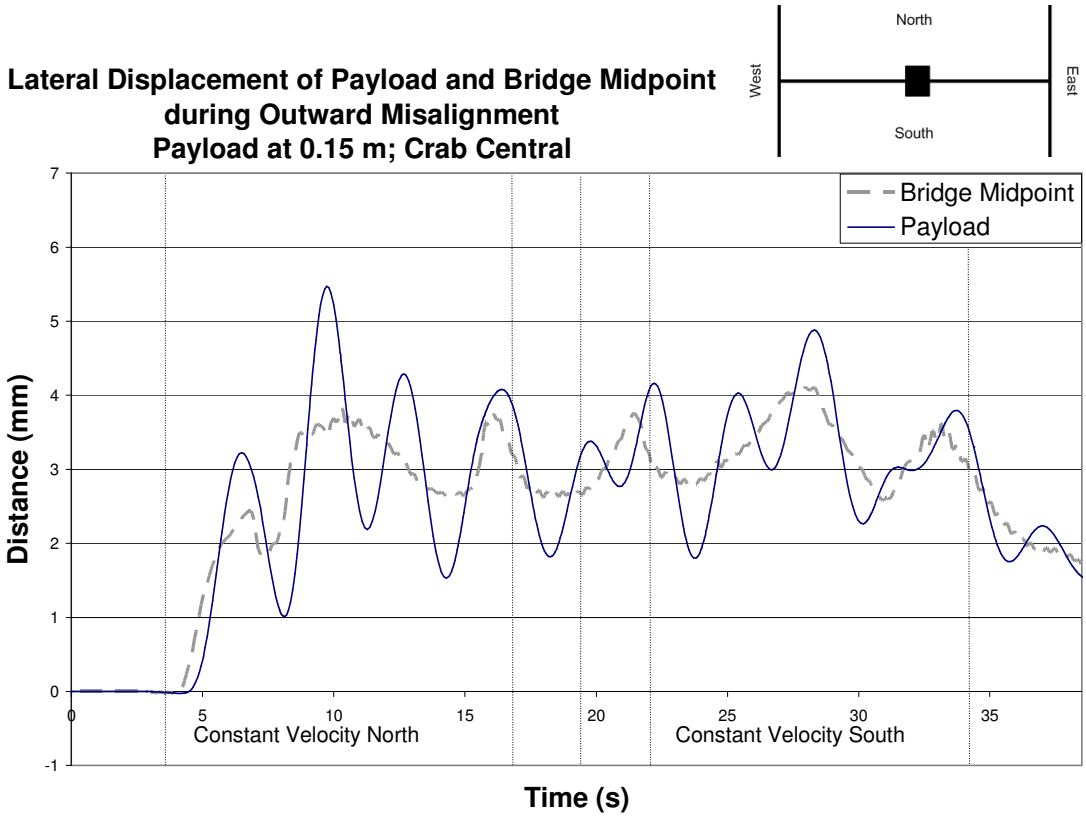

Figure 6-11: Lateral deflections experienced at the payload and the midpoint of the crane bridge during outward misalignment for the payload at 0.15 m and the crab central on the bridge.

The graph of lateral horizontal wheel forces (Figure 6-12) also reflects the anomaly caused by the swinging of the payload as can be seen by the force peak at time t = 6.76 seconds and the slight shift in forces at time t = 33.22 seconds. For the remainder of the time the forces behave in a predictable manner. The greatest force experienced (1.06 kN) is in a westerly direction at the south east wheel when it is at the point of maximum misalignment. The south west wheel experiences little force throughout the movement of the crane with the lateral force outward due to the dead weight of the payload being counteracted by the force of the crane attempting to move east with the outward misalignment. The north west wheel has a relatively constant force of approximately 0.40 kN acting in an easterly direction on it throughout the majority of the misalignment. The east wheels take the majority of the lateral forces with the north wheel and south wheel forces counteracting each other as the east endcarriage resists excessive bending.

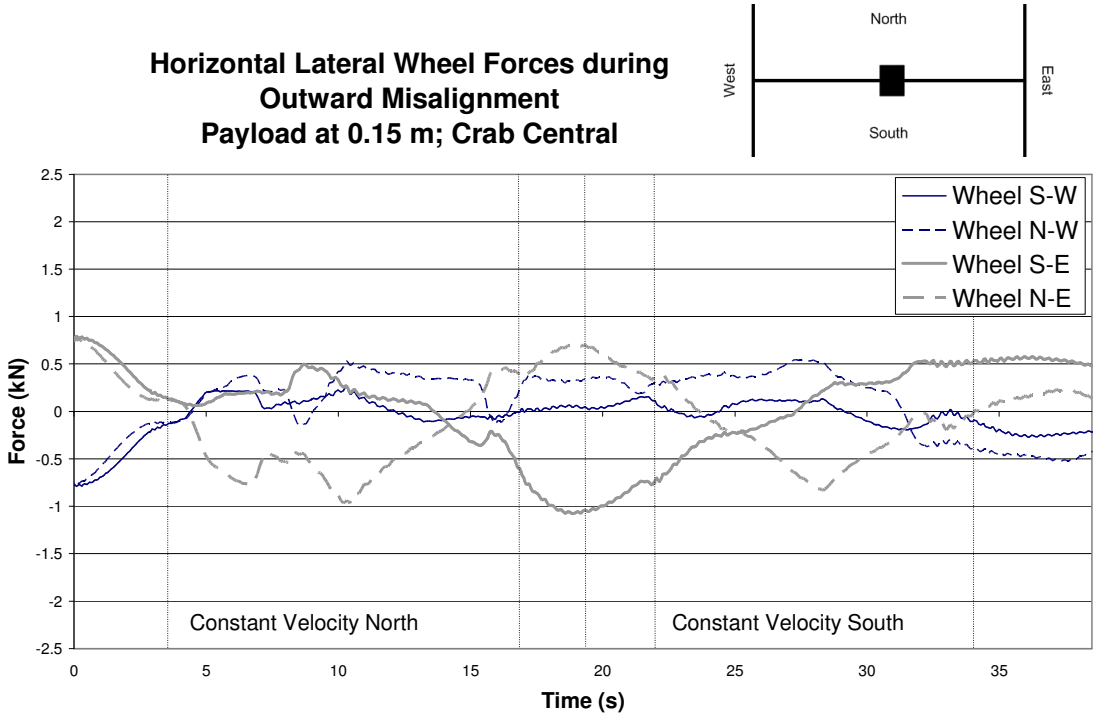

Figure 6-12: Horizontal lateral forces experienced at the wheels during outward misalignment for the payload at 0.15 m and the crab central on the bridge.

Crab West Eccentric

When the crab is positioned on the west of the bridge the results are smoother than the scenario with a central crab (Figure 6-13). As the crab is on the opposite side of the bridge from the misaligned rail, the payload does not experience a sudden lateral movement at the start of the misalignment and as such there are fewer anomalies in the wheel movement. Both west wheels are forced, by the outward misalignment of the east rail, to the east for the duration of the misalignment. The peak deflection when the south east wheel reaches the point of maximum misalignment (t = 19.06 s) is slightly rounded as the crane is already in the process of decelerating.

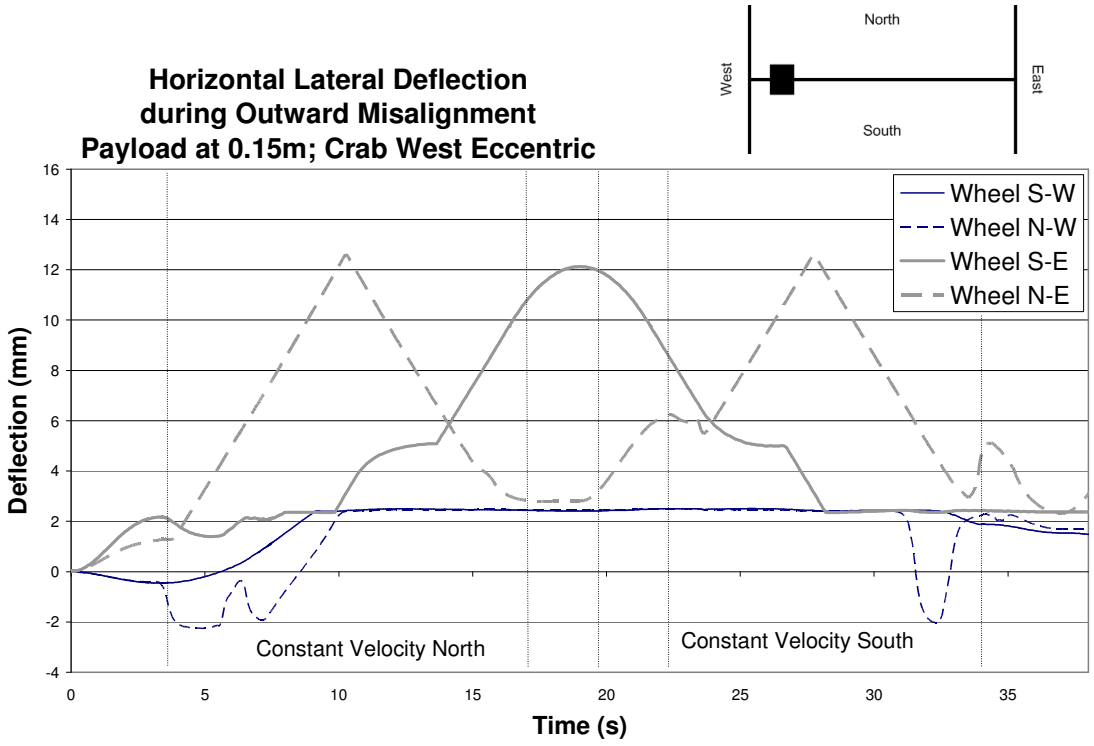

Figure 6-13: Horizontal lateral deflections experienced at the wheels during outward misalignment for the payload at 0.15 m and the crab placed eccentrically west on the bridge.

The forces decrease from their static loading as the crane starts to move (Figure 6-14). As the north east wheel is forced east by the misalignment the force increases. The forces at the remaining three wheels counteract the misalignment force. As the force at the north east wheel starts to decrease the force at the south east wheel increases as the east wheels run over the misalignment. The west wheels remain constant through this change so the forces at all four wheels remain in equilibrium. The largest force experienced is 1.16 kN in a westerly direction at the north east wheel during northward motion.

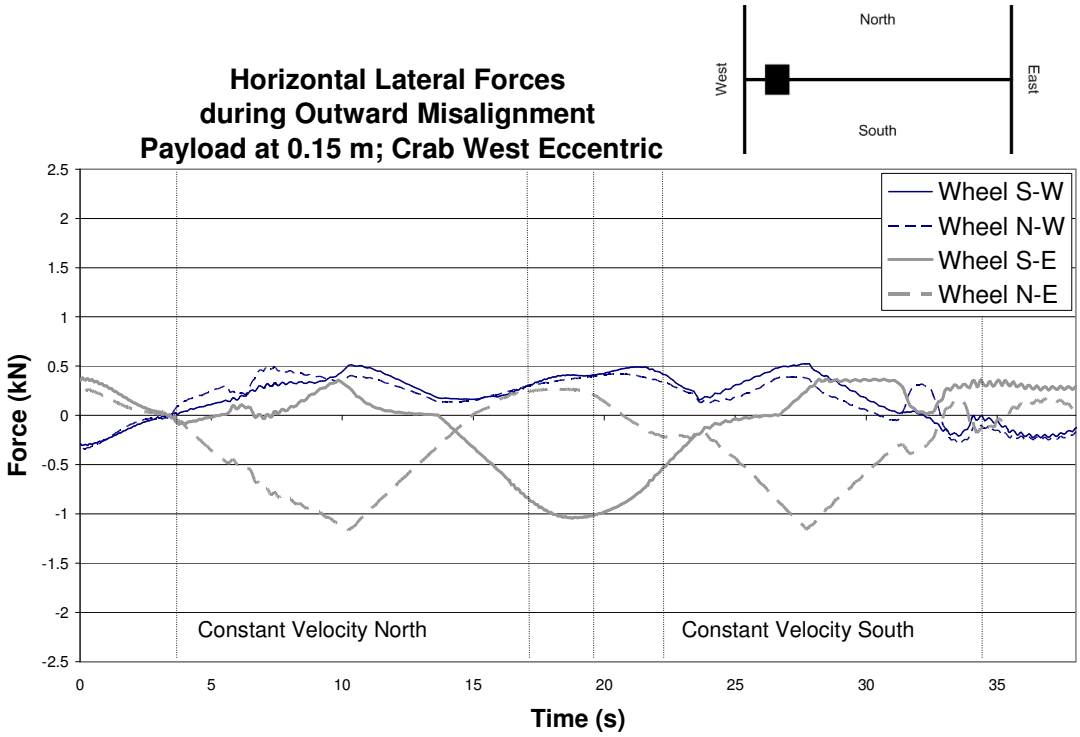

Figure 6-14: Horizontal lateral forces experienced at the wheels during outward misalignment for the payload at 0.15 m and the crab placed eccentrically west on the bridge.

Crab East Eccentric

For the first 15 seconds of crane travel, the deflections at the wheels are as expected (Figure 6-15). The north east wheel starts to move east as the rails misalign and as the misalignment increases the remaining wheels also move to the east. After 15 seconds there is an anomaly, again caused by the oscillation of the payload in the lateral direction (Figure 6-16). At this point the forces on the wheels are small and the payload oscillations have a noticeable effect on the forces at all wheels. As the north east wheel is the only wheel without its west flange pressed against the rail, it is the only wheel capable of moving east. As a result it is the only obvious deflection that occurs.

A similar effect occurs from time t = 22.9 seconds to t = 28.8 seconds. Here the payload is oscillating on the east of the midpoint of the crane, attempting to pull the crane east. All wheels except the north east wheel already have their west flanges against the rails and hence are prevented from moving east. The north east wheel is the wheel that is being forced east by the misalignment so it is pressing against the east of the rail. It is therefore free to move a maximum of 4.8 mm in an easterly direction in reaction to the swinging payload.

Misalignment

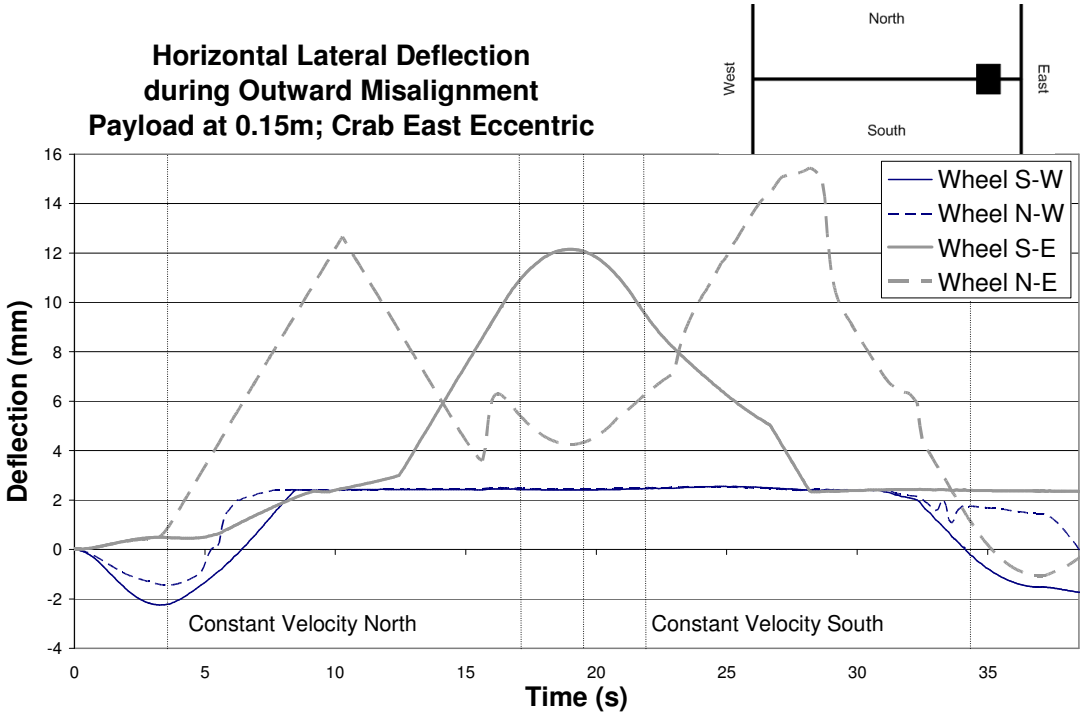

Figure 6-15: Horizontal lateral deflections experienced at the wheels during outward misalignment for the payload at 0.15 m and the crab placed eccentrically east on the bridge.

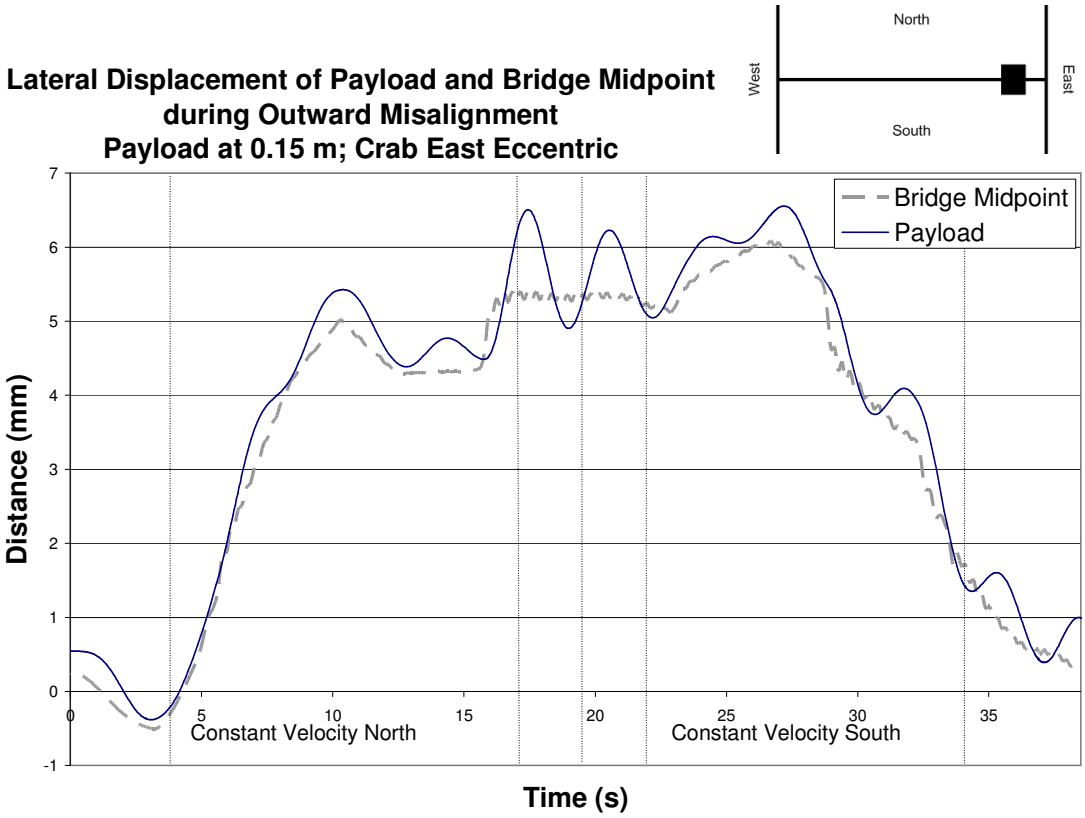

Figure 6-16: Lateral deflections experienced at the payload and midpoint of the crane bridge during outward misalignment for the payload at 0.15 m and the crab placed eccentrically east on the bridge

When the forces are considered (Figure 6-17), it is clear that the maximum horizontal lateral force (1.17 kN) occurs at the north east wheel when the crane is moving south. This corresponds with the point of maximum deflection. The west wheels consistently counteract the forces induced by the misalignment in the east wheels. The increase in forces due to the swinging of the payload at time t = 15.6 seconds and from time t = 22.9 seconds to t = 28.8 seconds is apparent at all wheels despite the fact that only the north east wheel was able to deflect substantially under these loads.

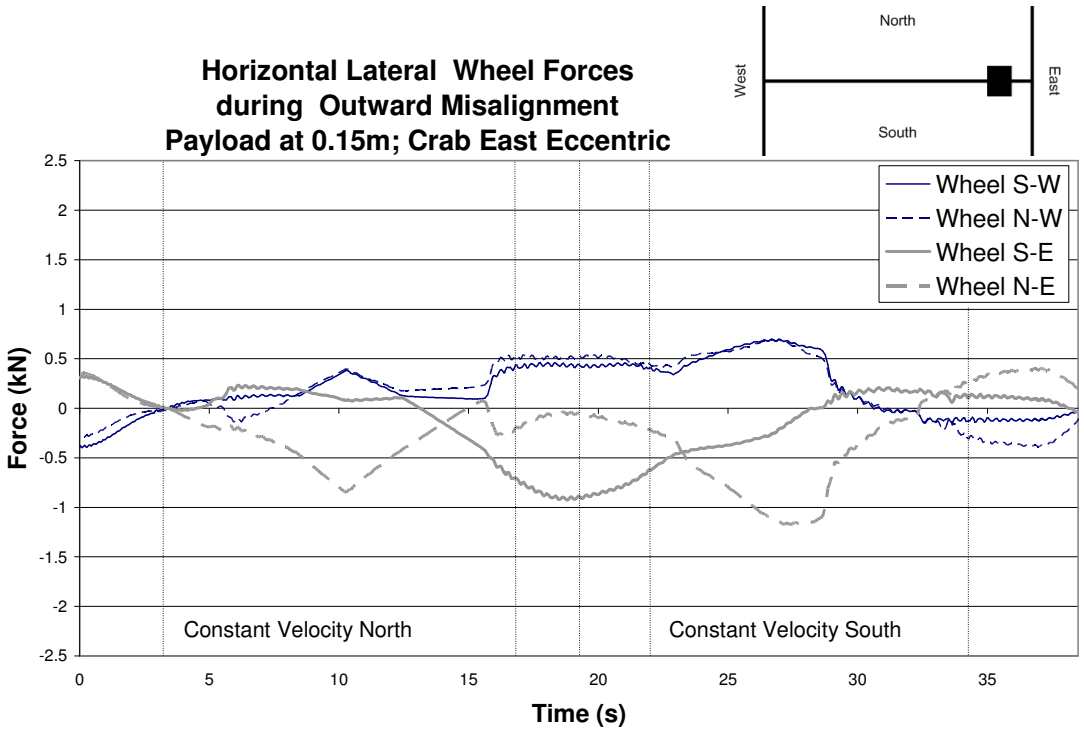

Figure 6-17: Horizontal lateral forces experienced at the wheels during outward misalignment for the payload at 0.15 m and the crab placed eccentrically east on the bridge.

6.4.2 Horizontal Longitudinal Force

Inwards Misalignment

The largest forces induced longitudinally into a rail occur when the payload is closest to that rail. The central crab cannot cause the dominant longitudinal force and as such is not considered in detail here.

The closest motor must account for the extra weight on the wheels as well as most of the forces caused by the swinging of the payload. The motor further away from the payload is only propelling the endcarriage so the forces are considerably more uniform with few oscillations. When the two graphs (west and east) below, are considered, it is clear that the largest longitudinal force experienced is in the west rail when the crab is eccentrically west on the crane bridge. This force (2.73 kN) occurs at time = 22.1 seconds when the crane is in the process of accelerating south.

When the crab is eccentrically east, the east motor does the majority of the work but the misalignment helps to counteract the skewing naturally induced by the eccentric crab. The

crane is attempting to rotate in a clockwise direction under the influence of the eccentric payload but the inward misalignment is forcing the crane to rotate anti-clockwise. When the crab is eccentrically west, the misalignment enhances the effect caused by the eccentric payload and as a result the driving forces required are larger.

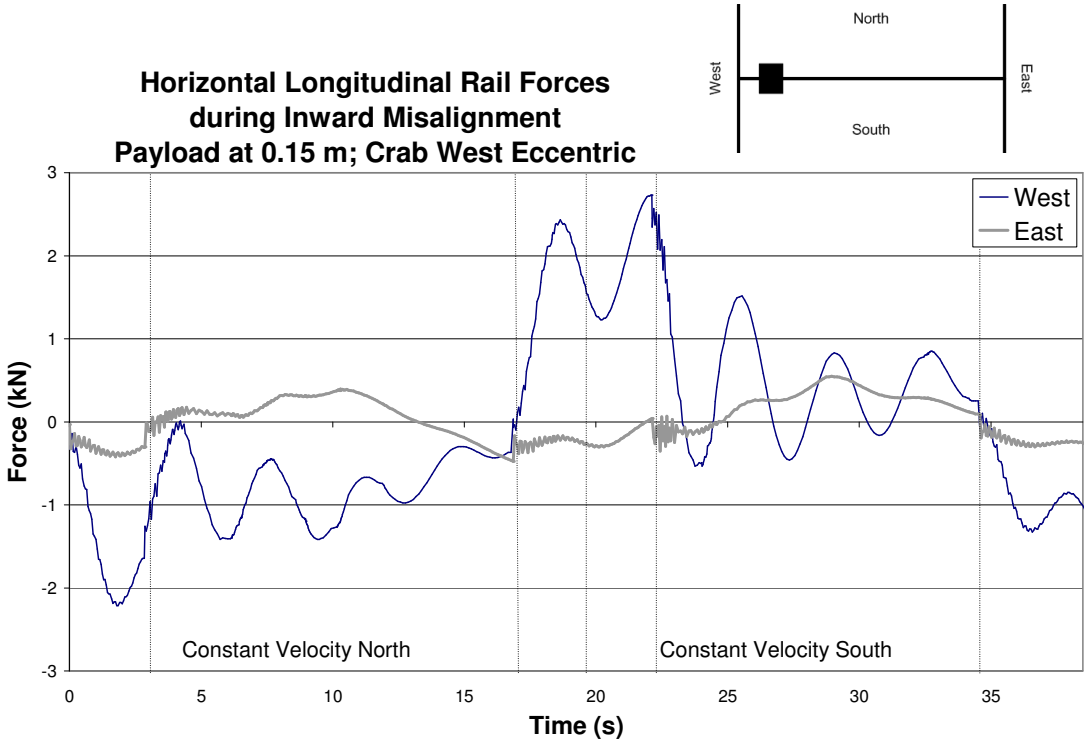

Figure 6-18: Horizontal longitudinal forces experienced at the rail during inward misalignment with the payload at 0.15 m and the crab placed eccentrically on the west of the crane bridge.

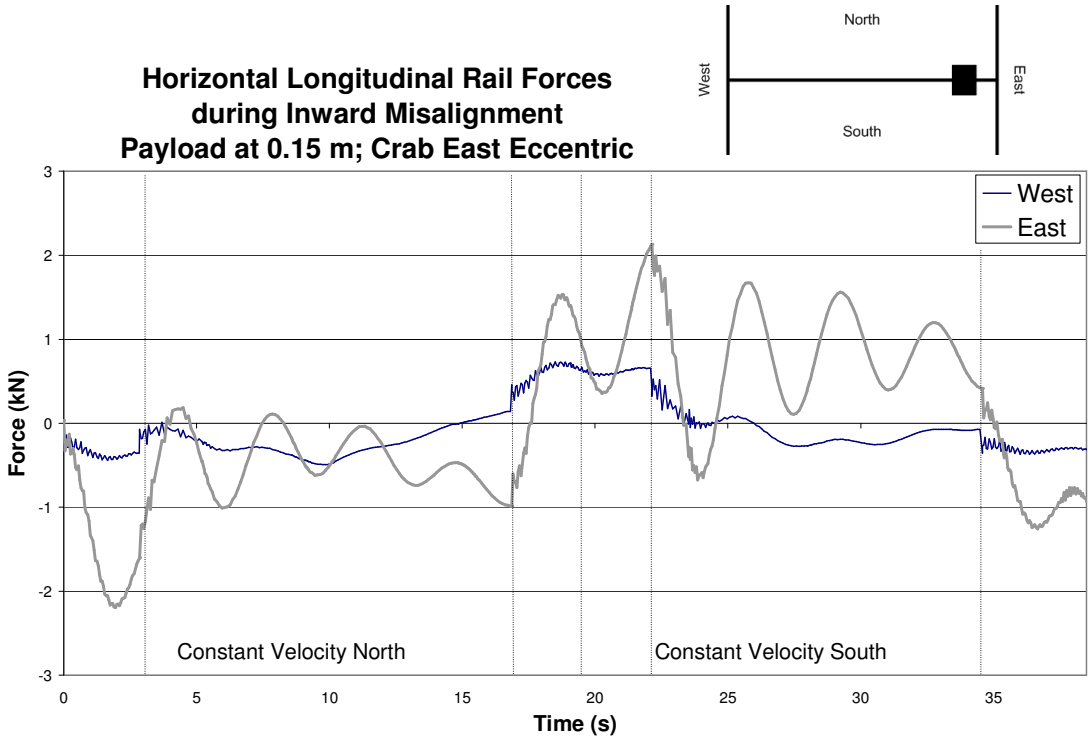

Figure 6-19: Horizontal longitudinal forces experienced at the rail during inward misalignment with the payload at 0.15 m and the crab placed eccentrically on the east of the crane bridge.

Outward Misalignment

While the eccentric crab cases remain the most critical for determining the longitudinal forces induced into rails, the more dominant case is the reverse of inward misalignment. When the crab is positioned on the west of the crane bridge, the natural tendency of the crane is to skew in an anti-clockwise direction during northward travel. As the east rail, misaligned outward, is trying to force the crane to skew in a clockwise direction, these two effects partially cancel each other out (Figure 6-20).

When the crab is on the east side of the crane bridge the skewing and misalignment forces are complementary resulting in a greater difference in east and west rail forces than those found when the crab was eccentrically west on the crane bridge (Figure 6-21). The maximum longitudinal force induced into the rails is 2.47 kN into the east rail at 22.6 seconds.

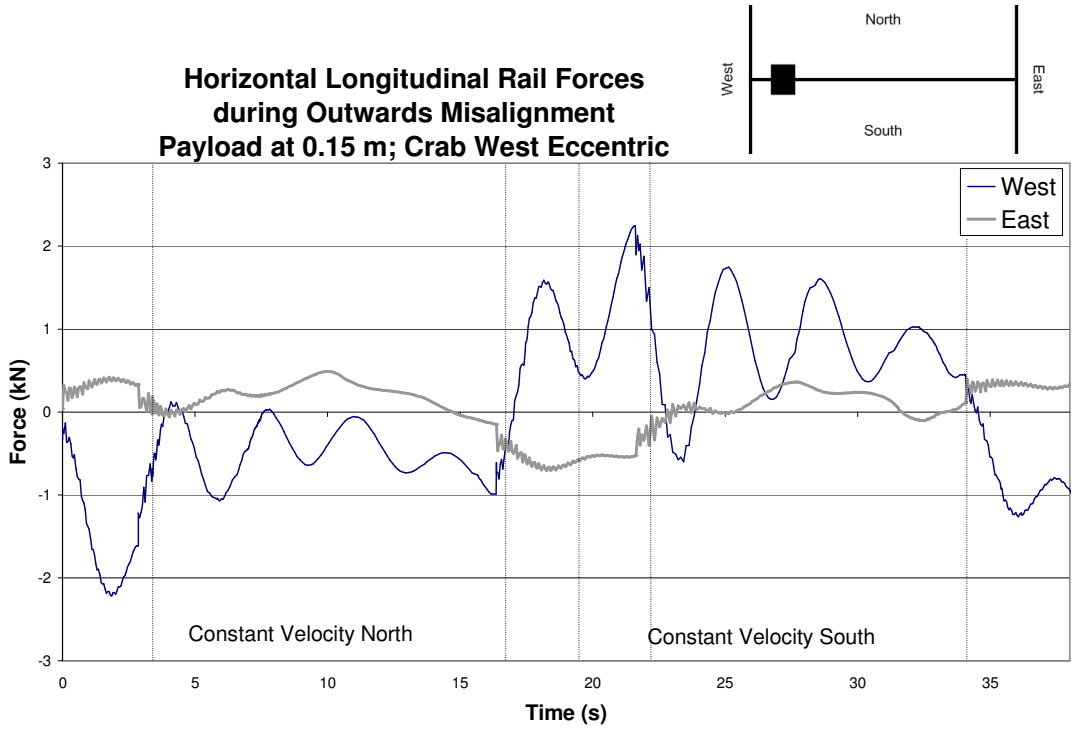

Figure 6-20: Horizontal longitudinal forces experienced at the rail during outward misalignment with the payload at 0.15 m and the crab placed eccentrically on the west of the crane bridge.

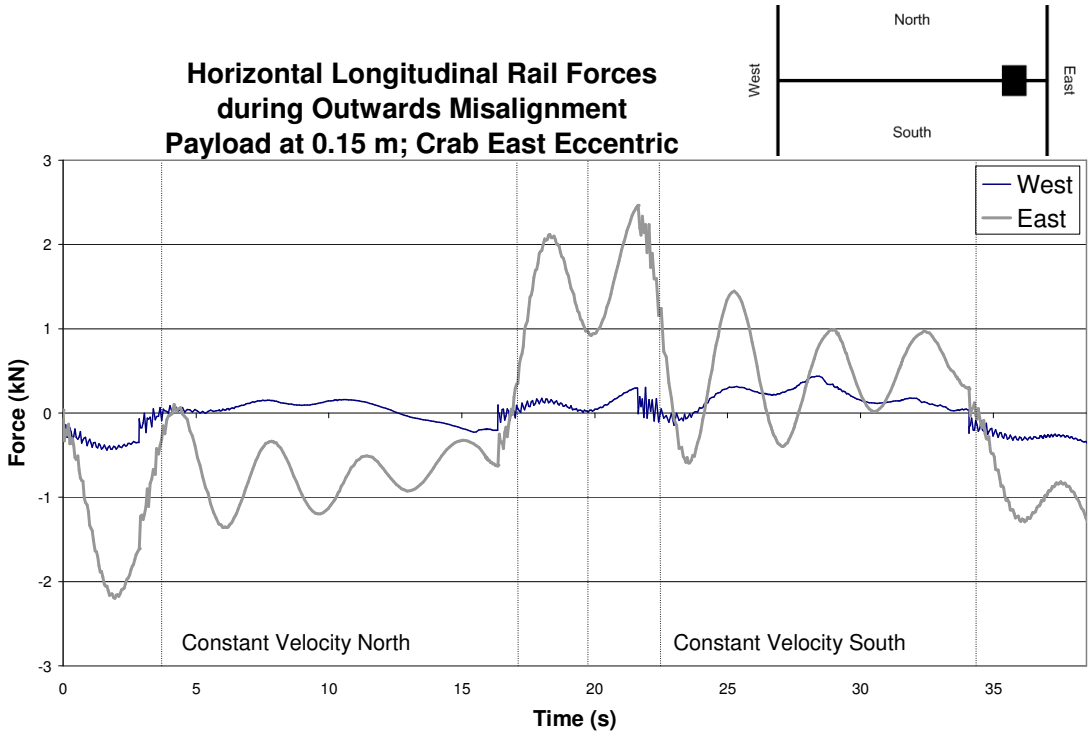

Figure 6-21: Horizontal longitudinal forces experienced at the rail during outward misalignment with the payload at 0.15 m and the crab placed eccentrically on the east of the crane bridge.

6.5 Discussion

The largest horizontal force experienced during misalignment is 2.11 kN during inward misalignment with a central crab (Figure 6-5). According to both the current South African loading code [1] and the draft South African code [3], the horizontal lateral force that should be designed for as a result of misalignment is 2.13 kN (inwards or outwards) at each wheel.

Although appearing only slightly higher in magnitude than the largest force from the numerical results, this design value is in fact considerably higher, as it occurs at each wheel as opposed to the numerically calculated forces in Figure 6-22. The highest force to occur at all wheels simultaneously is only 1.27 kN (Figure 6-5).

Allowing for a design force of 2.13 kN at each wheel is conservative, especially as misalignment is often the dominant case for design lateral loading. It would be inappropriate to assume that a force of only 1.27 kN acted at each wheel as, although it is accurate for the crane as a whole, it underestimates the peak lateral force that can be experienced at one wheel.

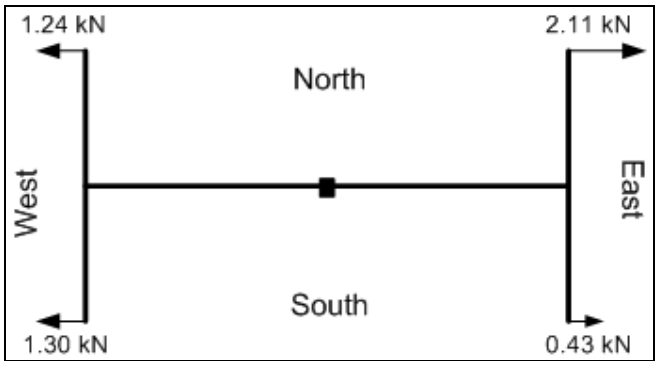

Figure 6-22: Lateral forces at wheels when NE wheel is at maximum misalignment with a central crab.

An interesting point should also be noted about the longitudinal forces exerted onto the rails during crane motion. The current South African loading code [1], Eurocode [2] and draft South African code [3] all assume that the maximum longitudinal force into the rails comes from the normal longitudinal travel case due to the acceleration and deceleration of the crane. According to the South African code [1] this value should be 2.89 kN in each rail while the Eurocode [2] and draft South African code [3] agree on 2.04 kN.

The maximum force as calculated with the numerical model for the acceleration and deceleration of the crane was 2.17 kN during normal longitudinal travel. During misalignment this value increases to 2.73 kN as shown in (Figure 6-18). This is larger than that estimated by both the Eurocode [2] and the draft South African code [3] and marginally smaller than the force estimated by the current South African code [1].

6.6 Conclusion

Misalignment occurs when either the wheels of the crane are not correctly aligned on the rails or the rails themselves are not straight. To simulate inward misalignment in the finite element model the east rail was kinked 15 mm westwards at a point adjacent to a column. For outward misalignment the east rail was kinked 15mm east.

During inward misalignment the crane behaves in a steady manner. As the misalignment increased the lateral forces experienced by the wheels increased. Slight skewing occurred in the case of the crab positioned eccentrically on the west side of the crane bridge. The largest lateral force (2.10 kN) was experienced with a central crab as the north east wheel crossed the point of greatest misalignment.

During outward misalignment the crane is more unstable. The misalignment initially causes a reduction in horizontal lateral forces as it alleviates the lateral forces due to static loading. The forces then develop inwards as the misalignment continues to increase. The greatest lateral force (1.17 kN) was experienced with an east eccentric crab as the north east wheel crossed the point of greatest misalignment. It is interesting to note that for both inward and outward misalignment these peaks occurred during southward travel when the driving wheels were pulling rather than pushing the crane. The lateral movement of the payload was observed as having a far larger influence on the forces experienced at the wheels than during inward misalignment.

The misalignment predictions in both the South African code [1] and the draft South African code [3] overestimate the lateral forces experienced by all four wheels at the same time. Although empirically based, they do provide an accurate reflection the force that can be reached at each wheel independently.

The longitudinal forces experienced during misalignment are greatest during inward misalignment when they reach a peak of 2.73 kN. This is greater than that experienced during longitudinal motion and slightly smaller than that allowed for by all three codes considered.

Misalignment is a potentially hazardous scenario for a crane. Wheel flanges are frequently touching the rails, which leads to a rapid wearing down of the steel and shortens the lifespan of the rails and the wheels. The forces induced are large, both in the lateral and the longitudinal direction, and need to be accounted for during design.

7 SKEWING

Skewing is when the crane is not running straight along its rails. Three of the common ways it can be induced are by an eccentric payload, failure of one motor or oblique hoisting.

During skewing, the crane rotates and moves laterally as well as longitudinally. Often this causes the flanges of the wheel to come into contact with the crane rail. This leads to wear of the wheel flanges and large horizontal forces are transmitted into the crane supporting structure.

Many cranes have synchronised motors to adjust the motor speed for an eccentric payload. This alleviates the most common cause of skewing and leaves only those due to mechanical error or bad practice. Both the current Eurocode [2] and the draft South African loading code [3] state that oblique hoisting due to the misalignment of the crab and the payload is forbidden. The remaining case, the failure of one electric motor, is studied here in detail.

When an electric motor fails the brakes automatically come on. When the crane is needed in a hurry the motor will get disconnected and the crane will be used with one motor until the other is repaired. Although this is considered extremely bad practice, as with the oblique hoisting, it still occurs.

This chapter analyses the Eurocode [2] and the current South African code's [1] approach to skewing. It follows with the methods that were used to imitate skewing in the laboratory and the numerical model, analyses the results obtained from the numerical model and compares them to the codes.

7.1 Codification

The current South African code [1] considers horizontal lateral forces in Chapter 5.7.4. The design lateral force is considered to be the most adverse force produced by acceleration and deceleration of the crab, misalignment of the crane wheels or gantry rails and skewing of the crane in plan.

In the case of skewing, where the crane is not guided by rollers, the code requires that a force (P_2) be applied at each wheel as shown in Figure 7-1 below. The force can be applied in either direction as shown, depending on which has the most severe effect.

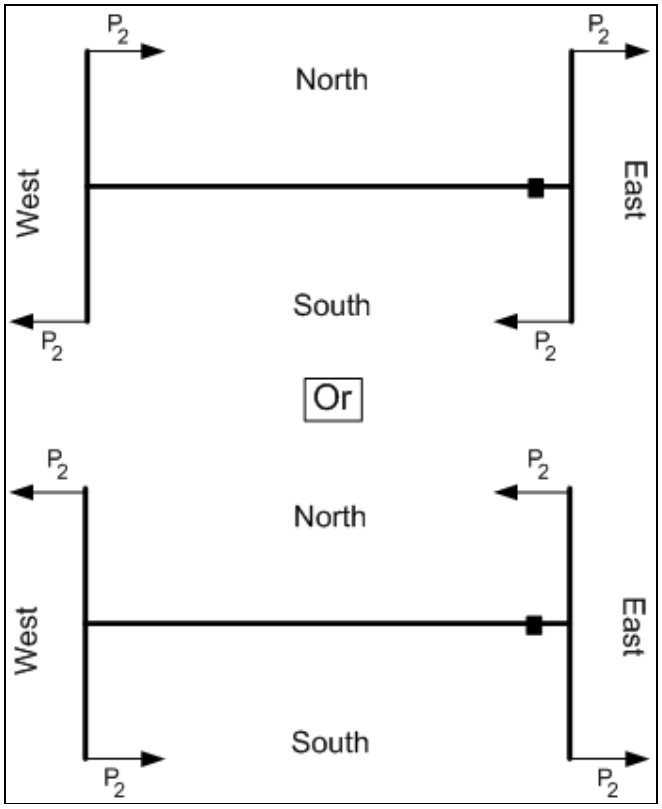

Figure 7-1: Skewing options in the current South African loading code

$P_2 = 1.5 * P_1$

where: P_1 is the force calculated in 5.7.4b of the current code and discussed in detail in Chapter 6 of this thesis.

The Eurocode [2] handles the phenomenon of skewing in far more detail (Figure 7-2). The forces are considered to be:

$H_{S,i,j,T} = f * \lambda_{S,i,j,T} * \Sigma Q_r$

where: i is the number of the rail (1 and 2 refer to rail West and East respectively)

j indicates the wheel pair under consideration

f is the non positive factor discussed below

Skewing

$\lambda_{S,i,j,T}$ is the force factor discussed below

T indicates the transverse force

ΣQ_r is the total vertical load on all wheels

f = $0.3*(1-\exp(-250*\alpha)) \leq 0.3$

where: α is the angle of skewing. In the case of the Stellenbosch crane f = 0.21

$\lambda_{S,1,j,T}$ = $\zeta_2/n * (1-e_j/h)$

$\lambda_{S,2,j,T}$ = $\zeta_1/n * (1-e_j/h)$

where: $\zeta_{1 \text{ and}}\ \zeta_2$ are the ratios of the distance of the instantaneous centre of rotation from rail 1 and rail 2 respectively, divided by the total distance

n is the number of wheel pairs

e_j is the distance of the wheel pair from the relevant guidance means

h is the distance from the centre of rotation to the relevant guidance means

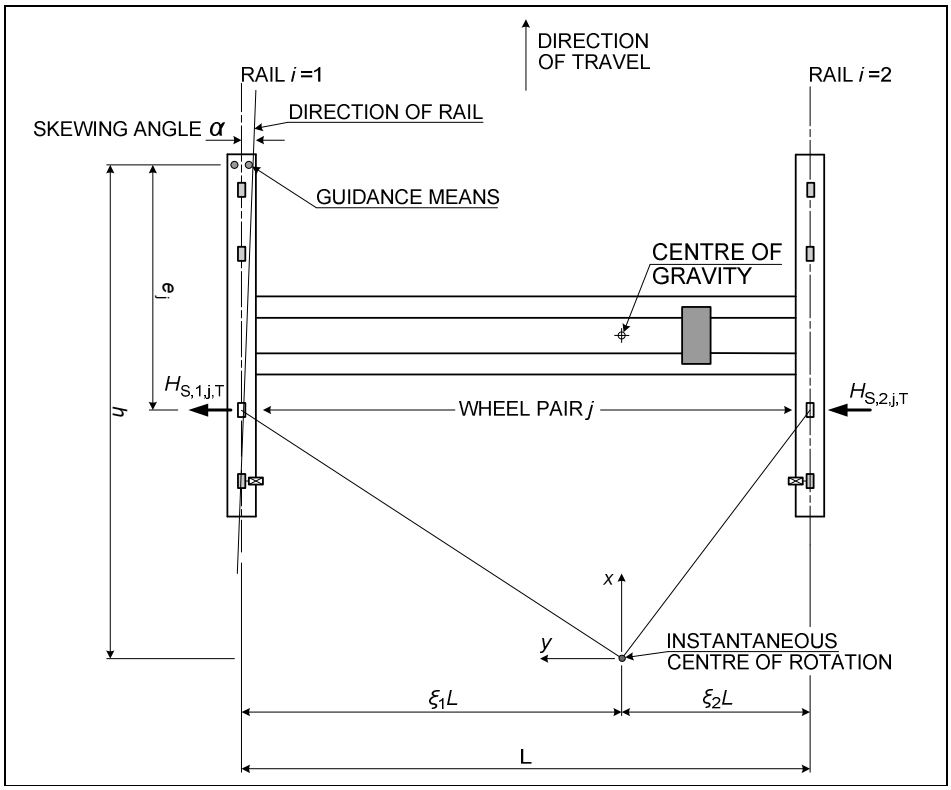

Figure 7-2: Diagram illustrating terms used in the Eurocode and draft South African code.

Skewing

This method of calculating the lateral skewing forces takes into account the distance of the wheels from the instantaneous centre of rotation and the maximum angle of skewing that can occur. It is important to note that this method of calculating the forces, although detailed, is primarily based on skewing caused by an eccentric payload rather than skewing induced by the failure of an electric motor.

The draft new South African loading code [3] follows the same calculation method as the Eurocode.

The expected forces as calculated from the above equations will be compared to the actual forces obtained from the numerical model to determine whether this calculation method is still viable if a motor fails.

7.2 Experimental Setup

The crane in the Stellenbosch Laboratory has synchronized motors. This means that if one motor is carrying more load than the other they adjust their torque to minimize the amount of skewing experienced. With this feature, the only practical methods of inducing skewing are to disconnect one motor or pick up the payload obliquely. Both of these tests were completed by Johan de Lange in the laboratory.

With one electric motor disconnected, the crane was accelerated at $0.16\ m.s^{-2}$ for 2.17 seconds, then decelerated again and allowed a period of free movement (Figure 7-3). The deceleration was followed by a free motion step to determine how the crane reacted to the residual lateral forces present at the end of the deceleration step.

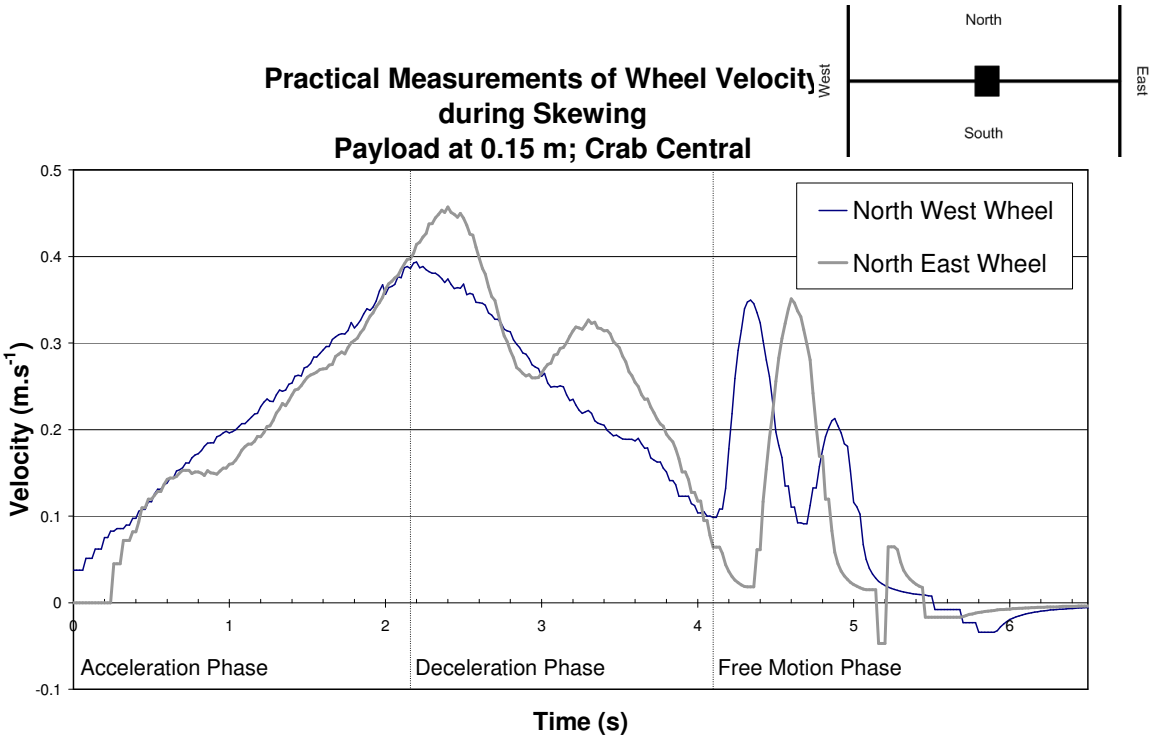

Figure 7-3: Experimental velocity measurements taken at Northern wheels with a central crab 0.15 m above the ground.

The oblique lifting of the payload, although covered in the experimental tests [4], will not be dealt with in detail here. The Eurocode [2] and the draft new South African code [3] both explicitly state that this form of hoisting is not permitted and any small unavoidable eccentricities that might occur are taken into account in the inertial forces.

7.3 Numerical Model

As in normal longitudinal motion, the movement of the numerical model was controlled by applying acceleration and deceleration boundary conditions to the wheels. The values for these steps were obtained from the experimental tests (Figure 7-3). In the skewing load case, the movement boundary conditions were only applied to the South-West wheel as the motor on the eastern endcarriage (south-east wheel) had been disconnected.

The initial numerical skewing tests were run with a central crab to a maximum speed of 0.39 $m.s^{-1}$ in order for the model to be calibrated with the experimental tests. The calibration was then confirmed with an eccentric crab on the east of the crane bridge with a maximum velocity of 0.39 $m.s^{-1}$ to ensure that the model was an accurate representation of the physical scenario.

After the model was fully calibrated the acceleration step on the numerical model was altered to allow the crane to reach its maximum velocity of 0.55 $m.s^{-1}$. The largest lateral forces should occur at this speed. The physical experiments were not done to this velocity and it is possible that a single motor would not be able to move a crane at its rated speed, especially with an eccentric crab. If this is the case, the results from the maximum velocity runs in the numerical model will be conservative.

The model was analysed with the crab placed eccentrically on the west of the crane bridge, in the centre and on the east of the crane bridge. For each crab position a scenario was run with the payload at the bottom (0.15 m above ground) and at the top (2.2 m above ground). These six cases provide a full spectrum of results of what is occurring to the crane during skewing.

7.4 Calibration

The acceleration and deceleration conditions from the experimental results were applied to the model with a central crab and a payload 0.15 m above the ground. The model was then calibrated so the numerical results closely followed the experimental results.

The movement of the crane in the free motion step was governed by the braking coefficient of the working motor and the rolling frictional coefficient of the non-motorised wheels. The braking co-efficient of the working motor (south west wheel) was interpreted as a frictional value in the numerical model but is substantially higher than a purely frictional interface would be. The final coefficients selected for the model were:

Braking Frictional Coefficient = 0.017
Rolling Frictional Coefficient = 0.005

Other factors such as the frictional coefficients of the wheel flanges, the frictional coefficients in the lateral directions on the wheel flats and the damping co-efficients of the payload, had a small influence on the overall results and were adjusted accordingly.

In Figure 7-4 below the north west wheel, with the western end carriage driven by the motor, is following the set acceleration and deceleration conditions. The north east wheel is strongly affected by the swinging of the payload and during the acceleration phase lags behind its

western counterpart. The wheel velocity from the numerical model is extracted for the two northern wheels to match the information given by the encoders in the physical experiments.

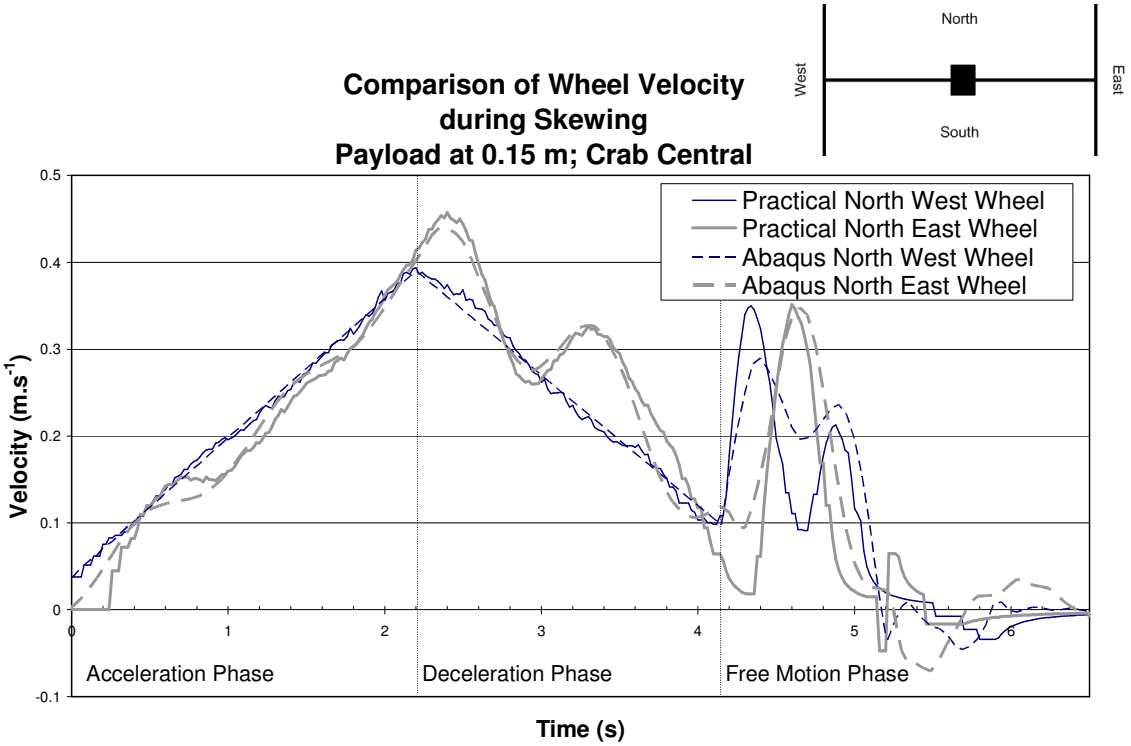

Figure 7-4: Comparison of the experimental measurements and numerical results for northern wheel velocity

During the free motion step the payload induces movement in the crane despite the working brake on the western endcarriage. It is interesting to note that the velocity at the wheels induced by the swinging of the payload reaches a similar magnitude as when the crane was being driven. In the experimental results the north-western wheel reaches a higher peak than it does in the numerical results (0.35 $m.s^{-1}$ and 0.29 $m.s^{-1}$ respectively) but this was considered an acceptable discrepancy.

When the horizontal lateral forces are considered the differences between the experimental and numerical model are more pronounced (Figure 7-5). Only the northern wheels are shown in the graph, to maintain clarity. The lateral forces experienced by both northern wheels during the experiments and during numerical modelling follow the same pattern of behaviour. The forces increase during acceleration and then decrease and increase in the negative direction during deceleration. In free motion, the forces oscillate as induced by the swinging payload.

Skewing

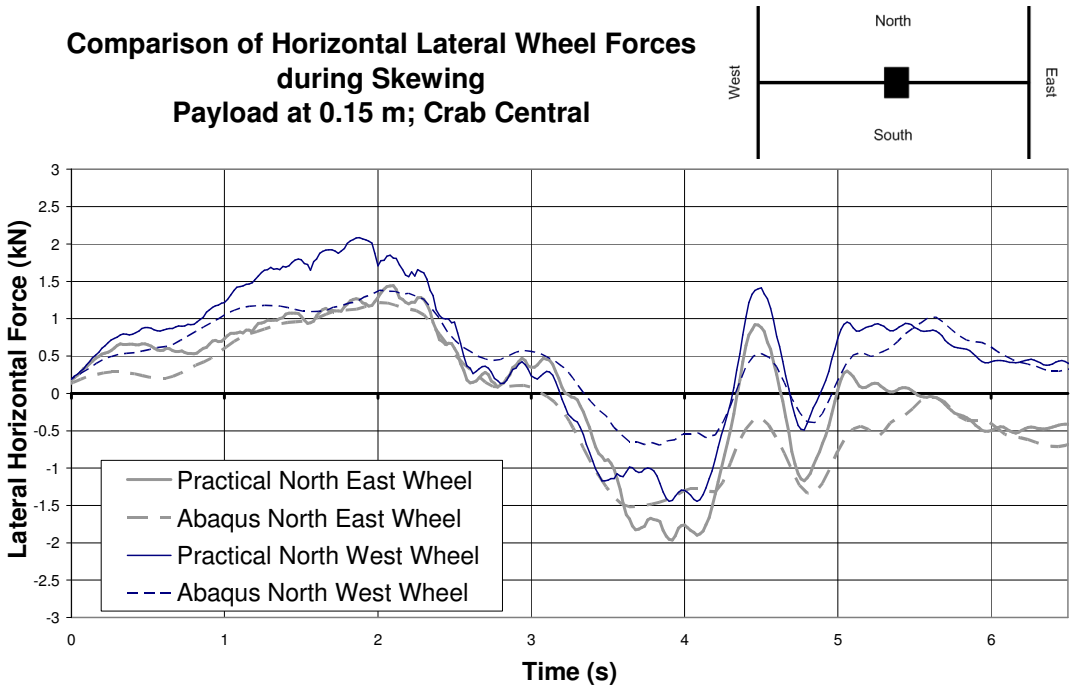

Figure 7-5: Comparison of the experimental measurement and the numerical results of the horizontal lateral forces at the Northern wheels for a central crab.

The maximum lateral force experienced in the experiments was 2.09 kN towards the end of the acceleration phase (time = 1.88 s) while the force experienced in the numerical model at this time was only 1.26 kN. The maximum peak experienced by the numerical model was -1.52 kN towards the end of the deceleration phase (time = 3.67 s).

This difference in forces with a central crab could be due to several inaccuracies, for example:

- Numerically the wheel flanges in the numerical model are currently modelled as longer than the actual wheel flanges, which could have a softening affect on the forces experienced.
- Experimentally, the strain gauges are being utilised at the low end of their rated measuring range and inaccuracies are expected to occur.

When the forces due to an eccentric crab, positioned as far from the working motor as possible (East), are considered, a high correlation is found (Figure 7-6).

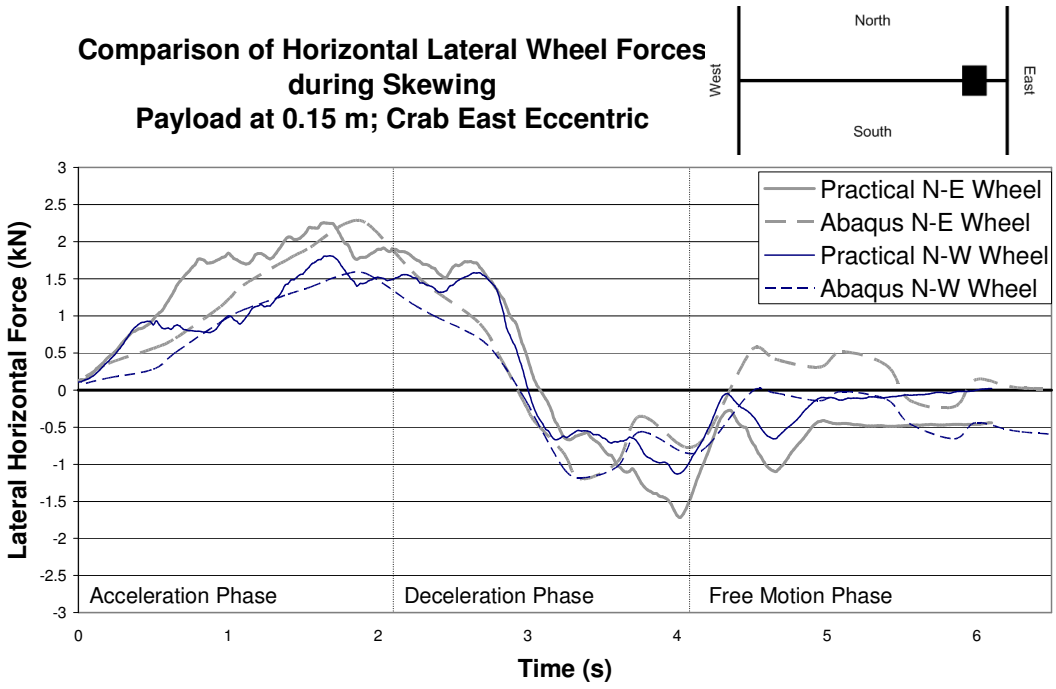

Figure 7-6: Comparison between the experimental and numerical results for lateral wheel forces at the northern wheels with the crab positioned eccentrically east on the crane bridge.

Only the northern wheel forces are shown in Figure 7-6 to demonstrate the correlation with the experimental results. The southern wheels experience similar forces in the opposite direction to their northern counterparts but this will be seen in Section 7.5.

With an eccentric crab the experimental results and numerical model show similar force peaks. From the physical experiment the highest peak is 2.27 kN occurring at time = 1.64 seconds. In the numerical model this peak is at time = 1.93 seconds but the value of the force has a good correlation at 2.28 kN.

It was judged from these graphs that the behaviour of the numerical model accurately represented the behaviour of the physical crane. The numerical model was correspondingly extended to determine the forces induced in the supporting structure if the crane was accelerated to its maximum velocity (0.55 $m.s^{-1}$) while skewing was taking place.

7.5 Results

Vertical wheel forces have been covered in detail in Chapter 4 and will not be considered again here. Little vertical oscillation is induced into the crane during skewing and as a result the vertical loads experienced at the wheels remain constant.

In all cases tests were completed for the payload both at the bottom (0.15 m above the ground) and at the top (2.2 m above the ground). It was found that, in line with the previous load cases, the payload had a greater influence on the forces experienced by the crane when it was at the bottom than when it was fully hoisted.

The one instance when the force induced by a payload at the top exceeds the force induced when the payload is at the bottom is discussed in detail, however a detailed study of the results for the payload at the top will be omitted here. The full set of graphs can be found in Appendix C.

All the results that follow below are generated with a maximum velocity of 0.55 $m.s^{-1}$ and adhere to the set acceleration and deceleration pattern shown in Figure 7-7 obtained from the experimental tests. The movement during the free motion step changes depending on the position of the crab. The graph represents the case with a central crab.

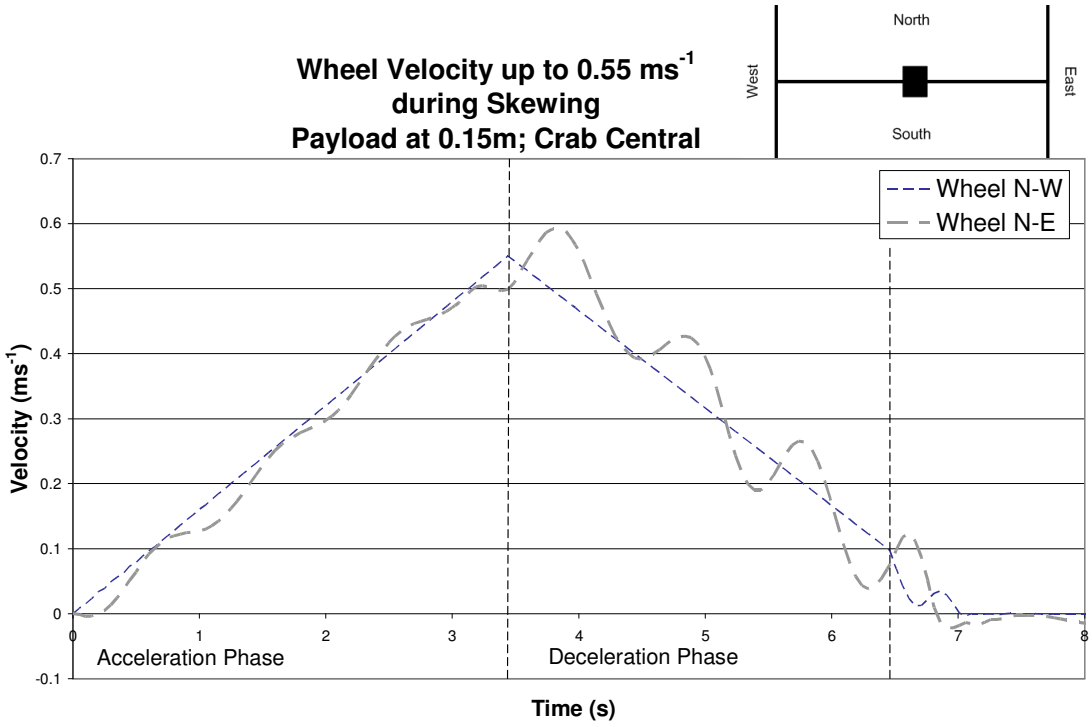

Figure 7-7: Wheel velocity graph showing the set acceleration and deceleration applied to the finite element model

7.5.1 Horizontal Lateral Wheel Forces

Central Crab

As the crane starts to move in the longitudinal direction the western wheels, with the working motor, move outwards laterally (Figure 7-8).

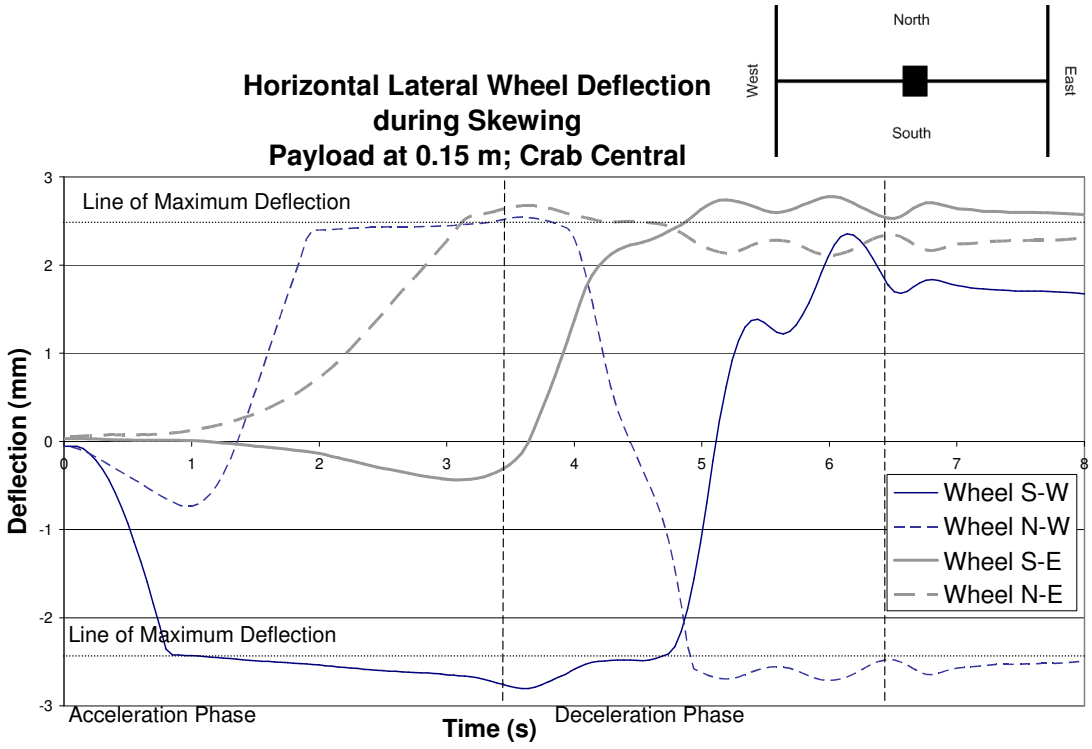

Figure 7-8: Horizontal lateral deflection experienced at the wheels with the payload 0.15 m off the ground, the crab in a central position and the South-East motor deactivated

The eastern wheels remain in a constant lateral position for the first second of travel. After the first second the bridge can no longer transmit the longitudinal forces from west to east without skewing occurring. As a clockwise moment is induced by the working motor into the crane, the crane wheels are forced to deflect laterally until they reach the pattern shown by Figure 7-9 at time = 3.1 s. It is interesting to note that the western wheels assume this position quickly while the eastern wheels move more slowly. The flexibility of the crane bridge accounts for this difference. In the figure below it is plain that not only the East endcarriage but the bridge as well must bend in order to achieve this position.

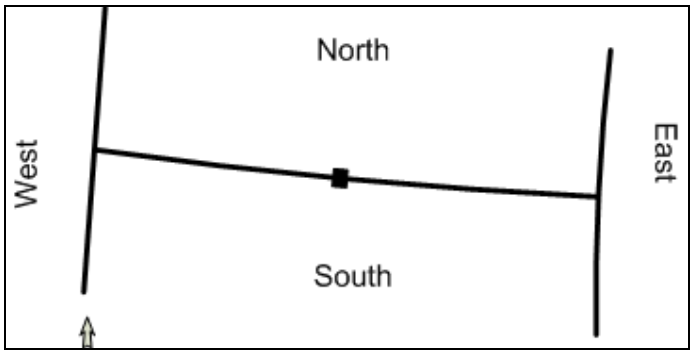

Figure 7-9: Flexing of the crane after 3.1 seconds of skewing

Skewing

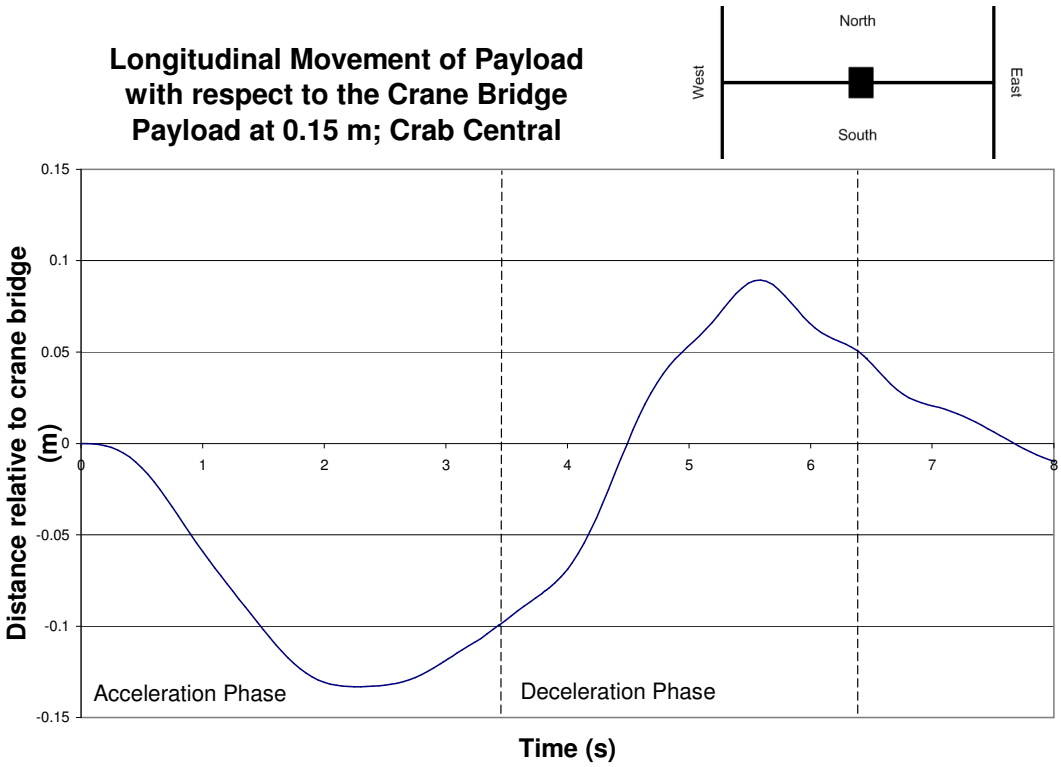

Figure 7-10: Longitudinal movement of payload with respect to the centre of the crane bridge during skewing

At time = 3.44 seconds the crane stops accelerating and starts decelerating. At this point the payload, although still behind the crane, is already in the process of swinging through (Figure 7-10). As it swings and the western endcarriage of the crane decelerates, the eastern endcarriage is still accelerating through. The bend in the eastern endcarriage straightens out and the south east wheel moves out to the rail. The northwest wheel responds to the deceleration in moving outwards to its own rail. As the crane pivots under the braking motion and the swinging payload the south west, braking wheel is forced inwards as shown in the figure below.

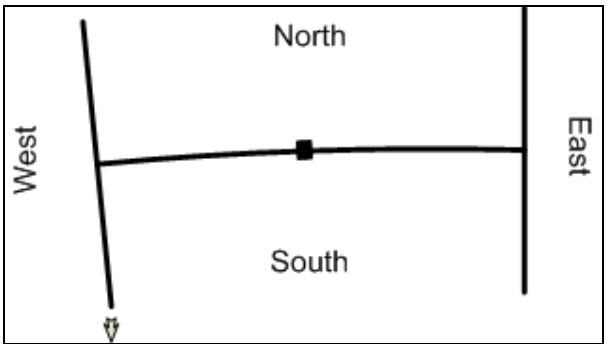

Figure 7-11: Flexing of crane after 8 seconds of skewing

In several places the horizontal deflection of the wheels exceeds the maximum gap between the wheel and rail flanges of 2.4 mm. When this occurs the rails themselves are being pushed outwards by the skewing of the crane.

The horizontal lateral forces experienced at the wheels as a result of the skewing of the crane can be seen in Figure 7-12. The largest force of 2 kN occurs at time = 3.59 seconds, just after the crane has started to decelerate. The pattern of forces experienced by both east and west sets of wheels is the same. The apparent difference in values occurs primarily because of the static outward forces of 0.76 kN that exist at the start of the crane's movement.

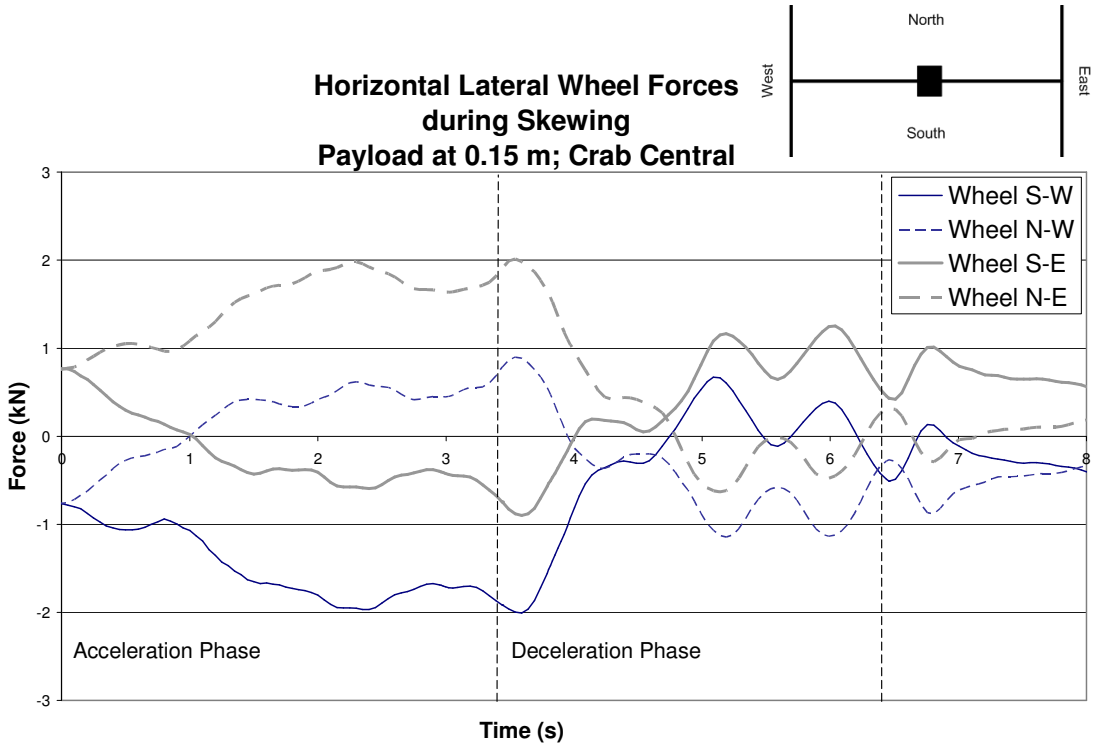

Figure 7-12: Horizontal lateral forces experienced at the wheels during skewing with the payload at 0.15 m above the ground and a central crab.

The forces change directions between time t = 4 and t = 5 seconds as the payload swings through, moving from their peak values as seen in Figure 7-13 to their final values in Figure 7-14.

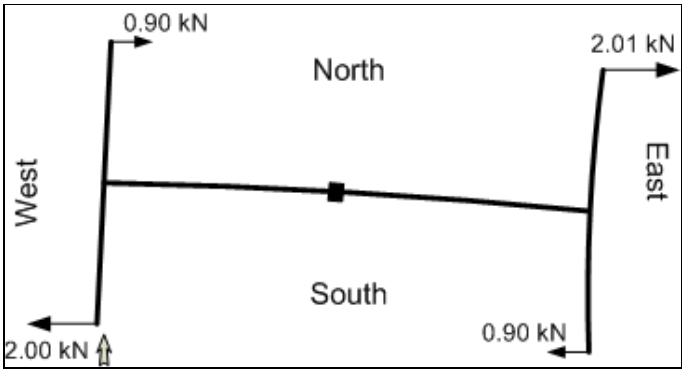

Figure 7-13: Lateral wheel forces after 3.1 seconds of skewing

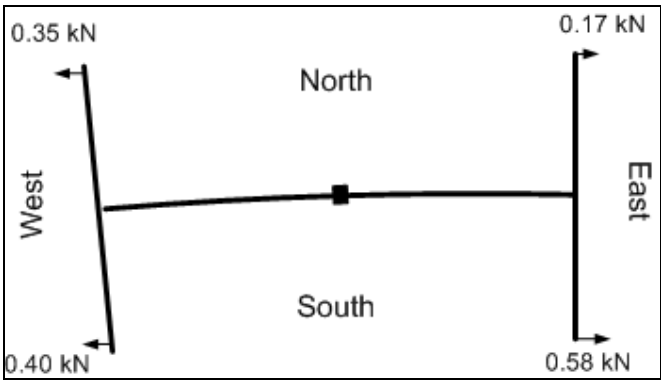

Figure 7-14: Lateral wheel forces after 8 seconds of skewing

It should be remembered that these forces incorporate the initial outward forces induced by the static weight of the payload.

West Eccentric Crab

When the crab is positioned 0.75 m away from the west endcarriage the bulk of the weight of the payload is being carried by the wheels with the working motor. This minimises the eccentricity of the centre of gravity of the crane from the working motor and decreases the skewing effect on the crane as a whole.

As the crane starts to move the south west, driving wheel slides outwards laterally. It is attempting to propel the crane north but the inertia of the crane resists movement. Once the crane is accelerating both northern wheels swing to the east as a result of the clockwise moment on the crane. The static loading on the south east wheel is balanced by the force due to the skewing of the crane. As a result the south east wheel remains centred on its rail and the east endcarriage flexes to account for the different deflection in its wheels (Figure 7-15).

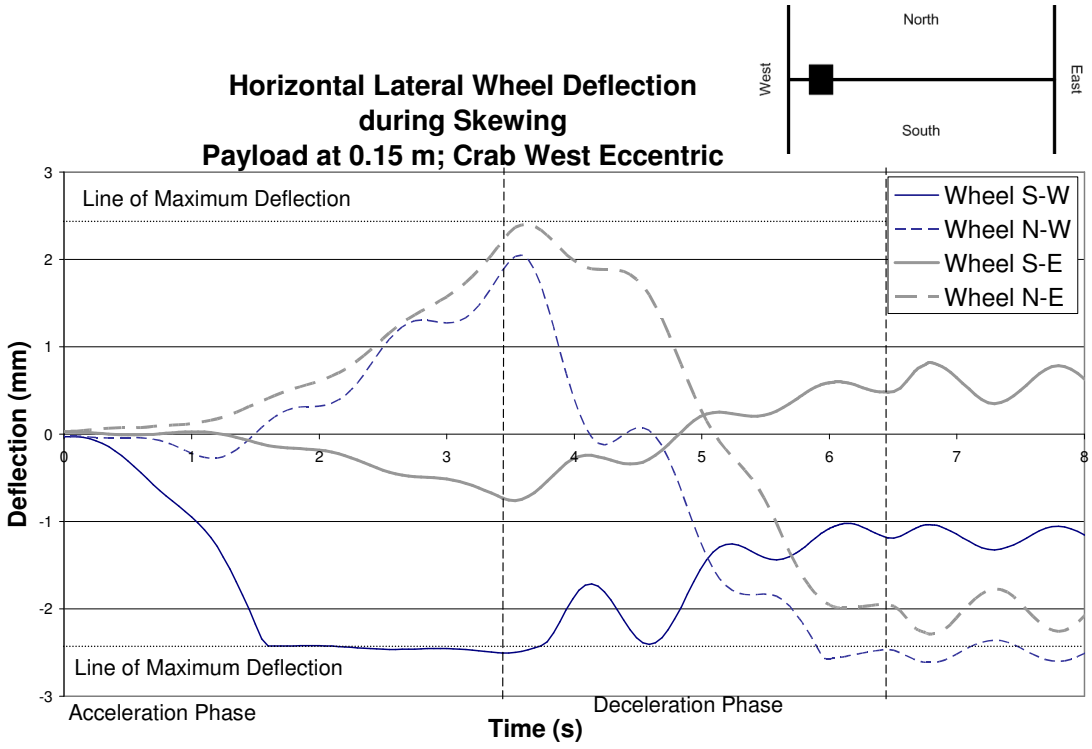

Figure 7-15: Horizontal lateral displacements experienced at the wheels with the payload at 0.15 m above the ground and the crab positioned eccetrically on the West side of the bridge.

When the crane starts to decelerate (time = 3.44 s) the crane swings around in an anticlockwise direction as a result of the braking south west wheel and the forward momentum of the payload. This means both northern wheels move away from the east rail flanges and towards the west. This motion moves the driving south west wheel east away from its rail. The south east wheel still feels little overall effect from the manoeuvring of the crane. At the end of the motion it is apparent that the whole body of the crane has moved to the west.

When considering the forces in Figure 7-16 it is apparent that they are considerably smaller than seen in Figure 7-12 with the crab in a central position. As the positioning of the crab adjacent to the endcarriage with the working motor minimises the eccentricity in the test, these results are to be expected.

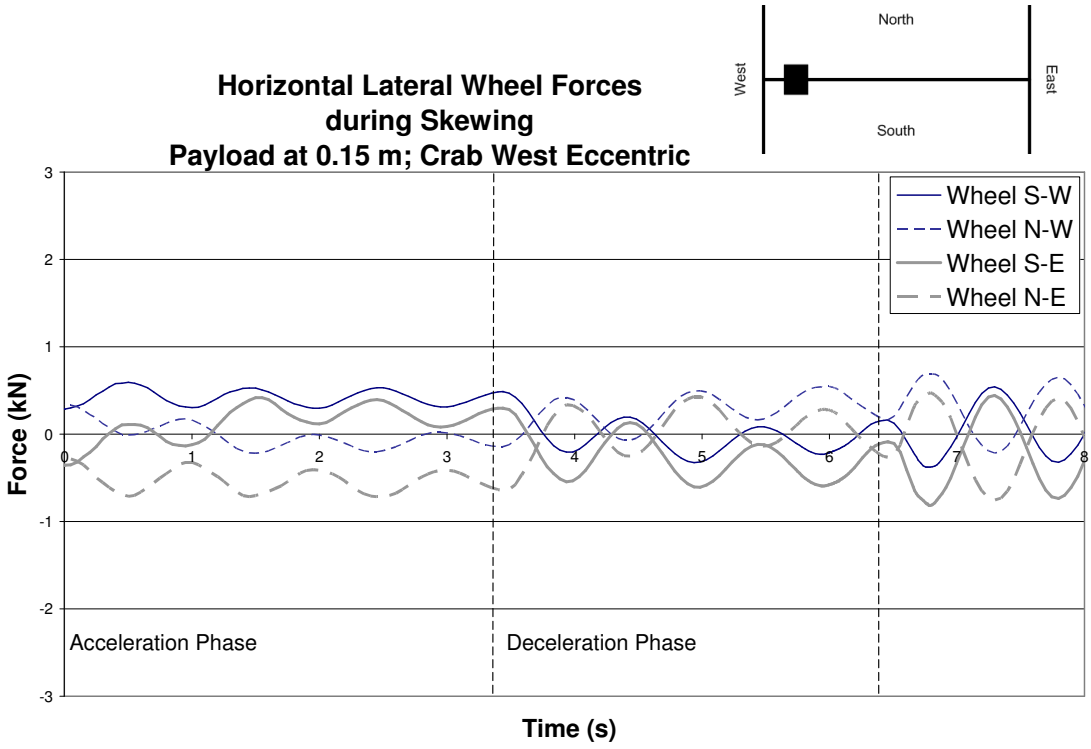

Figure 7-16: Horizontal lateral forces experienced at the wheels with the payload at 0.15 m above the ground and the crab positioned eccentrically on the West side of the crane bridge.

East Eccentric Crab

With the crab positioned 0.75 m away from the east endcarriage and with the east motor deactivated, the centre of gravity of the system is the farthest distance possible from the working motor. This means that a large moment is applied to the crane by the motor.

As the crane starts to move, the west endcarriage skews laterally almost immediately with the northern wheel moving east and the southern wheel moving west (Figure 7-17). The west endcarriage is highly mobile as it is lightly loaded but it is restrained from moving north rapidly and skewed by the inertia of crane bridge and east endcarriage.

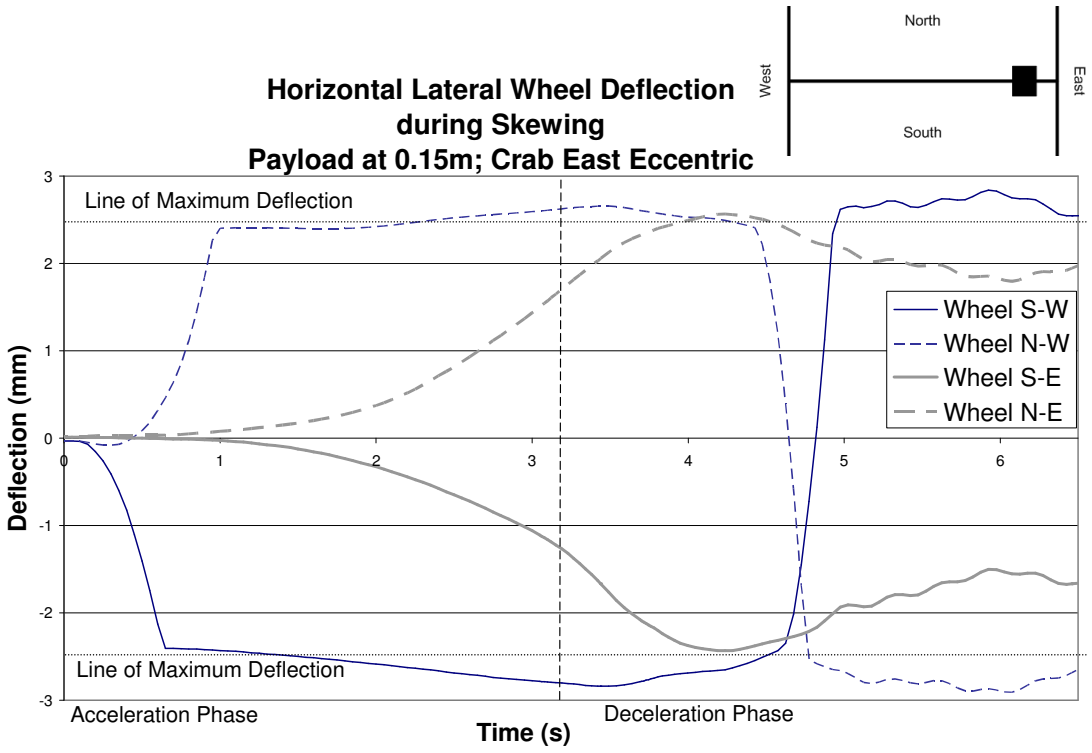

Figure 7-17: Horizontal lateral deflections experienced at the wheel with the payload at 0.15 m above the ground and the crab positioned eccentrically on the East side of the crane bridge.

The east endcarriage also skews after the crane has started moving but far more gently than the west endcarriage. The forces skewing the east endcarriage are smaller than those acting on the west endcarriage, as some of the moment acting on the crane is already taken up in the flexing of the west endcarriage and the bridge. Once the brakes are applied and the payload swings through, the west endcarriage rotates quickly in an anticlockwise direction until the north flange is as far west as possible and the south flange as far east. The east endcarriage, carrying most of the load of the payload experiences a slight rotation but little lateral movement occurs at the wheels. The shape of the crane at time t = 6 seconds can be seen in Figure 7-18 below.

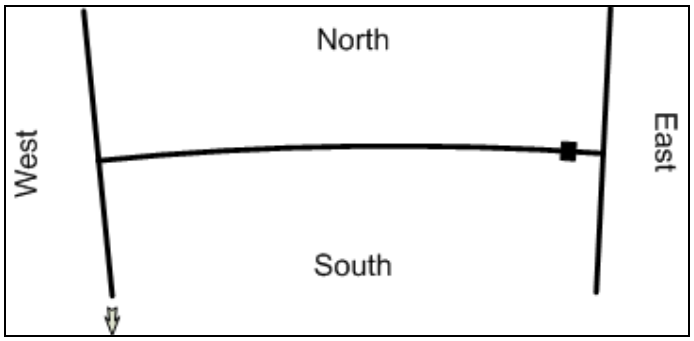

Figure 7-18: Skewing in crane with East eccentric crab after 6s

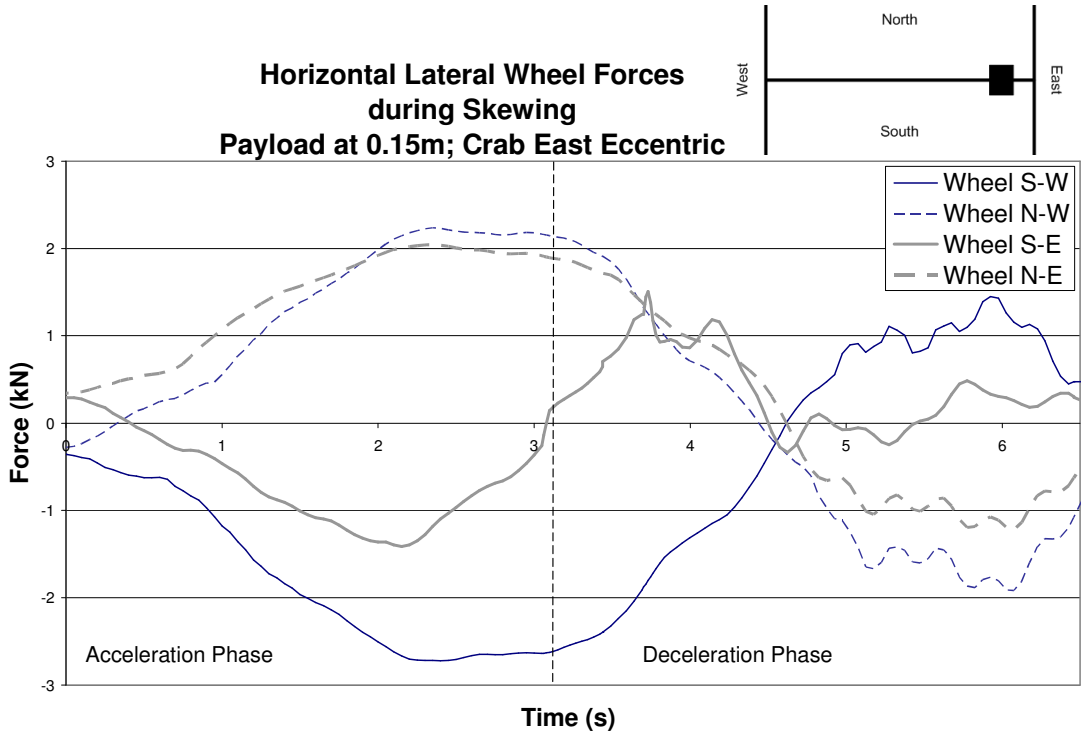

Figure 7-19: Horizontal lateral forces experienced at the wheels for the payload 0.15 m above the ground with the crab placed eccentrically on the East of the Crane Bridge

The largest of the lateral horizontal forces is experienced by the wheels on the west endcarriage. These forces reach a peak of 2.71 kN in a westerly direction at the south west wheel when time = 2.4 seconds. The payload then starts to swing through and the horizontal forces reduce again. The corresponding forces experienced at the other wheels at this moment in time can be seen in the diagram below.

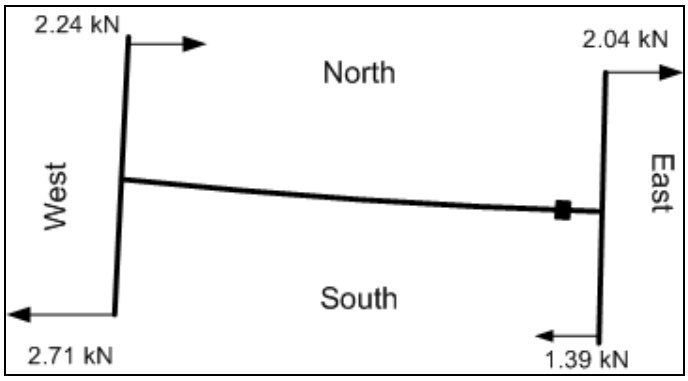

Figure 7-20: Horizontal lateral wheel forces after 2.4 s of skewing with the crab placed eccentrically on the east of the crane bridge

It should be remembered that these forces include the static outwards forces developed when lifting the payload. If these are ignored, the forces at the eastern wheels remain substantially lower than the forces experienced at the western wheels.

In the case of the crab east eccentric on the crane bridge, the payload at the top should also be considered. The lateral deflection experienced at the wheels follows a similar pattern to the payload at the bottom although a smaller deflection occurs at both eastern wheels throughout the motion of the crane when the payload is fully hoisted (Figure 7-21).

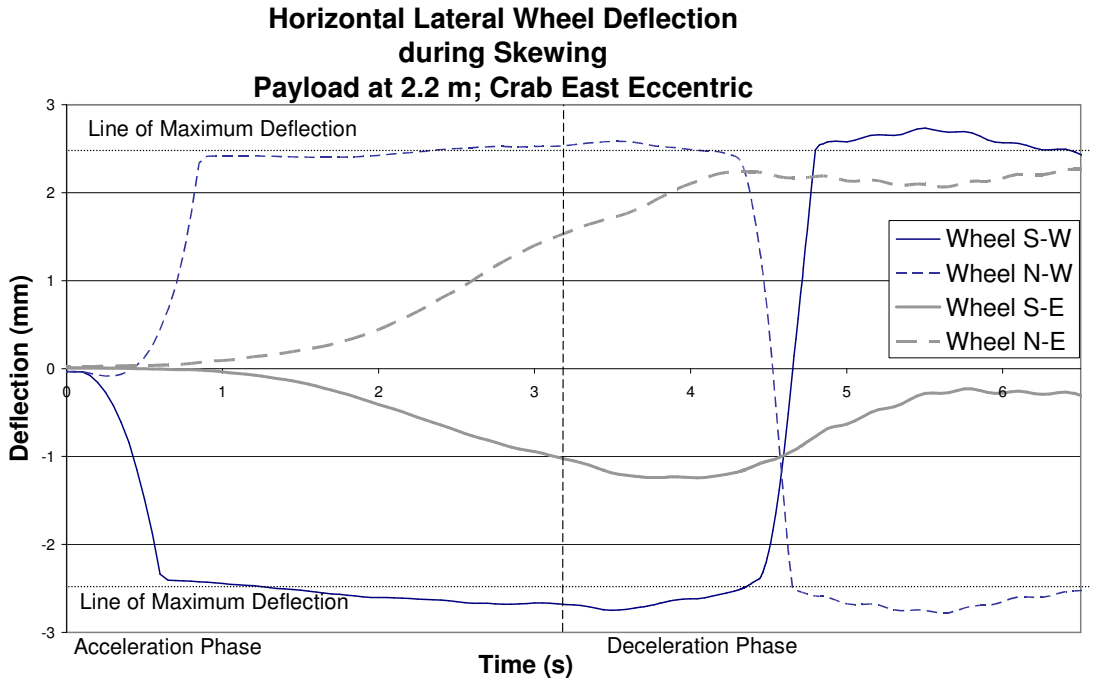

Figure 7-21: Horizontal lateral deflections experienced at the wheel with the payload at 2.20 m above the ground and the crab positioned eccentrically on the East side of the crane bridge.

When one regards the forces induced when the payload is at 2.20 m above the ground (Figure 7-22) it is apparent that, although the pattern experienced by the forces is the same as when the payload is 0.15 m above the ground, the maximum force is slightly higher. When the payload is fully hoisted the peak force is 2.78 kN at time = 1.95 seconds, 0.07 kN higher than the force experienced when the payload is at the bottom. This slight increase is probably induced by the position of the payload at the time. The payload is at its maximum displacement from the crane bridge at time = 2.1 seconds when the payload is fully hoisted and time = 2.7 seconds when the payload is just lifted off the ground. When the payload is fully hoisted the time of the peak of the payload's longitudinal swing is closer to the time the maximum lateral force is experienced. This could lead to the slight increase in force seen between the two cases.

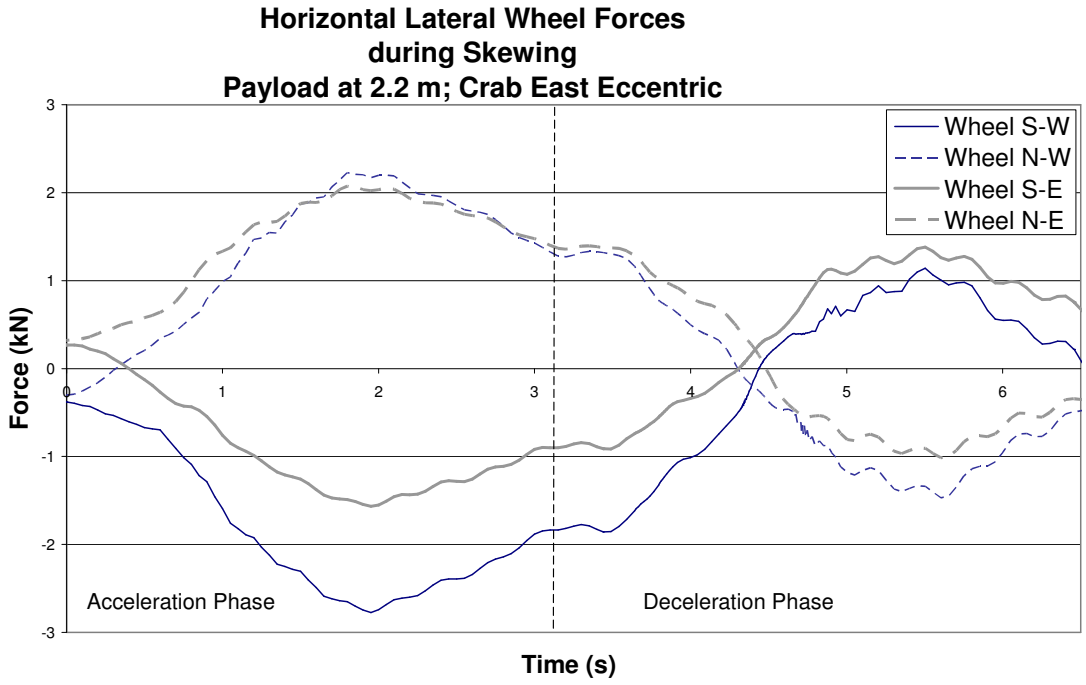

Figure 7-22: Horizontal lateral forces experienced at the wheels for the payload 2.20 m above the ground with the crab placed eccentrically on the East of the Crane Bridge

It is also interesting to note that in the numerical results there is relatively little difference in the wheel forces between the tests done to a velocity of 0.39 ms^{-1} and the tests done to a velocity of 0.55 $m.s^{-1}$ (Figure 7-23). This is due to the position of the payload at the end of the acceleration and deceleration steps. In the 0.39 ms^{-1} case, the payload has just swung forward to its full extent when the crane starts to decelerate and this enhances the effect caused by the deceleration. In the 0.55ms^{-1} case, the payload is already swinging back and hence this enhancement doesn't occur (Figure 7-24). A similar effect occurs at the end of the deceleration phase where, for the 0.39 ms^{-1} velocity case, the payload beginning to swing through again. This leads to high velocities and forces experienced after the motor is braked while in the 0.55 ms^{-1} case the payload is mid-swing and the effect dies out quickly.

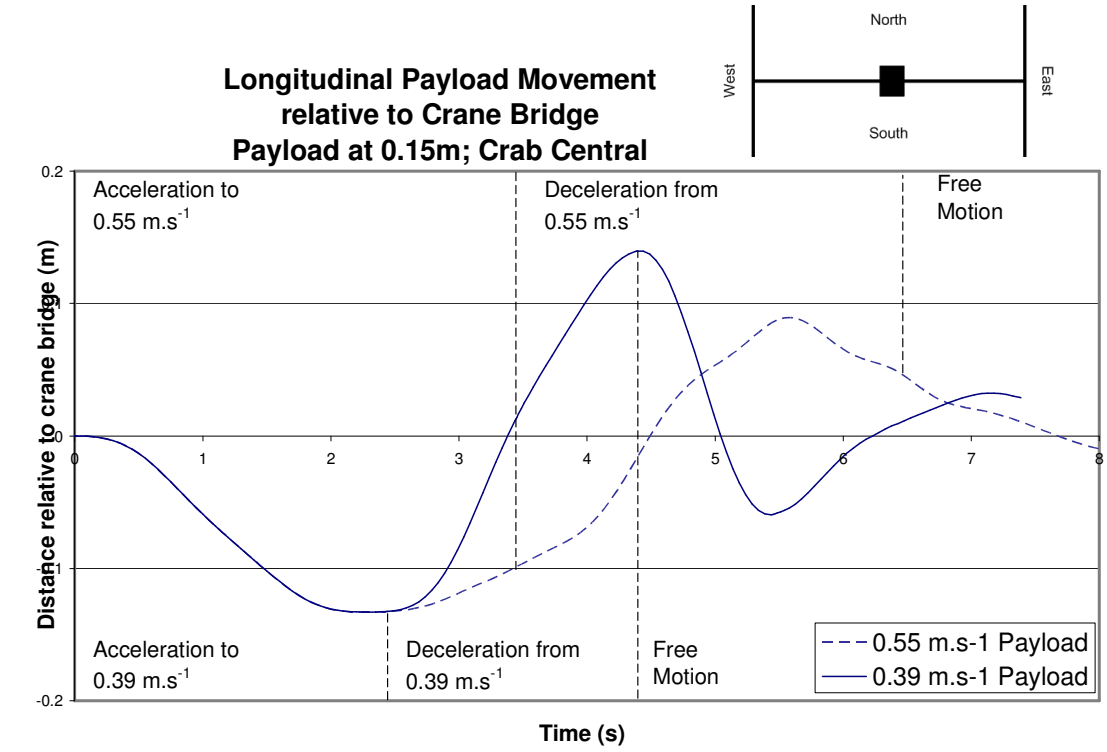

Figure 7-23: Numerical velocity results for the crane accelerated to 0.39 m.s^{-1} and 0.55 m.s^{-1}

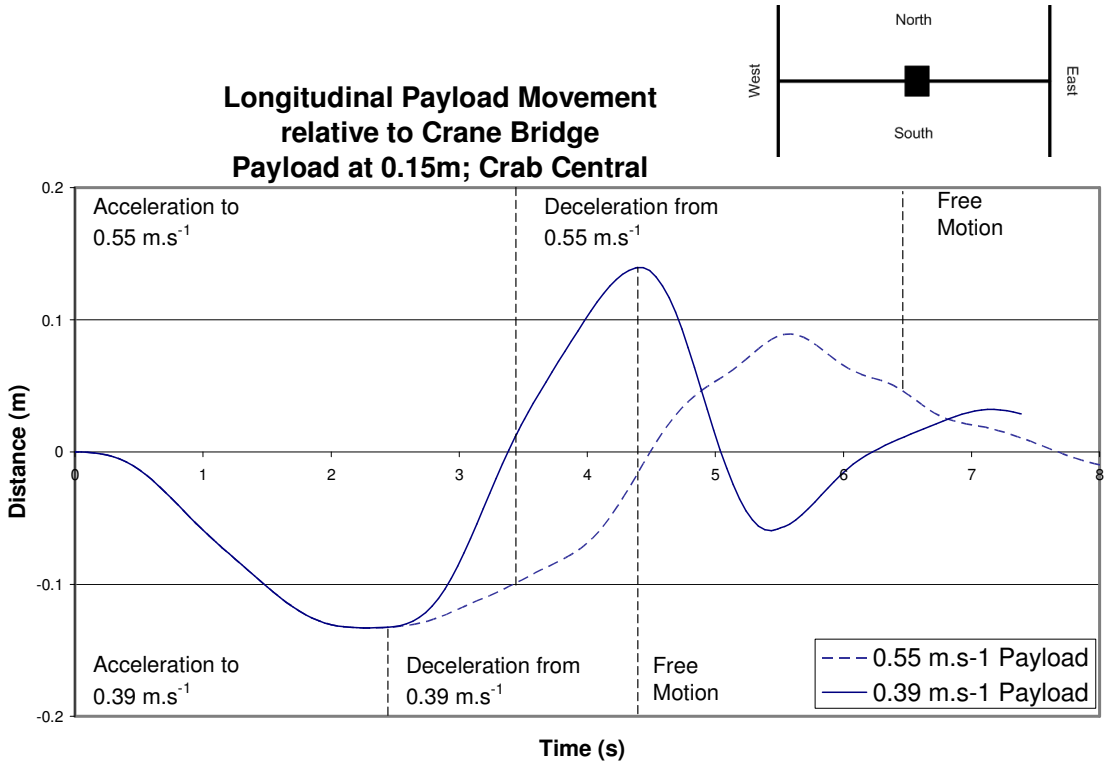

Figure 7-24: Longitudinal payload motion relative to the crane bridge during skewing for 0.39 m.s^{-1} and 0.39 m.s^{-1}. Payload at 0.15 m with crab placed centrally on the bridge.

7.5.2 Horizontal Longitudinal Forces

The dominant longitudinal forces will always occur at the rail with the working motor. The longitudinal forces induced at the east rail due to friction between the rail and wheel flanges are slight in comparison to the forces induced in the west rail by the acceleration and deceleration of the working motor.

As the payload is moved closer to the east endcarriage, the peak negative force in the west rail (due to acceleration of the crane) increases. A greater force required at the wheel to move the crane forward as the eccentricity between the working motor and the centre of gravity of the crane increases. The greatest negative force experienced in the west rail is -2.56 kN at time t = 2.4 seconds. After this point, in all load cases, the payload starts to swing through even though the crane is still accelerating. This reduces the force required to move the crane.

When the payload is close to the West endcarriage the greatest positive force (due to deceleration of the crane) occurs. When the payload's mass is carried purely by the Western wheels, a large force needs to be applied at the wheels to slow the crane down. This braking causes the large positive force of 2.47 kN seen in Figure 7-25.

Throughout the acceleration and braking motion the simulation with the crab east eccentric and 2.20 m above the ground follows the same path as the situation where the payload is 0.15 m above the ground. It is therefore omitted from the longitudinal results.

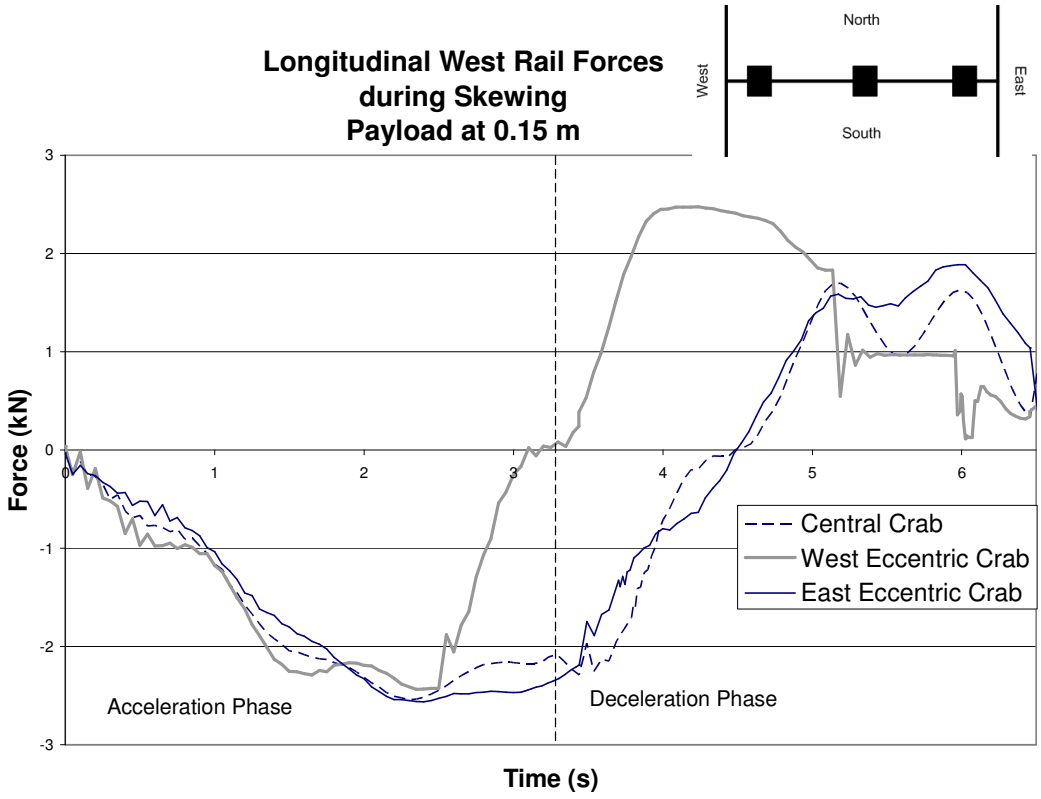

Figure 7-25: Longitudinal forces experienced in the West rail during skewing for various payload positions

7.6 Discussion

According to the current South African loading code [1], a force P_2 should be applied to each wheel as shown in the diagram below where $P_2 = 1.5 * P_1$ and P_1 is the lateral horizontal calculated for misalignment. The design skewing force, P_2, for the crane in the Stellenbosch Laboratory is therefore be 3.2 kN at each wheel.

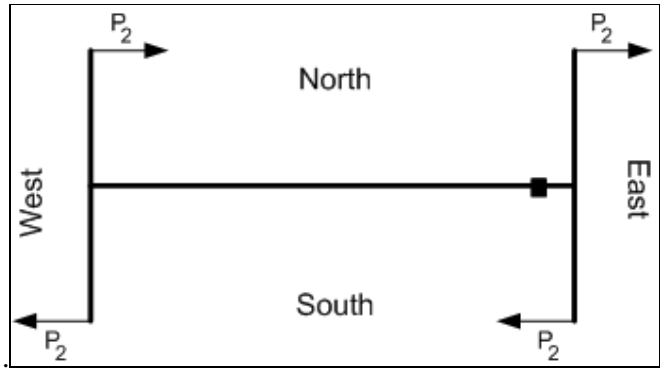

Figure 7-26: SABS definition of skewing forces

Skewing

Under the Eurocode [2] and draft South African Code [3], using the equations discussed in Section 7.1, the design skewing forces are as in Figure 7-27 below.

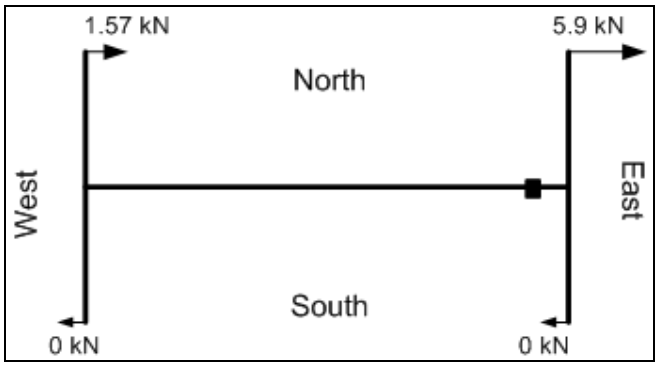

Figure 7-27: Skewing forces as calculated for the Stellenbosch crane according to Eurocodes

As has been discussed earlier, the Eurocode and draft South African code are primarily concerned with skewing as a result of an eccentric payload. In these codes it is assumed that a moment is induced around the centre of gravity of the crane under normal operating conditions and must be balanced by the lateral forces at the front wheels. In the laboratory crane, this effect is counteracted primarily by the synchronized motors as discussed in Chapter 5.

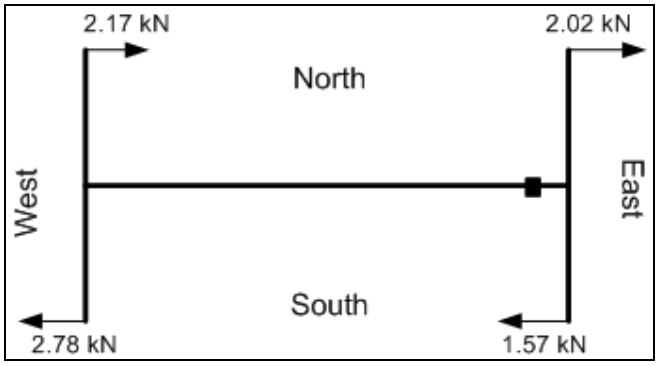

Figure 7-28: Maximum skewing forces as calculated by the finite element model

The most critical forces from the numerical model are as shown in Figure 7-28. While the calculations in the current South African loading code [1] are a gross simplification of skewing, with little allowance for the method of skewing or the eccentricities involved, the predicted forces are of the correct magnitude. They are conservative at each wheel but do assume that forces occur at all four wheels.

The Eurocode [2] and draft South African code [3] misrepresent this form of skewing. If the maximum design skewing force of 5.90 kN (Figure 7-27) was used for calculations, the crane girder would be overdesigned. The predicted force distribution does not reflect the forces calculated at the wheels by the numerical model as, according to the codes, the horizontal lateral forces at the driving wheels are minimal.

7.7 Conclusion

Skewing can be caused by the carrying of an eccentric payload, the failure of one motor or oblique hoisting of the payload. Oblique hoisting is considered bad practice and many motors today are synchronised to alleviate skewing induced by an eccentric payload. Skewing caused by the failure of one motor is still a recurring problem in practice.

This was simulated in the laboratory by the disconnection of the east motor. The numerical model was adjusted to reflect this failure and then calibrated against the experimental results and extended to determine what forces occur when the crane attains its full velocity with only one motor working.

As the payload is placed further east, the eccentricity of the centre of gravity of the crane to the working motor (south west wheel) is increased. As a result of this, the lateral horizontal forces are at their largest when the crab is furthest east. The lateral wheel forces are a direct result of the moment that the motor induces into the crane.

In the most extreme case, with the crab positioned eccentrically east on the crane bridge, the western wheel flanges are mostly running against the rails. This causes a significant amount of wear and tear on the rails and flanges and should be avoided. Constant running of the crane with only one motor will rapidly reduce the lifespan of the wheels and rail.

The current South African loading code [1] conservatively represents the lateral forces experienced by the crane during skewing, exceeding the greatest measured force by a margin of 0.5 kN. The calculation is very general and based on an empirical rule of thumb rather than actual theory with respect to eccentricities induced in the crane.

The Eurocode [2] and draft South African code [3] do not take into account the instance where one motor fails. These codes are designed for the case where both motors are working but the

payload is eccentric. As such the calculations do not give valid results to compare with the case of one motor failing.

Skewing induces high lateral loads into the crane supporting structure. The lateral loads are roughly 3.5 times greater than the loads caused purely by hoisting the payload. The loads induced by skewing must be compared to those caused by misalignment and the acceleration and deceleration of the crab and the combination of forces that lead to the worst case must then be taken into account in the design of the structure.

8 DISCUSSION

Throughout the load cases discussed in the preceding four chapters, several important points recur. These include the influence of the payload on the loads experienced whether the forces investigated at the wheels are vertical, horizontal lateral or horizontal longitudinal and the flexibility of the crane bridge and endcarriages.

The four load cases each contribute to factors in the design codes. The factors given in the codes must be compared to the actual values calculated by the numerical model to determine how accurate the predicted forces from the codes are.

8.1 Payload Influence

A strong payload influence was noted throughout the different load cases. The influence is related to the position of the payload along the bridge, the height of the payload above the ground (length of the cables) and the oscillations of the payload with respect to the midpoint of the bridge.

In the vertical payload motion load case the oscillations experienced in the vertical forces at the wheels are mostly due to the oscillation of the payload during hoisting and lowering and the resulting vibration it establishes in the crane. The east-west distribution of the payload weight to the wheels is dependent on the payload position on the crane bridge.

In all cases where lateral horizontal forces are considered, the payload's influence is felt. The position of the payload on the bridge naturally induces different lateral forces whether in normal longitudinal motion, misalignment or skewing, but the swinging motion of the payload with respect to the midpoint of the crane bridge also heavily influences the behaviour of the crane. This can be seen in the period of rapid movement that occurs with an eccentric crab during longitudinal motion as well as the anomalies that occur during outward misalignment. Here, although the crane supporting structure is causing the crane to misalign outwards, the lateral swinging of the payload is dominant enough to overcome the misalignment forces experienced at the wheels and move the wheels even further out.

When considering the longitudinal horizontal forces that the wheels are transmitting to the rails, it is observed that the wheel force oscillates significantly with the longitudinal swinging

of the payload. Depending on the position of the swing the payload is either pulling the crane forward or holding it back. The driving force at the wheels is altered to maintain a steady velocity. As a result when the payload is holding the crane back the longitudinal force transmitted into the rails is considerably more than calculated by simple Newtonian calculations neglecting the payload motion.

The height of the payload above the ground and hence the length of the payload cable also has an influence on the wheel forces. When the payload is at its highest point (2.20 m above the ground) the frequency of oscillation of the payload, and therefore the oscillation of the wheel forces, is far higher than when the payload is just lifted off the ground (0.15 m above the ground). When the payload is at the top the angle the cables form at the pulley (0.95 rad) is considerably greater than the angle the cables form when the payload is at the bottom (0.15 rad). Fully hoisted, the pulley is more inclined to run along the cables than cause the cables to sway. At the same time, when the payload is fully hoisted it has a high eigenfrequency. This makes it less excitable by low frequency events. As a result, when the graphs of the two different payload heights are considered, the graphs with the payload fully hoisted are observed to be smoother than those with the payload at the bottom, and the displacement and force pattern at the wheels is more predictable. The full influence of the payload is always more apparent when the payload is at the bottom.

8.2 Crane Flexibility

It is often assumed that a crane acts as a rigid body and as such rigid body mechanics are applied to it when attempting to calculate wheel forces. Under this assumption if one wheel was deflected laterally, the remaining wheels of the crane would also deflect.

Throughout the load cases studied in the preceding four chapters it has been shown that this is not strictly true:

During normal longitudinal travel with an eccentric payload it was observed that in response to the slight skewing induced by the eccentric payload, the crane bridge and endcarriages were both flexed in the equilibrium position the crane found, both during northward and southward travel.

In misalignment, it was apparent that one wheel could be deflected 15 mm outwards, forcing the endcarriage to bend, and yet the pattern of forces of the opposite endcarriage remained the same, not indicating the couple that would have been expected if the crane was a rigid body.

In skewing, the two endcarriages and the bridge bend substantially as the crane attempts to accommodate the uneven forces it experiences. This can be observed in the pattern of lateral deflections followed at the crane wheels during motion.

While calculations involving the forces induced into the crane supporting structure by an electric overhead travelling crane generally assume that rigid body mechanics apply, for the test crane in the Stellenbosch Laboratory at least, this is inaccurate. This will lead to expectations that completely misrepresent the crane's behaviour, for example where skewing is considered in the Eurocode [2] the crane is treated as rotating around an instantaneous centre of rotation. This assumption only works with the concept of the crane as a rigid body.

It should be noted that the test crane in the laboratory at Stellenbosch University is an 8.28 m spanning 5 ton single girder crane. This is lightweight when compared with the cranes found commonly in industry. When the cranes under consideration have two box girder bridges, it is likely that the behaviour of the crane will follow rigid body mechanics far more closely than the test crane.

8.3 Vertical Wheel Loads

The dominant load case for determining vertical wheel loads is the vertical movement of the payload. When the payload is hoisted and lowered, the vertical force oscillations experienced at the wheels are greater than when the crane is moving longitudinally.

The South African loading code [1] has a simple approach to calculating the design vertical wheel loads from a crane onto the crane supporting structure. The total weight of the crane, including payload, is multiplied by a dynamic factor to account for oscillations. This load is distributed between the wheels according to the centre of gravity of the crane and payload combination.

The Eurocode [2] accounts for the design vertical wheel loads in more detail than the current South African code [1]. The total wheel load is split into the load due to the weight of the

crane, multiplied by a dynamic factor to account for the oscillation of the crane (φ_1), and the load due to the weight of the payload, multiplied by a dynamic factor to account for the payload oscillation (φ_2). The dynamic factor φ_1 is an empirical value given a maximum of 1.1, while φ_2 is calculated based on the payload hoisting speed.

From the numerical results discussed in Chapter 4.6, it was observed that the scenario which induced the largest oscillations in the crane occurred when the payload was lowered from 2.2 m above the ground to 1.2 m. If only the eccentric payload is considered, as this leads to the largest wheel loads, the greatest force oscillation experienced due to the vibration of the crane was 1.07 times the weight of the crane.

The greatest force oscillation due to the payload alone, with the crab eccentrically placed on the crane bridge, was calculated in the experimental tests as 1.11 times the weight of the payload. This occurred when the motor cut out as the payload was hoisted from 1.2 m above the ground to 2.2 m above the ground.

The two factors mentioned above correlate to φ_1 and φ_2 in the Eurocode respectively. According to the Eurocode the values that should be allowed for in the design of the crane supporting structure are $\varphi_1 = 1.13$ and $\varphi_2 = 1.10$. These exceed both of the dynamic factors calculated in the numerical model but not excessively.

In order to compare the numerical results with the global dynamic factor as allowed for in the current South African code [1], it is necessary to divide the total vertical wheel load on the supporting structure by the weight of the crane and the payload together. As the maximum partial dynamic factors occurred in different load cases, it is necessary to do this for all cases to determine which is dominant. The case with the greatest global dynamic factor is where the payload is lifted from 1.2 m above the ground to 2.2 m above the ground and the motor cuts the hoisting off suddenly. This global dynamic factor is $\varphi_0 = 1.10$ for an eccentric crab.

The design global dynamic factor according to the current South African code [1] for a class 2 crane is 1.2. This is extremely conservative when compared to the numerically calculated value. If the same process is followed with the Eurocode [2] to determine a global dynamic factor from the weights of the crane and payload and partial dynamic factors as discussed

previously, the global factor becomes $\varphi_0 = 1.12$. This is a slightly conservative and therefore a good prediction of the force involved.

The draft South African code [3] closely follows the Eurocode [2] in its approach to vertical wheel loads on the crane supporting structure. This provides a good estimate of the actual forces experienced by the crane in the numerical model and the partial dynamic factors used for the dead weight of the crane and the dead weight of the payload separately show an understanding of the mechanics involved during vertical payload movement.

8.4 Horizontal Lateral Wheel Loads

Horizontal lateral wheels forces can be induced by a wide range of causes. During hoisting, normal longitudinal travel, misalignment, skewing and acceleration and deceleration of the crab, longitudinal forces of different magnitudes are transmitted into the crane supporting structure via the wheels.

The current South African code [1] assumes that the design lateral horizontal forces are the most adverse of the lateral forces that are predicted to occur during misalignment, skewing or acceleration and deceleration of the crab.

The Eurocode [2] considers the lateral forces induced by normal longitudinal motion, skewing and the acceleration and deceleration of crab. The design lateral horizontal force is taken as the most adverse of these forces.

The greatest forces from each load case are shown in Table 8-1.

	SABS 0160	**Eurocode 1991-3**	**Numerical Model**
Vertical Payload Movement	-	-	0.84 kN
Normal Longitudinal Travel	-	2.75	0.76 kN
Misalignment	2.13 kN	-	2.11 kN
Skewing	3.2 kN	5.90 kN	2.77 kN
Acc / Dec of Crab	1.3 kN	1.3 kN	-

Table 8-1: Maximum lateral forces at wheels as predicted in the codes and calculated in the numerical model

From this table it appears that skewing is by far the most dominant case according to both codes and the numerical model. It should be noted that this table only represents the largest forces experienced, not the forces at each wheel.

The current South African code [1] assumes that the force of 3.2 kN acts at each wheel during skewing and the layout is such that the four forces form a couple. In contrast to this the forces during misalignment, although acting at each wheel, either point inward or outward simultaneously at each wheel. The resultant force on the crane supporting structure can be larger from misalignment than from skewing as the forces on each endcarriage complement each other rather than counteracting each other as in the case during skewing. For this reason all cases must be studied for each crane design to determine which case will cause the most adverse forces on the crane supporting structure.

In the case of misalignment, the predicted force according to the South African code [1] is 2.13 kN acting at each wheel. This is slightly higher than the maximum force experienced at a wheel according to the numerical model. Because the numerical crane is flexible rather than a rigid body as assumed in the code, the remaining three wheel forces are substantially lower than the maximum force experienced. This means that if the induced couple was divided among all four wheels equally, the magnitude of the force at the wheel would only be 1.27 kN at each wheel. As a result the current South African code accurately predicts the maximum force due to misalignment at one wheel but overestimates the forces due to misalignment on the crane as a whole.

In the case of skewing, the predicted force according to the South African code [1] is 3.2 kN acting at each wheel. As in the misalignment case, this is slightly higher than the maximum force experienced at a wheel as calculated by the numerical model. According to the numerical model, the remaining three wheels experience smaller forces than 2.78 kN. If the forces were represented at each wheel as the code predicts, the numerically calculated force at each wheel would only be 2.14 kN. Here the South African code [1] is fairly conservative with the maximum force experienced at one wheel and extremely conservative when the whole crane is considered.

The method the Eurocode [2] uses to represent skewing entails calculating a different force at each wheel according to the distance from the relevant guidance means and the instantaneous

centre of rotation of the crane. The maximum predicted force (7.96 kN) is far in excess of the numerically calculated force (2.71). The predicted force distribution at the wheels also completely misrepresents the actual force distribution as calculated by the numerical model. Eurocode [2] predicts minimal forces at the southern wheels while the numerical model calculates the largest force to be at the south west wheel. The method of calculating skewing forces in the Eurocode is not designed to account for the failure of one motor and completely misrepresents the forces involved.

The acceleration and deceleration of the crab was outside the scope of this thesis and further work is required to determine whether the factors used in the South African code [1] and Eurocodes [2] are relevant.

The draft South African code [3] follows guidelines from both the current South African code [1] and the Eurocode [2]. The calculations for skewing and the acceleration and deceleration of the crab are adopted from the Eurocode [2] while the misalignment calculations come from the current South African code [1]. Although the factors used in the current South African code [1] were empirical with little scientific backing, they do represent the horizontal lateral forces involved at the wheels accurately, albeit conservatively when considering the crane as a whole. The Eurocode, although based on scientific theory, does not take into account skewing induced by the failure of one motor and as such misrepresents the forces involved. As the draft South African code [3] has adopted the Eurocode [2] method of predicting skewing forces, these inaccuracies will continue in the new South African code [3].

8.5 Horizontal Longitudinal Wheel Forces

The current South African code [1] and the Eurocode [2] make allowances for the longitudinal horizontal forces that the crane imparts to the rails. These forces must be designed for in the longitudinal bracing system of the crane to ensure stability during the crane's motion. Both codes accept that the leading longitudinal forces that must be withstood by the bracing system are the forces transmitted into each rail during acceleration and deceleration of the crane and the force transmitted into the end stops of the crane supporting system when the crane impacts on the end stops.

The situation of the crane impacting on the ends stops is an accidental case and outside the scope of this thesis. For more details regarding the forces involved and the numerical modelling of the crane impact, refer to Reference 5 in the Bibliography.

For ease of comparison the horizontal longitudinal forces predicted by the design codes and calculated by the numerical model are presented in Table 8-2 below.

	SABS 0160	Eurocode EN 1991-3	Numerical Model
Normal longitudinal motion	2.89 kN	2.86 kN	2.17 kN
Misalignment	-	-	2.73 kN
Skewing	-	-	2.56 kN

Table 8-2: Horizontal Longitudinal Forces as predicted by the design codes and calculated by the numerical model.

The forces predicted as being generated by the crane's impact with the end buffer in both the current South African code [1] and the Eurocode [2] are the largest longitudinal forces expected to occur. As this is far in excess of the longitudinal forces generated by the acceleration and deceleration of the crab, the bracing system will be designed to withstand the accidental impact loads and will be conservative in comparison to the normal loads.

It is nevertheless interesting to note that while both codes assume that the largest longitudinal force due to crane acceleration and deceleration occurs during normal longitudinal travel, according to the numerical model it occurs during misalignment. The longitudinal forces induced into the rail during both misalignment and skewing are in excess of those induced during normal longitudinal travel.

The current South African code [1], using an empirical factor for determining the forces, predicts a force slightly higher than the actual force experienced during misalignment. This is an acceptable level of conservatism.

The Eurocode [2], calculating the forces in a more technical manner allowing for the maximum drive forces permitted at the driving wheels and taking friction into account, reaches a similar value for the longitudinal forces as the current South African code [1]. Although this overestimates the longitudinal forces involved during normal longitudinal motion of the crane, it accurately represents the forces that can be induced when misalignment and skewing are also considered.

As the draft South African code [3] incorporates the Eurocode's [2] methods of calculating the longitudinal forces, it is safe to assume that the draft South African code [3] will accurately predict the longitudinal forces occurring as a result of the acceleration and deceleration of the crane whether during normal longitudinal travel, misalignment or skewing.

8.6 Conclusion

When studying the movement and forces induced by an electric overhead travelling crane, it is essential to include the effect of the payload in the calculations. The effect of the payload oscillations alone have a large influence on the lateral and longitudinal forces experienced at the crane wheels.

The possibility of the crane not reacting as a rigid body should also be considered. While it is difficult to generalise about cranes in practice without further research, it is sufficient to state that the test crane demonstrates that some cranes are flexible in the movement of their bridge and endcarriages. This has a significant effect on the movement of the crane and the distribution of the forces at the wheels.

The current South African code is simplistic, relying on empirical factors to determine the correct loads. While these factors lead to predicted forces in the correct range of values, the Eurocode's method are more scientifically based. The draft South African code [3] is predominantly incorporating the methods used by the Eurocode [2] to calculate design forces for the supporting structure of an electric overhead travelling crane.

The only situations within the scope of this thesis which the Eurocode [2] does not accurately predict are the cases of misalignment and skewing. As such the draft South African code [3] adopts the current South African code's [1] calculations for misalignment. Although they are empirical methods they have been shown to give a fair estimate of the forces involved. In the case of skewing the draft South African code [3] has adopted the Eurocode's [2] calculations, despite the fact that they poorly predict the skewing forces existing due to the failure of one motor. These inaccuracies will be carried over to the draft South African code [3].

9 CONCLUSION

There is an unacceptably high failure rate of electric overhead travelling crane supporting structures across the world. These failures occur even when the cranes and supporting structures are designed within the relevant design codes. This demonstrates a lack of understanding of the dynamic behaviour of cranes in many design codes.

Many papers have been written studying the dynamic behaviour of cranes. These have included complex mathematical models to calculate the influences of eccentricities and vibrations on the motion of the crane. Simplifications of the experimental cranes need to be made in order to create the mathematical models. Two common simplifications are that the payload is taken as a fixed load on the crane and that the crane is a rigid body in plan.

The influence of the payload on the movement of the crane and the forces experienced at the crane wheels should not be neglected. The position of the crab, carrying the payload, on the crane bridge is expected to have a large influence on results. It is a well established fact that a crane with an eccentric load will move in a different manner to a crane with a central load. It is more interesting to note that the oscillation of the payload in all directions also has an effect on the forces experienced. The self weight of the payload is frequently more than the self weight of the crane and as such payload oscillations heavily influence crane movement. The payload is effectively a pendulum that is permitted to sway in all horizontal directions while the crane is accelerating and decelerating and undergoing skewing and misalignment. While this is difficult to model mathematically, a numerical model demonstrates that the swinging of the payload, not only in the direction of movement but perpendicular to it as well had an influence on the results obtained. This can be observed in the payload induced anomalies seen in the misalignment model in Chapter 6.

It is also important to note that the length of the cables carrying the payload (the height of the payload above the ground) has a direct influence on the results. The oscillations induced by the payload on the wheel forces are of a higher frequency when the payload is fully hoisted rather than just lifted off the ground. The pulley tends to run along the cables with a fully hoisted payload rather than causing the cables themselves to swing as occurs with the payload 0.15 m off the ground. This leads to smooth, more predictable results for the payload fully

hoisted than just off the ground. The largest payload influence can be seen when the payload is at the bottom (0.15 m above the ground).

A crane should not be assumed to react as a rigid body. When the crane is a lightweight, single I-section girder crane, the bending of both the bridge and endcarriages plays a substantial role in the crane's movement. This affects the force distribution experienced at the wheels and the motion of the crane as a whole. It is possible that the larger industrial cranes with a dual bridges mirror the actions of a rigid body more closely, but further work needs to be done to clarify this.

The South African loading code [1] with respect to crane loads is in the process of being revised. The methods currently used in the code are simplistic and empirical in nature, with little theory to support them. The draft South African code [3] is taking the Eurocode [2] for its model. The Eurocode [2] has scientifically substantiated calculations for the different load cases experienced during crane motion. It does still make use of dynamic factors that are empirical in nature, to take account of dynamic load amplification that can occur during crane movement. It is essential to determine if the predicted loads according to the Eurocode [2] represent the physical loads induced by the crane before they are adopted into the South African code.

In this study several load cases of concern in the codes were run on a numerical model. These were the vertical payload movement, normal longitudinal travel, misalignment and skewing load cases. According to the codes the vertical payload movement case is the dominant case for vertical wheel loads, while normal longitudinal travel, misalignment and skewing all induce horizontal loads into the structure.

The results from the numerical analyses were compared to the code's predicted values. It was ascertained that the Eurocode [2] provided an accurate, slightly conservative estimate of the vertical and horizontal longitudinal forces that were transferred by the crane into the crane supporting structure. The code showed an understanding of where the forces originated and allowed for them appropriately. The dynamic factors that were applied correlated well with the numerical results. It is sensible for the draft South African code [3] to incorporate these load cases as allowed for in the Eurocodes [2].

Conclusion

The South African code [1], although following empirical values, gave a conservative estimate of the overall loads applied to a crane during misalignment. It did, however, provide an accurate representation of the magnitude of the load that could be experienced at one wheel. In the absence of alternate methods for calculating misalignment forces it is reasonable for this current South African code [1] method to be carried over into the draft code.

The Eurocode [2] failed to predict skewing in a manner that was representative of the different forms of skewing that could occur. The magnitude and distribution of the forces predicted at the wheels were incorrect when compared to the results from the numerical model. The current South African code [1] predictions of skewing forces more accurate than those predicted by the Eurocode [2] but still overconservative and based on empirical methods only. The draft South African code [3] has included the skewing calculations from the Eurocode [2]. Further work needs to be conducted to improve the skewing calculations. This will enable the code to predict, in a logical manner, the viable forces resulting from crane skewing.

In order to lengthen the life of crane supporting structures it is essential to understand and predict the loads applied on the structures by the movement of the crane. The influence of the payload and the flexibility of the crane must be taken into account when determining crane movement. The draft South African code [3] provides logical predictions of the forces induced during vertical payload motion, normal longitudinal crane motion and misalignment. These predictions remain slightly conservative even after the effects of the payload and the flexibility of the crane are taken into account. Further work needs to be completed in the estimation of forces induced by skewing. As of yet this is not reliably predicted by the code. Once this is achieved it is hoped that the better understanding of the forces at work shown in the draft South African [3] code will lead to a reduction in failures of electric overhead travelling cranes.

10 RECOMMENDATIONS FOR FURTHER WORK

The following recommendations are areas that need further elucidation to continue the work established in this thesis:

- Work must be completed to determine a method that allows accurate prediction of forces due to skewing.
- The load cases concerning the acceleration and deceleration of the crab and the impact of the crab into its end stops should be implemented into the numerical model to confirm the factors and calculations used in the codes.
- Further work on misalignment could be completed by placing the wheels in the numerical model at a cant. This would investigate the effect of misaligned wheels on the loads induced in the crane supporting structure.
- A step or gap in the crane rail could be introduced in the numerical model to study the effect on the forces experienced at the crane wheels.
- The wheel flanges in the numerical model should be adjusted to match the experimental wheel flange size to determine what effect this has on the misalignment and skewing load cases.

11 REFERENCE SHEET

[1] SABS 0160:1989 (Amended 1990). Code of Practice: The general procedures and loadings to be adopted in the design of buildings. South African Bureau of Standards, Pretoria, 1990.

[2] prEN 1991-3:2003 Eurocode 1: Actions on Structures; Part 3: Actions induced by cranes and machinery.

[3] SANS 10160 (Final Draft, June 2006) Code of Practice: Basis of Structural Design and Actions for Buildings and Industrial Structures. Section 10: Actions induced by cranes and machinery.

[4] Personal communication with T. Haas

[5] De Lange, J., 2007 "An experimental investigation into the behaviour of a 5-ton Electric Overhead Travelling Crane and its Supporting Structure" *Masters Thesis*, University of Stellenbosch

[6] Lobov, N. A. 1976. "Calculation of Dynamic Loads on an Overhead Travelling Crane during its movement." *Vestnik Mashinostroeniya,* Vol. 56, Issue 1. pp. 44-48

[7] Karmakar, R. and A. Mukherjee. 1989. "Dynamics of Electric Overhead Travelling Cranes. A Bond Graph Approach." *Mech. Mach. Theory,* Vol. 25, Issue 1. pp. 29-39

[8] Lobov, N. A. 1984. "Overhead Travelling Crane Loads when Track-wheel Flanges contact the Rails" *Vestnik Mashinostroeniya,* Vol. 64, Issue 7, pp. 22-26

[9] Oguamanam, D. C. D. and J. S. Hansen. 2001. "Dynamics of a Three-Dimensional Overhead Crane System" *Journal of Sound and Vibration,* 242[3], pp. 411-426

[10] Taylor, F., Uma Jayaram, Sankar Jayaram and Tatsuki Mitsui. 2002 "Validation of Virtual Crane Behaviour through Comparison with a Real Crane" *Proceedings of ASME 2002 Design Engineering Technical Conferences.*

[11] Personal communication with J. Dymond

[12] Sedlacek, G. and Grotmann, D. 1996. "EC 1: Actions induced by cranes", *IABSE Colloquium on Basis of Design and Actions on Structures, Background and Application of Eurocode 1*, Delft. IABSE Report Vol 74.

[13] Lobov, N. A. 1986. "Loads on an overhead travelling crane when it moves with a constant skew setting of the girder." *Vestnik Mashinostroeniya,* Vol. 66, Issue 12, pp. 13-17

[14] Lobov, N. A. 1982. "Loads on an Overhead Travelling Crane caused by transverse and rotary motions of the bridge girder." *Vestnik Mashinostroeniya,* Vol. 62, Issue 6, pp. 31-35

[15] Lobov, N.A., A.V. Masyagin and I. A. Dulev. 1989. "On lengthening the life of bridge crane track wheels" *Vestnik Mashinostroeniya,* Vol. 69, Issue 2, pp. 30-34

[16] Spitsyna D. N. and I. V. Anoskin. 1986. "Investigation into the dynamics of the metal structures of foundry cranes when accelerating" *Vestnik Mashinostroeniya,* Vol. 66, Issue 5, pp. 25-30

[17] Personal communication with R. Harrison 2002. "The role of wheel flanges in the interaction between gantries and cranes."

[18] Cadile J., 1976. "Classification of cranes" AISE Annual Convention, Pittsburgh, *Pennsylvania*.

APPENDIX A: ECCENTRIC CRAB DURING HOISTING

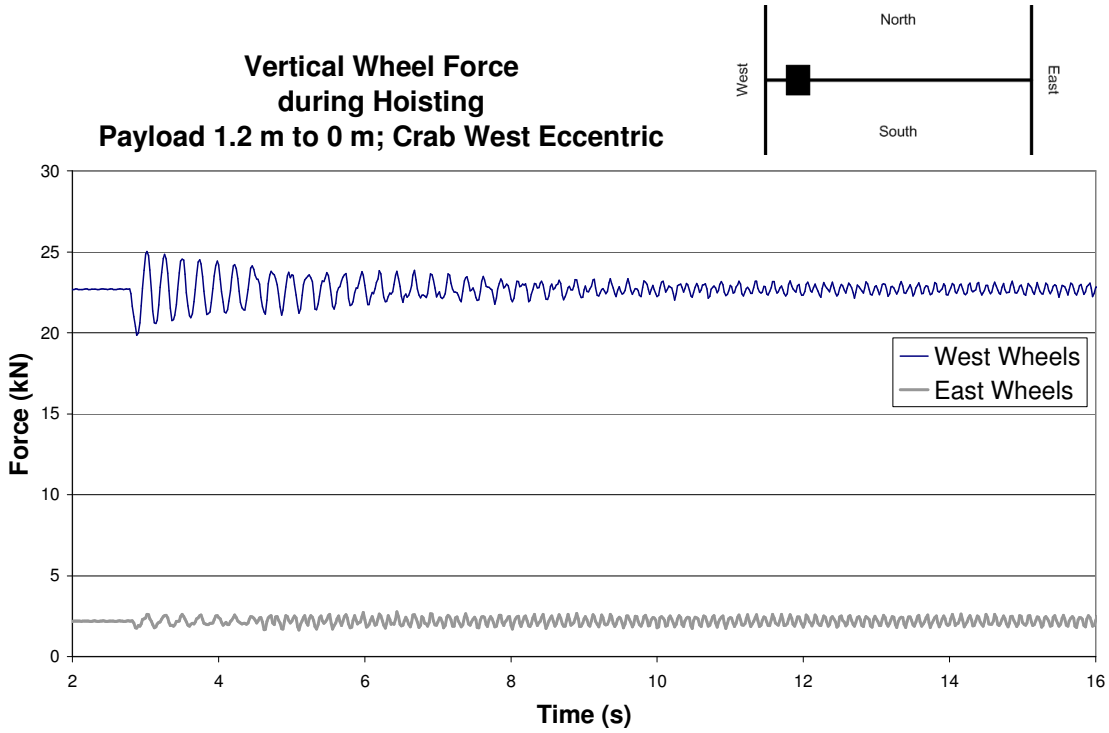

Figure A1: Vertical wheel forces as a result of hoisting the eccentric payload from 0 m to 1.2 m.

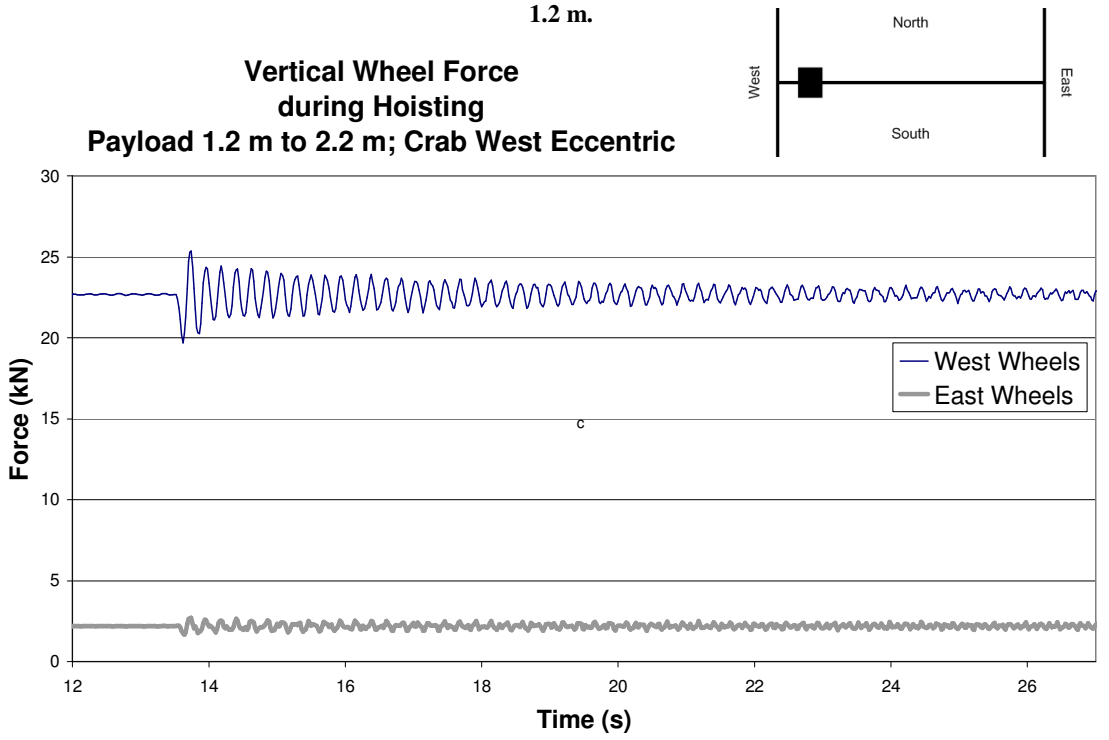

Figure A2: Vertical wheel forces as a result of hoisting the eccentric payload from 1.2 m to 2.2 m

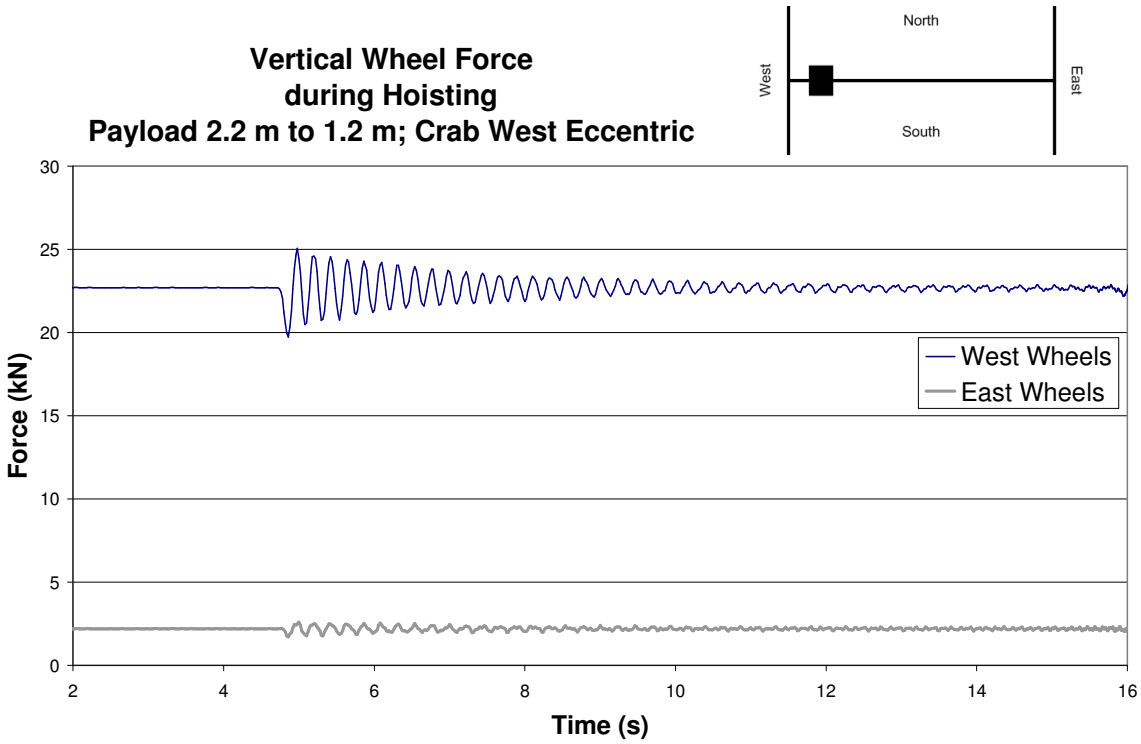

Figure A3: Vertical wheel forces as a result of lowering the eccentric payload from 2.2 m to 1.2 m

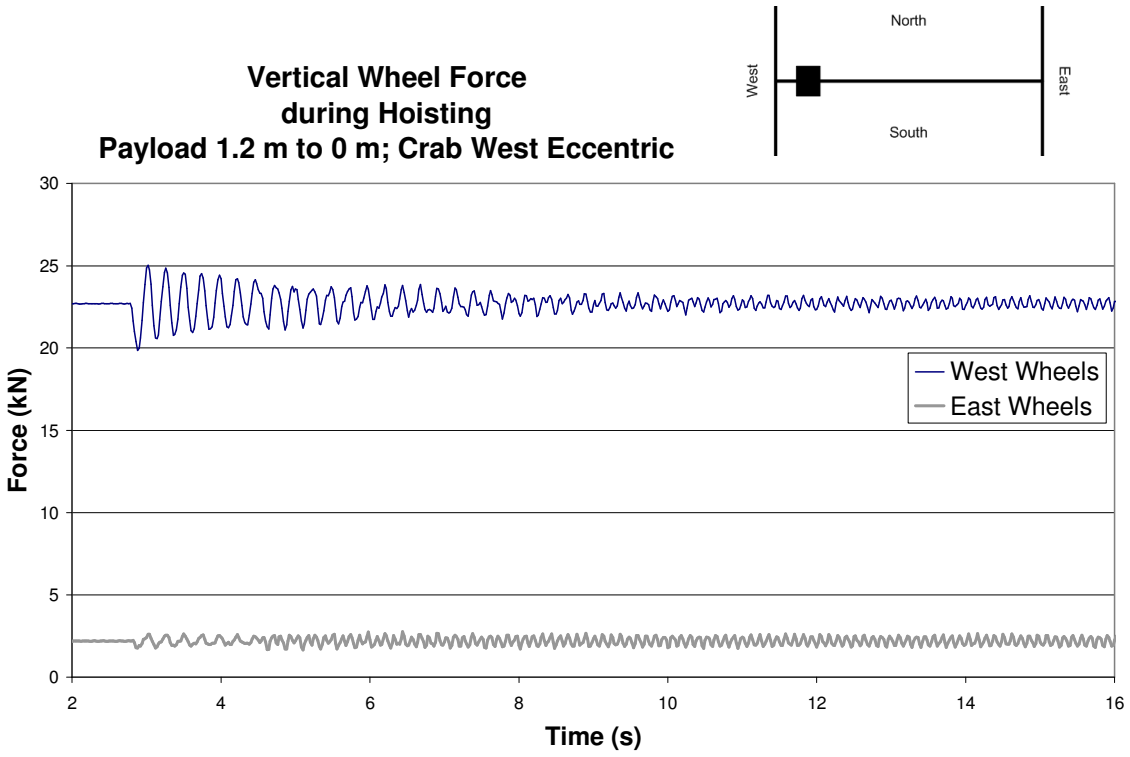

Figure A4: Vertical wheel forces as a result of lowering the eccentric payload from 1.2 m to 0 m

APPENDIX B: PAYLOAD AT 2.2 M DURING MISALIGNMENT

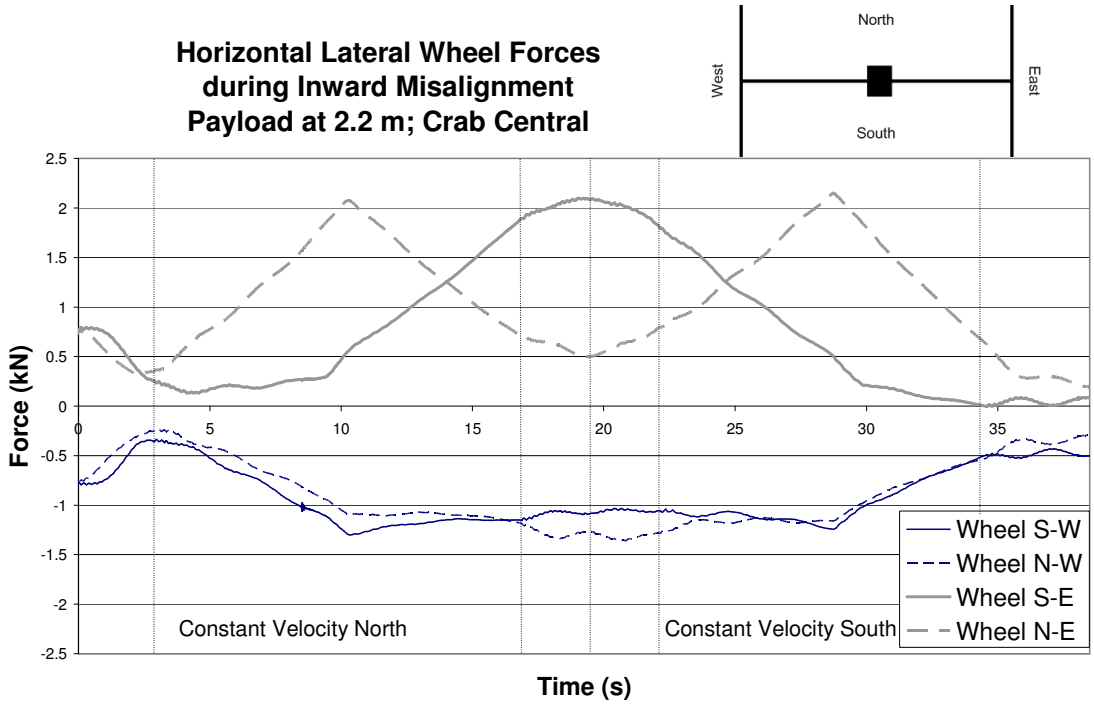

Figure B1: Horizontal wheel forces during inward misalignment with a central crab and payload at 2.2 m.

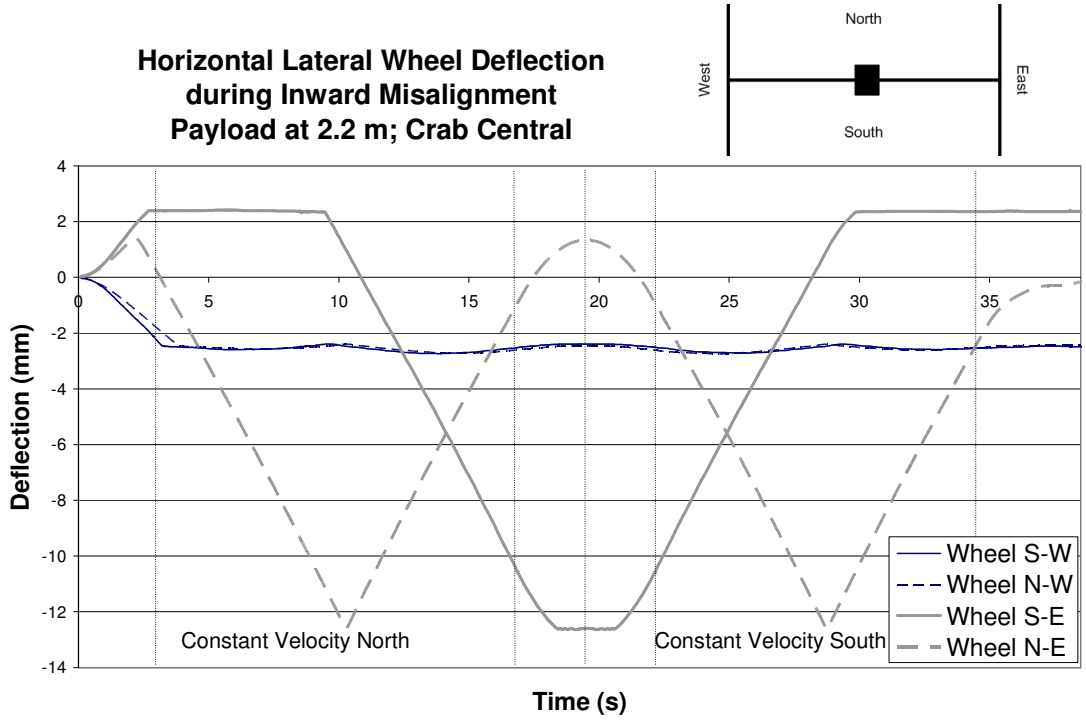

Figure B2: Horizontal wheel displacement during inward misalignment with a central crab and payload at 2.2 m.

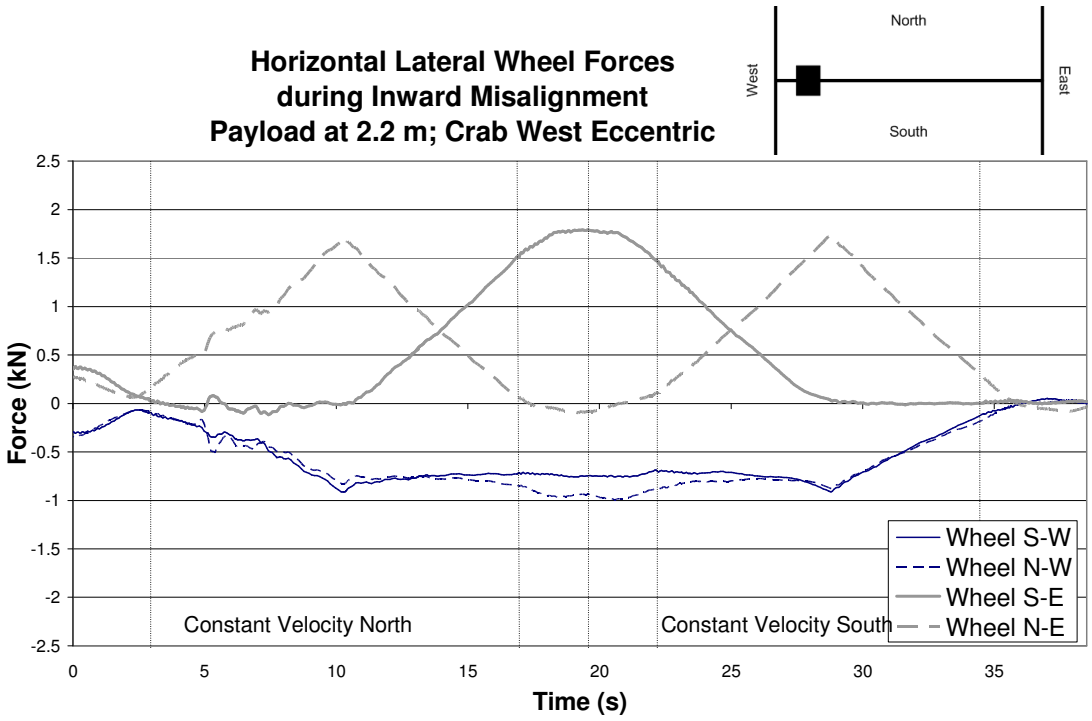

Figure B3: Horizontal wheel force during inward misalignment with a west eccentric crab and payload at 2.2 m.

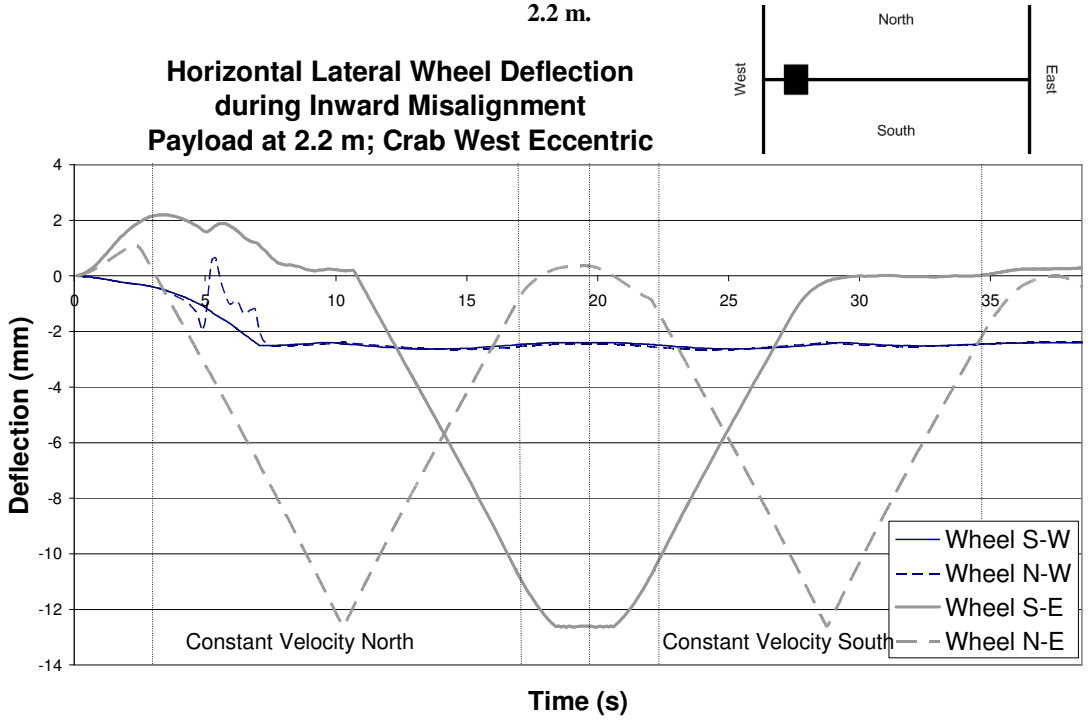

Figure B4: Horizontal wheel deflection during inward misalignment with a west eccentric crab and payload at 2.2 m.

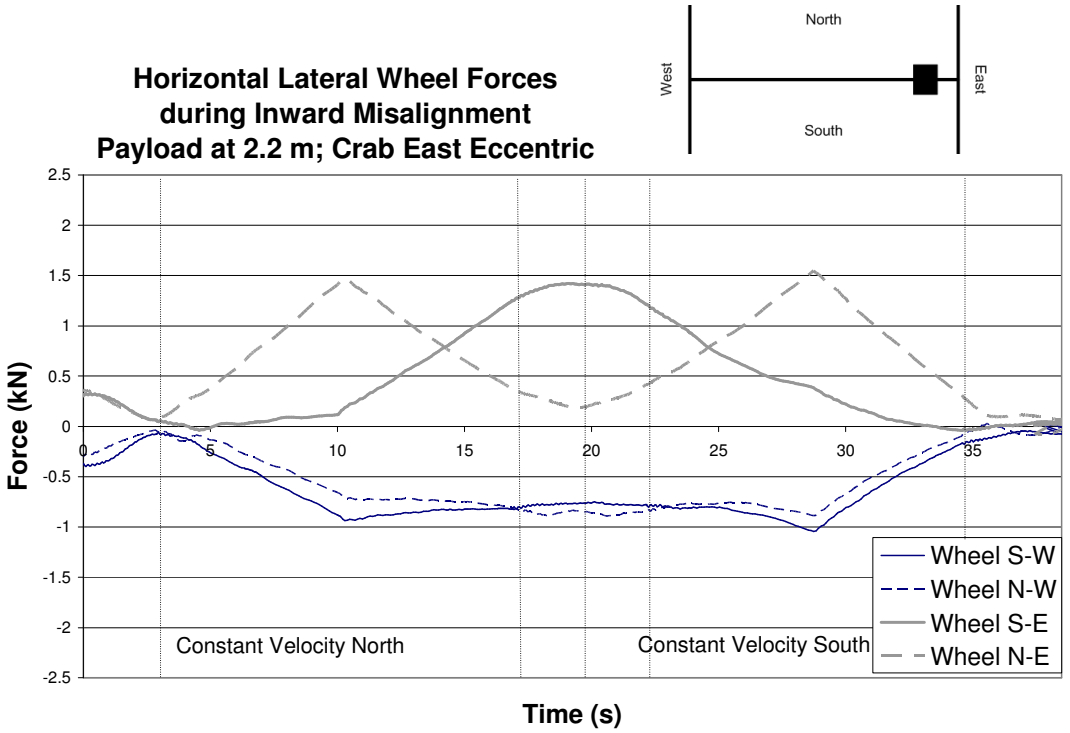

Figure B5: Horizontal wheel force during inward misalignment with an east eccentric crab and payload at 2.2 m.

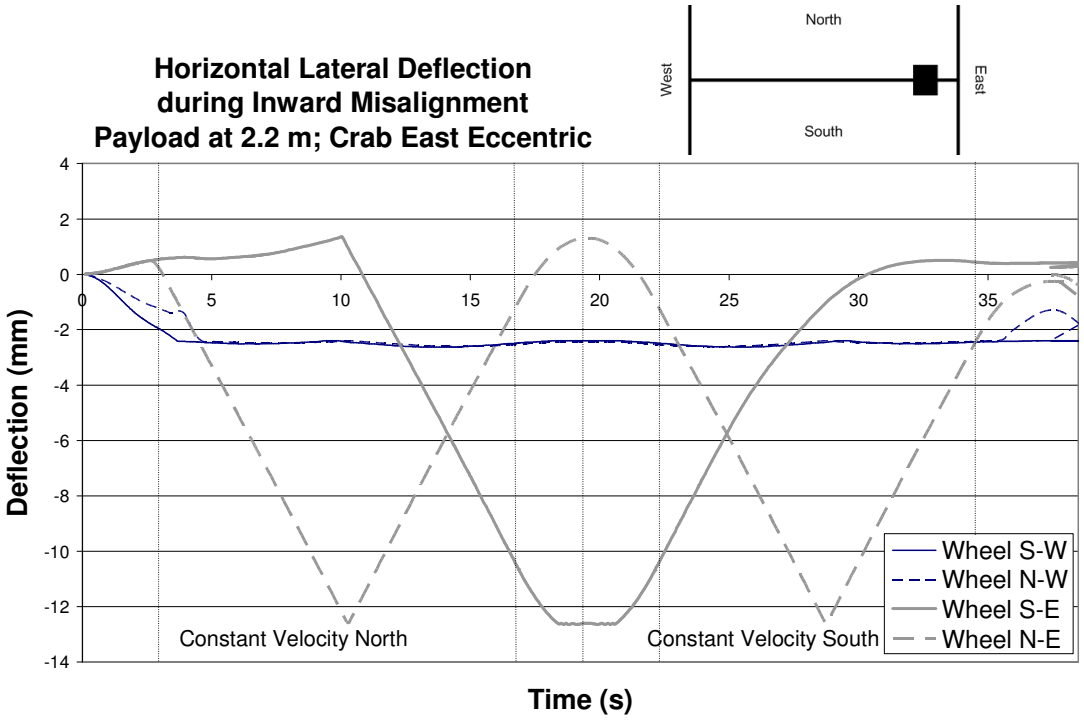

Figure B6: Horizontal wheel deflection during inward misalignment with an east eccentric crab and payload at 2.2 m.

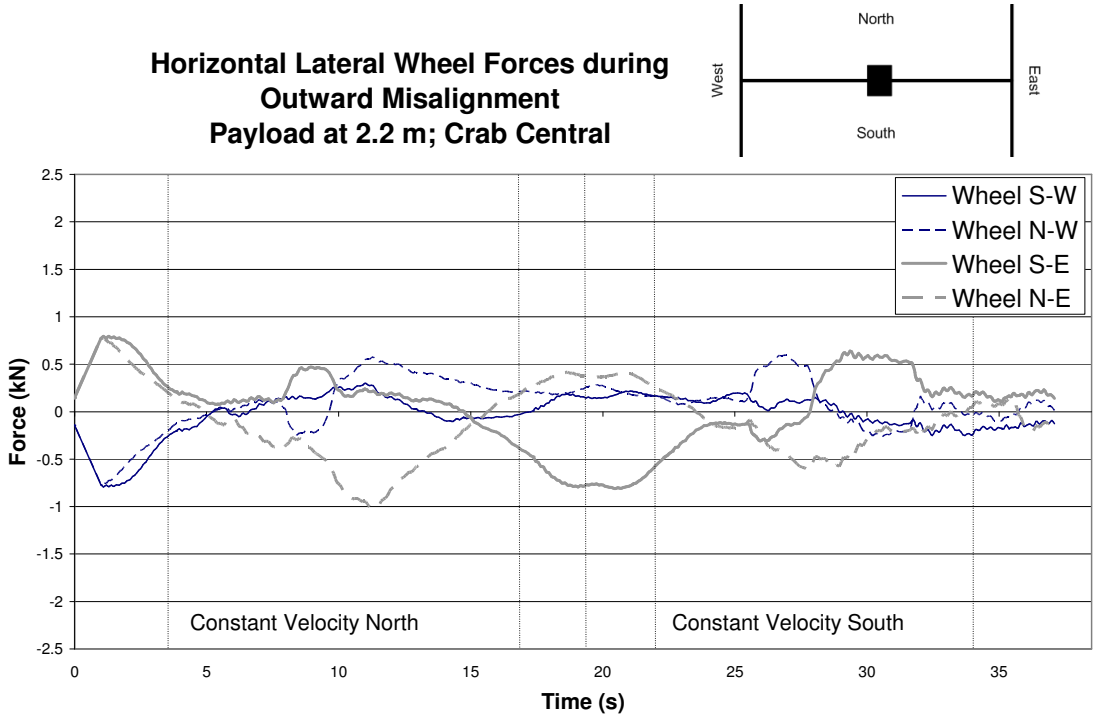

Figure B7: Horizontal wheel force during outward misalignment with a central crab and payload at 2.2 m.

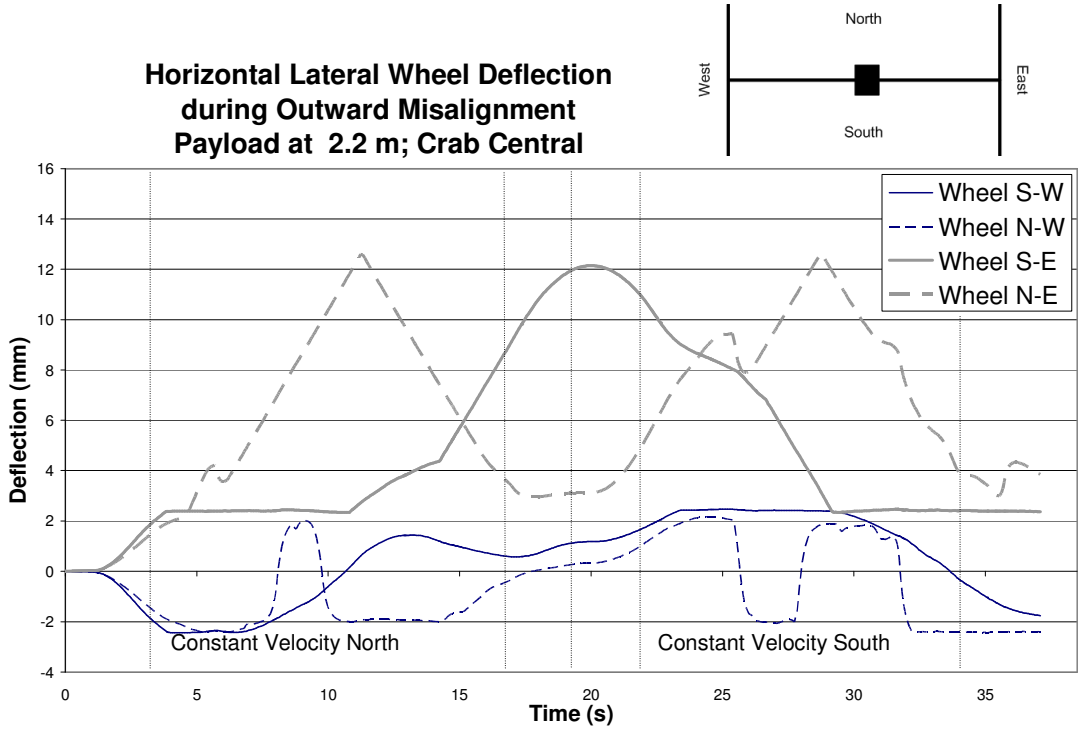

Figure B8: Horizontal wheel deflection during outward misalignment with a central crab and payload at 2.2 m.

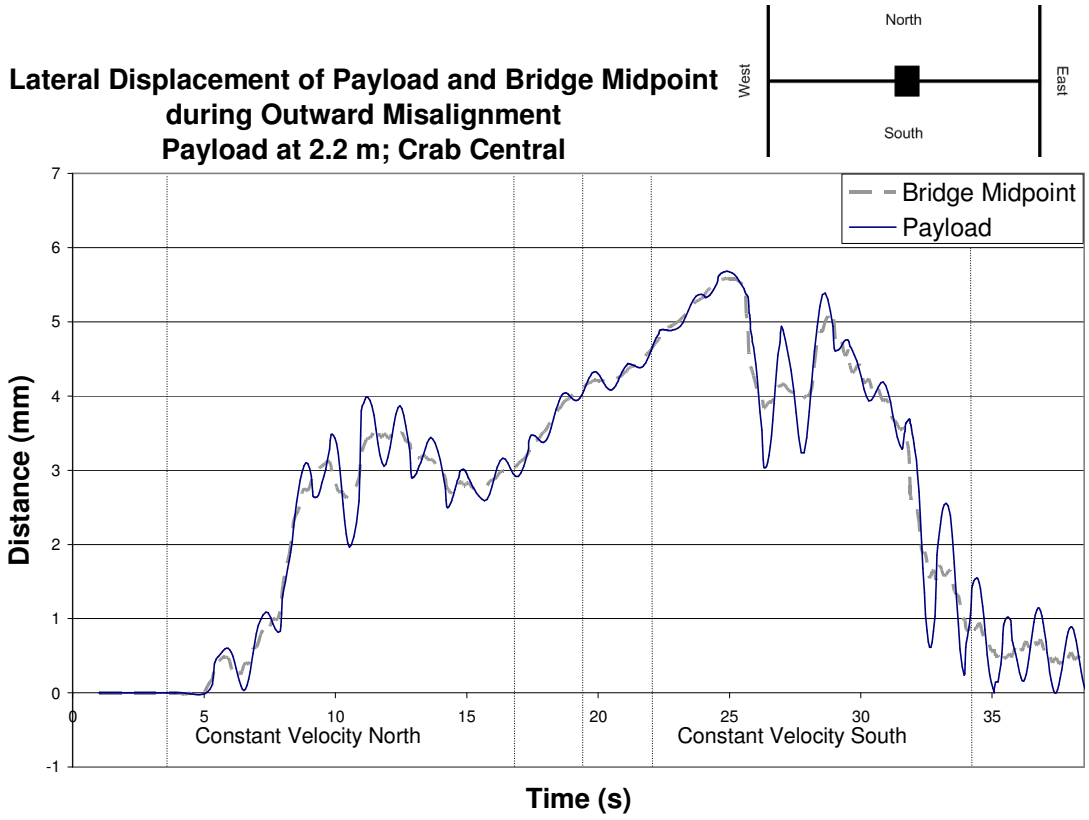

Figure B9: Lateral displacement of payload and bridge midpoint during outward misalignment with a central crab and payload at 2.2 m.

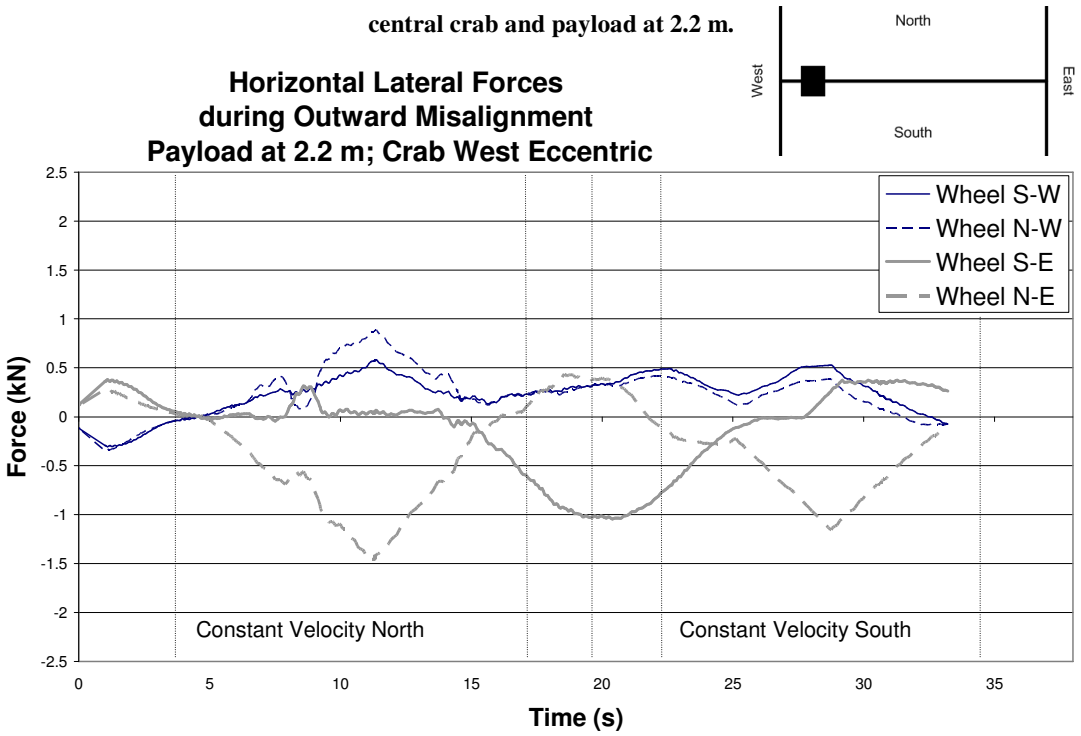

Figure B10: Horizontal wheel force during outward misalignment with a west eccentric crab and payload at 2.2 m.

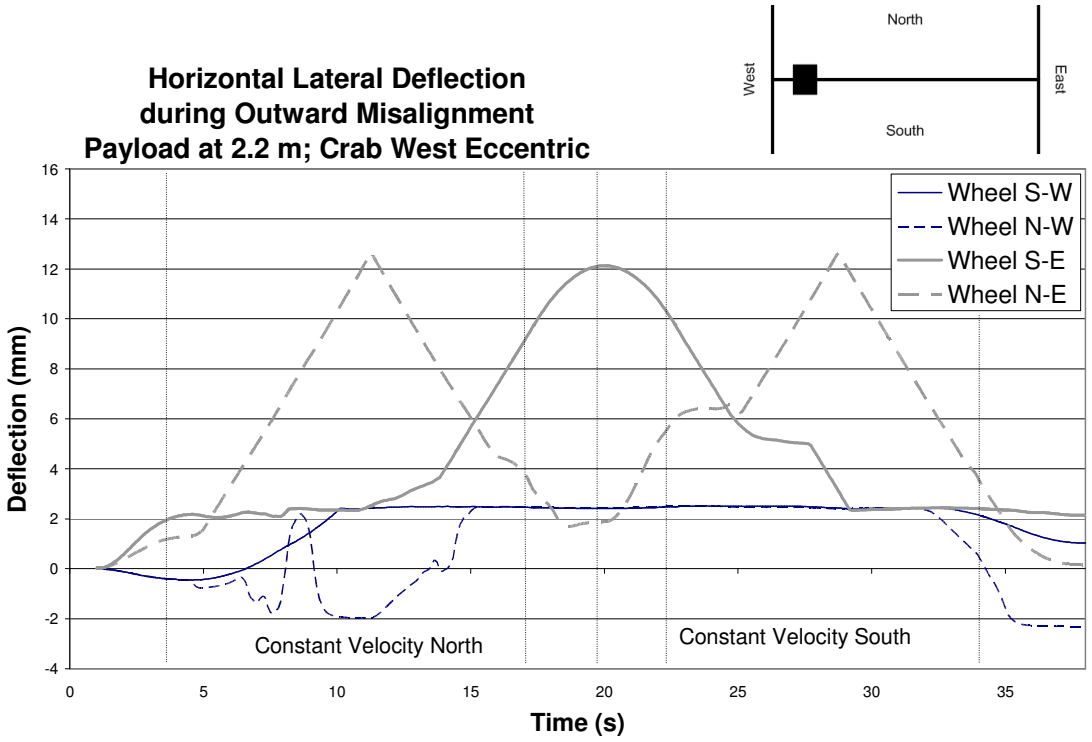

Figure B11: Horizontal wheel deflection during outward misalignment with a west eccentric crab and payload at 2.2 m.

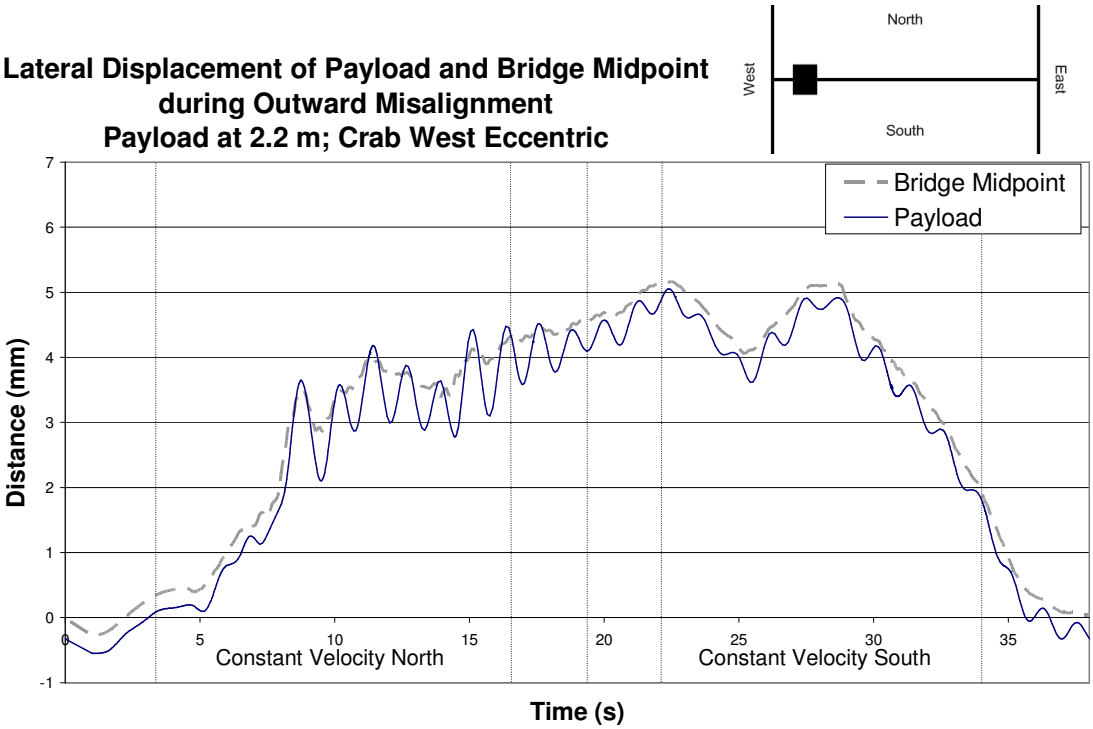

Figure B12: Lateral displacement of payload and bridge midpoint during outward misalignment with a west eccentric crab and payload at 2.2 m.

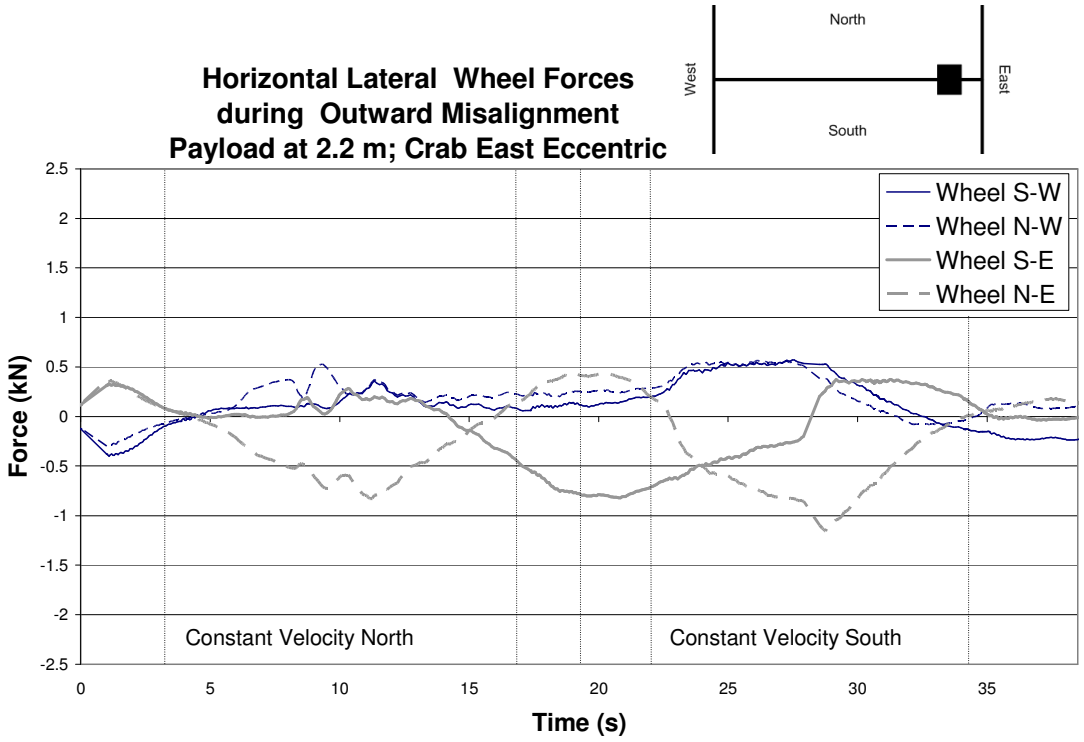

Figure B13: Horizontal wheel force during outward misalignment with an east eccentric crab and payload at 2.2 m.

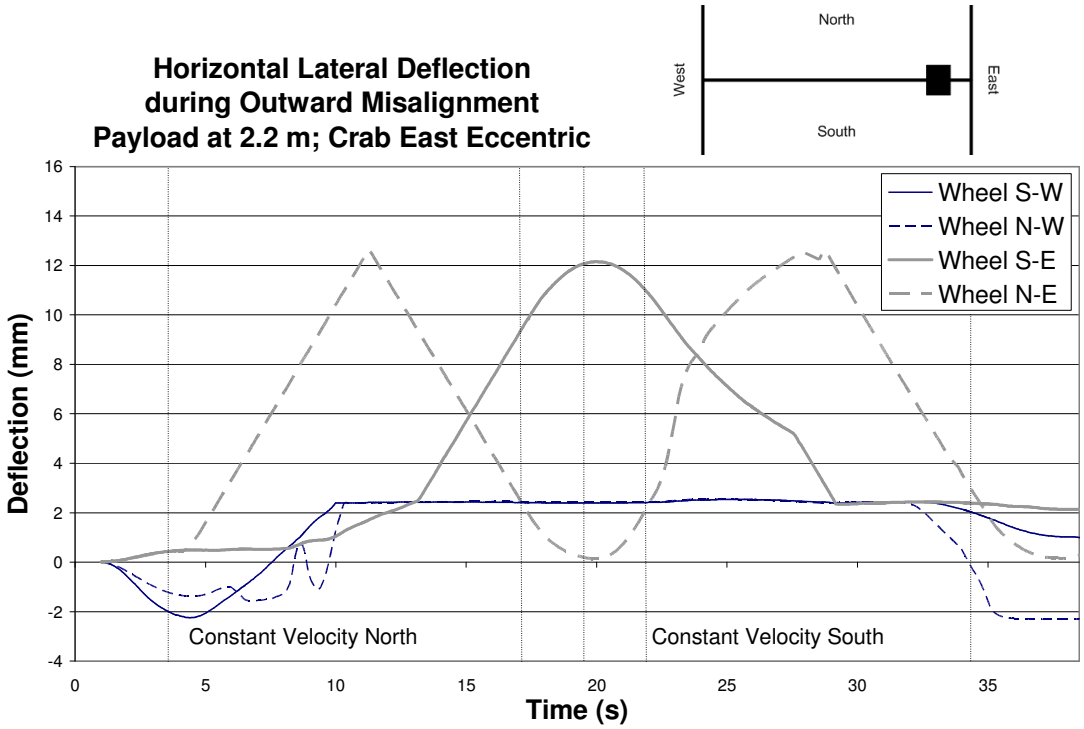

Figure B14: Horizontal wheel displacement during outward misalignment with an east eccentric crab and payload at 2.2 m.

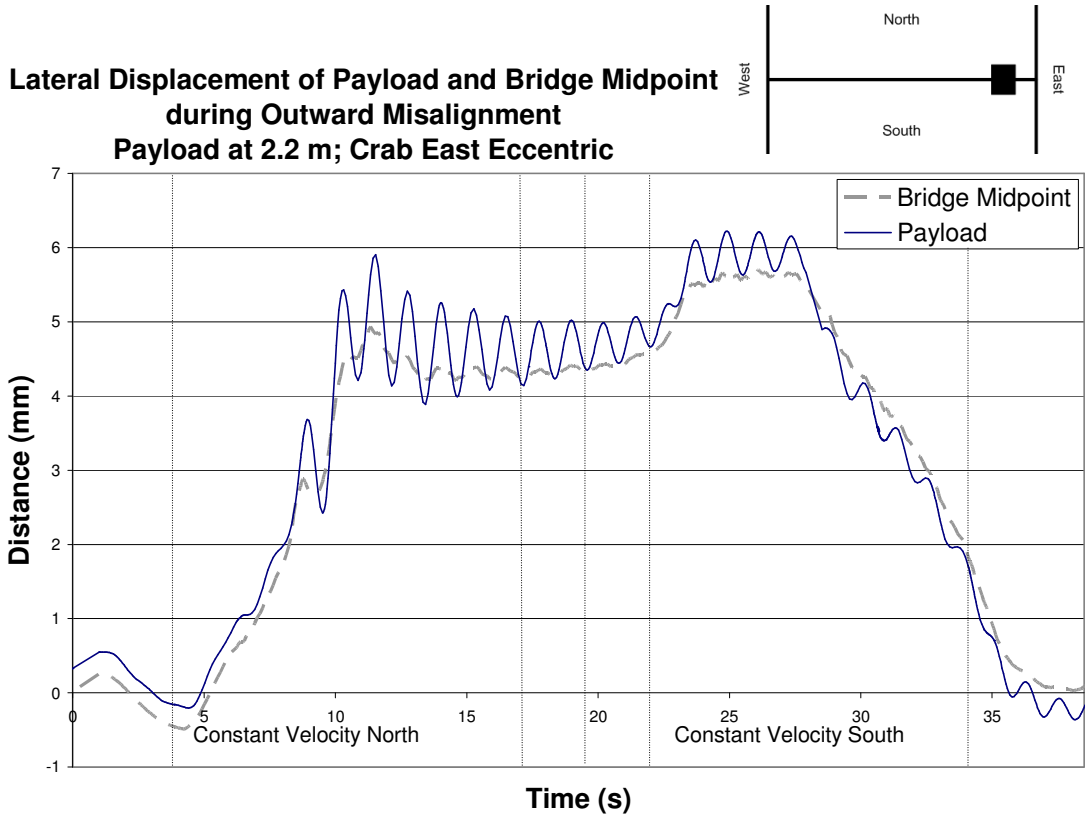

Figure B15: Lateral displacement of payload and bridge midpoint during outward misalignment with an east eccentric crab and payload at 2.2 m.

APPENDIX C: PAYLOAD AT 2.2 M DURING SKEWING

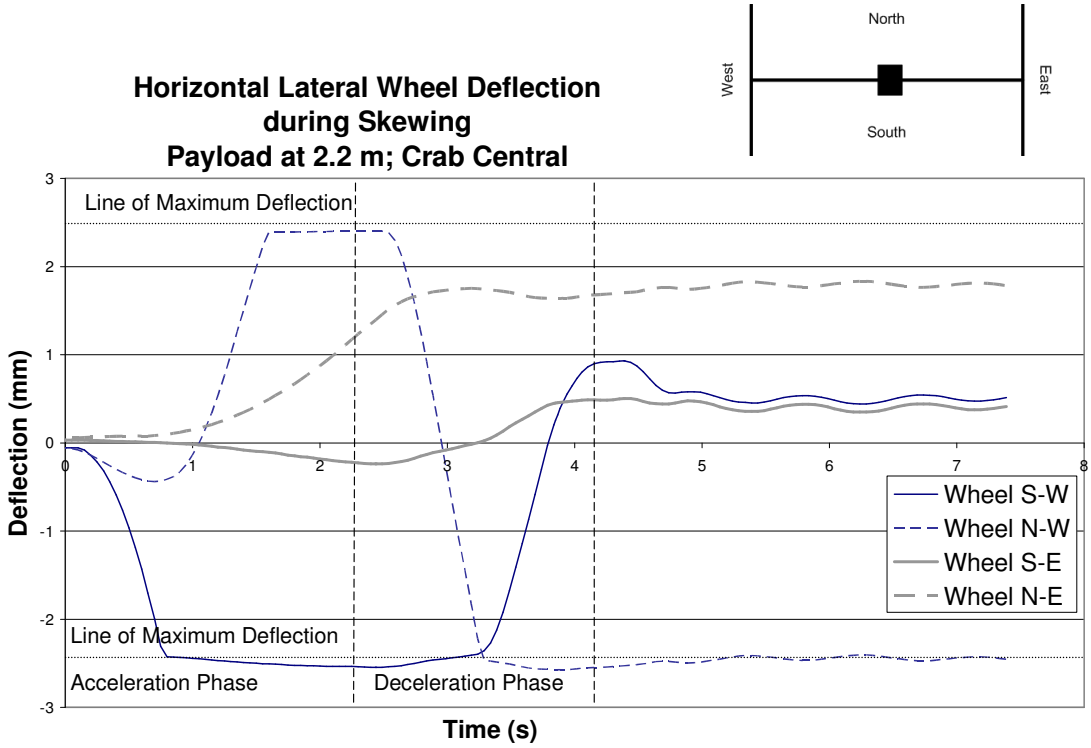

Figure C1: Horizontal wheel deflection during skewing with a central crab and payload at 2.2 m.

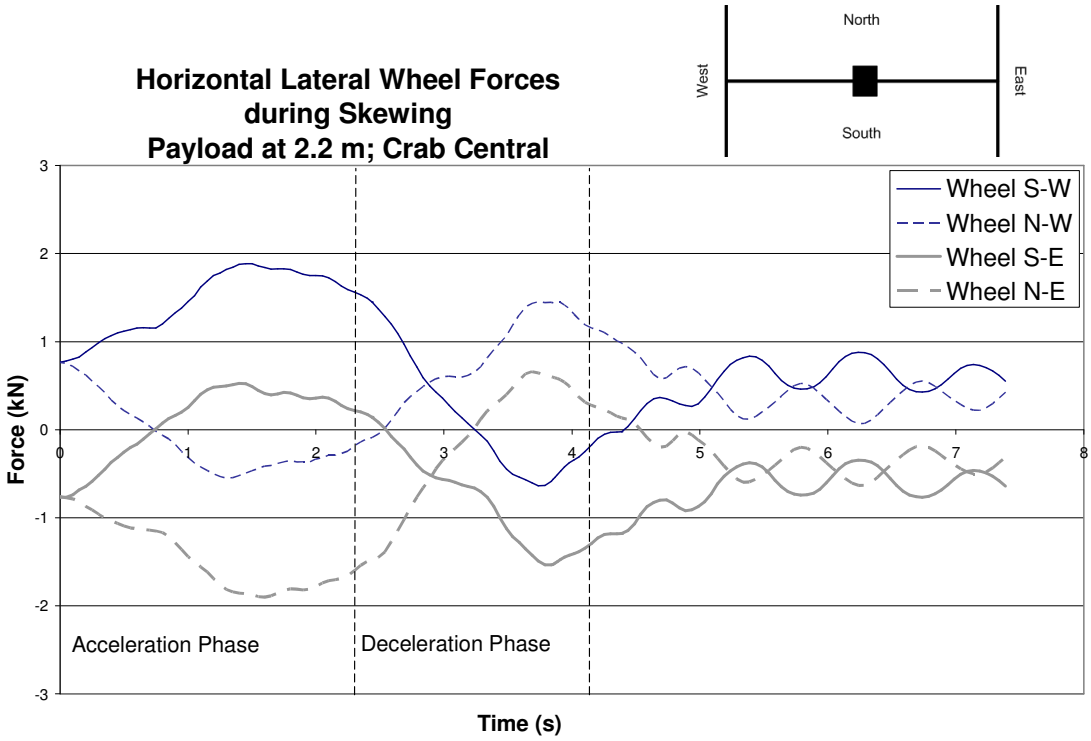

Figure C2: Horizontal wheel forces during skewing with a central crab and payload at 2.2 m.

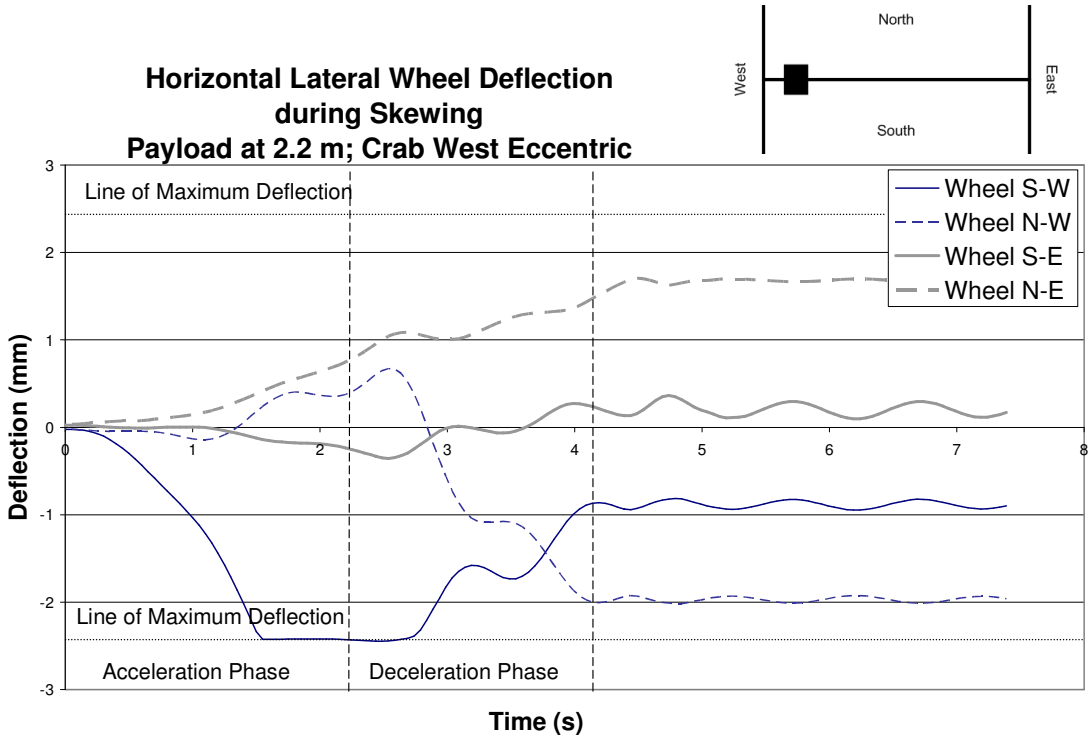

Figure C3: Horizontal wheel deflection during skewing with a west eccentric crab and payload at 2.2 m.

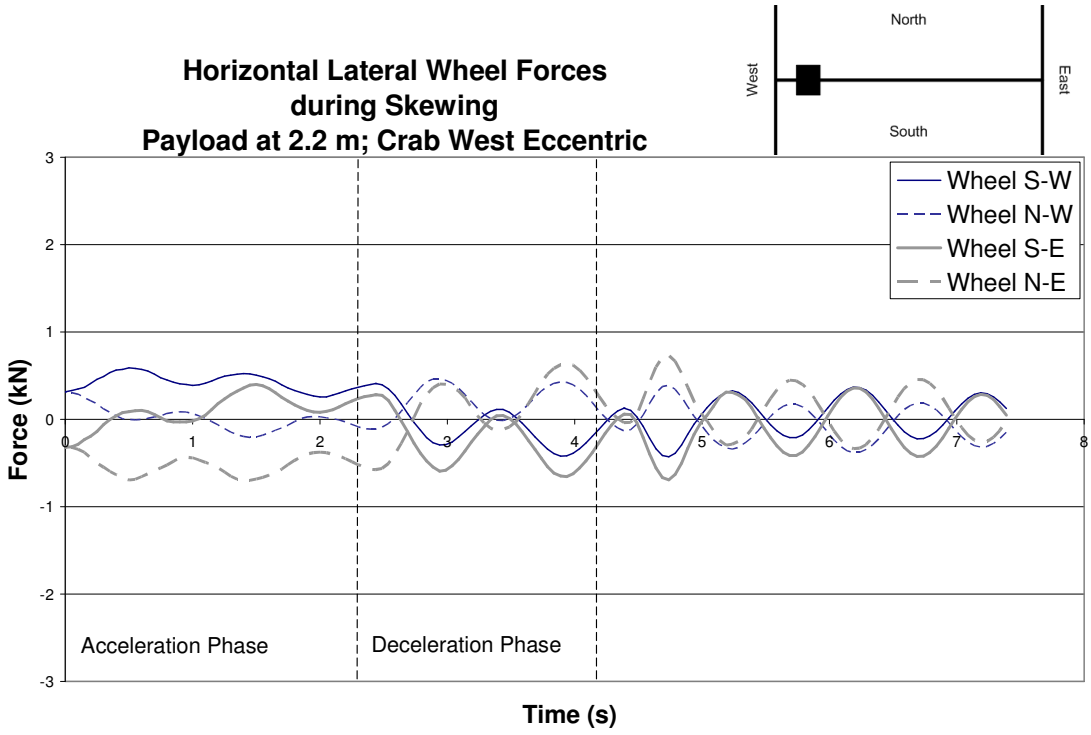

Figure C4: Horizontal wheel forces during skewing with a west eccentric crab and payload at 2.2 m.

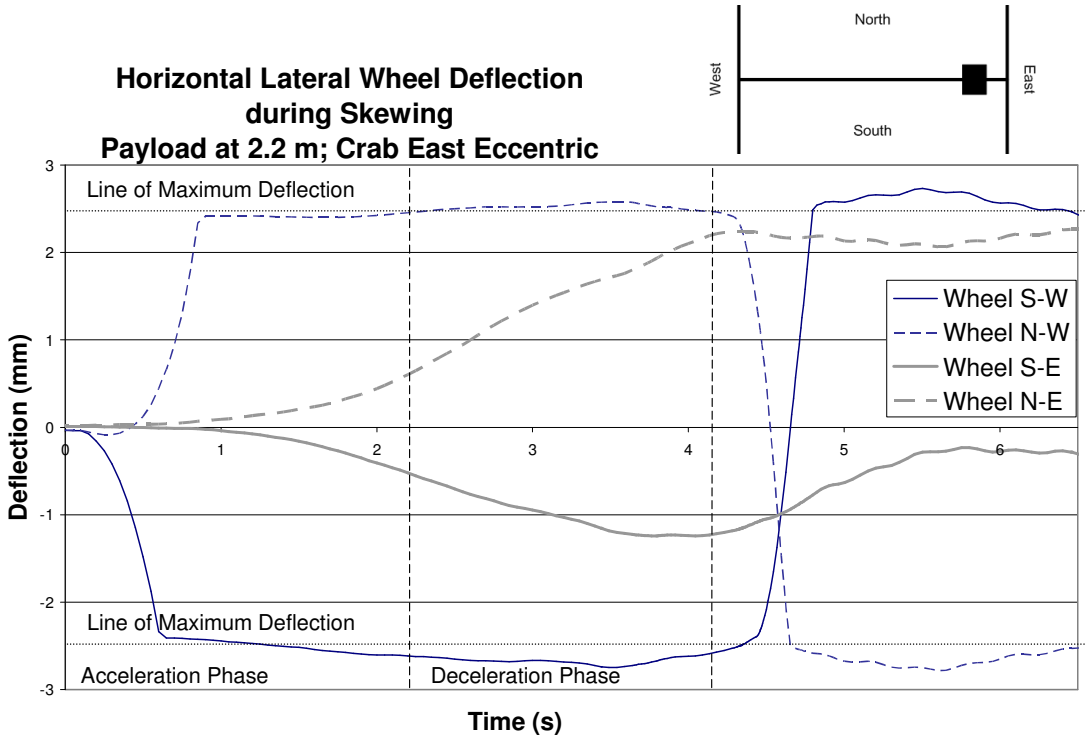

Figure C5: Horizontal wheel deflection during skewing with an east eccentric crab and payload at 2.2 m.

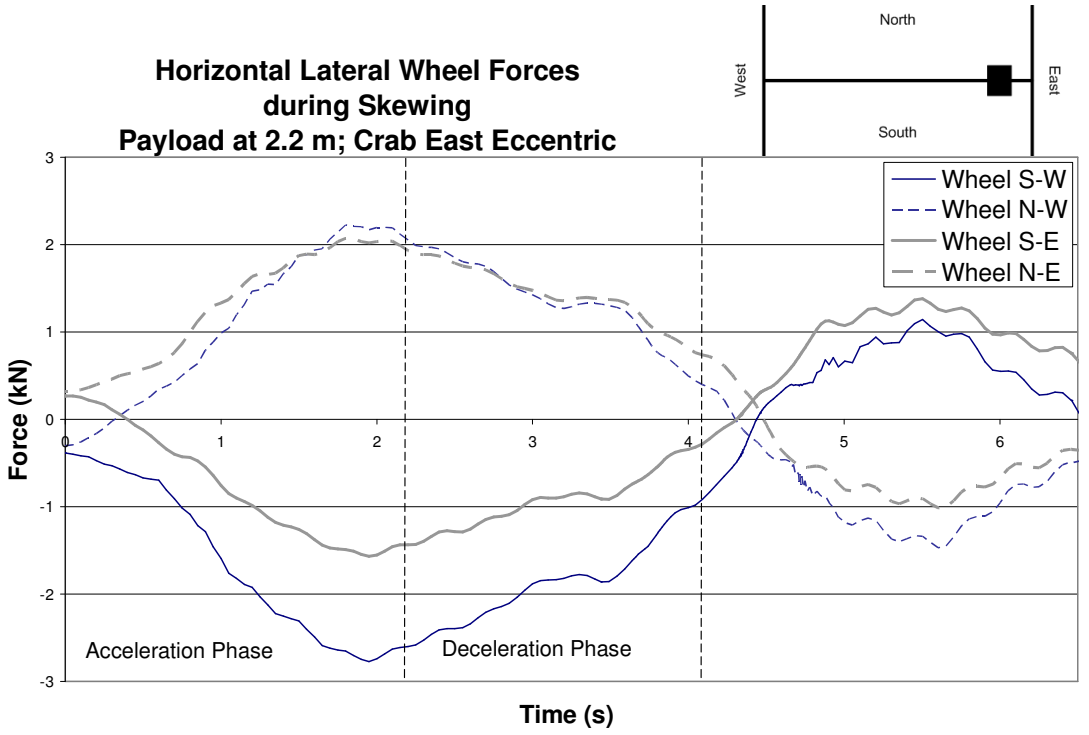

Figure C6: Horizontal wheel forces during skewing with an east eccentric crab and payload at 2.2 m.